

**Lipodendriplexes: A promising nanocarrier for enhanced nucleic
acid delivery**

Dissertation

zur

Erlangung des Doktorgrades

der Naturwissenschaften

(Dr. rer. nat.)

dem

Fachbereich Pharmazie der
Philipps-Universität Marburg

vorgelegt von

Imran Tariq

aus Lahore, Pakistan

Marburg/Lahn 2019

Erstgutachter: **Prof. Dr. Udo Bakowsky**

Zweitgutachter: **Prof. Dr. Cornelia M. Keck**

Eingereicht am: **12.07.2019**

Tag der mündlichen Prüfung am: **27.08.2019**

Hochschulkennziffer: 1180

EIDESSTATTLICHE ERKLÄRUNG

Ich versichere, dass ich meine Dissertation

„Lipodendriplexes: A promising nanocarrier for enhanced nucleic acid delivery“

selbständig ohne unerlaubte Hilfe angefertigt und mich dabei keiner anderen als der von mir ausdrücklich bezeichneten Quellen bedient habe. Alle vollständig oder sinngemäß übernommenen Zitate sind als solche gekennzeichnet.

Die Dissertation wurde in der jetzigen oder einer ähnlichen Form noch bei keiner anderen Hochschule eingereicht und hat noch keinen sonstigen Prüfungszwecken gedient.

Marburg, den.....

.....
(Imran Tariq)

A C K N O W L E D G E M E N T S

First of all, I would like to express my sincere gratitude to my research supervisor Prof. Dr. Udo Bakowsky for his continuous support during my whole Ph.D. research work. His guidance, immense knowledge, advice, patience and motivation helped me in all time of research. I could not have imagined having a better advisor and mentor for my Ph.D. study.

I would also like to thank my group leader Dr. Jens Schäfer for fruitful scientific discussions and guidance during my research work. His insightful thoughts, encouragement, but also for the hard question which incited me to widen my research from various perspectives. He really proved himself a fatherly figure.

I would like to express my humble gratitude to Dr. Shashank Reddy Pinnapireddy for his discussion and expertise in all cell culture experiments.

My sincere thank goes to Prof. Dr. Nadeem Irfan Bukhari, Dr. Abida Raza and Dr. Muhammad Farhan Sohail for their support during *in vivo* experiments in Pakistan.

I am grateful to Mr. Harshavardhan Janga for his tremendous help in RT-qPCR and flow cytometry experiments.

I thank my fellow lab mates for the stimulating discussions, for the whole days we were working together and for all the fun we had in the last four years. Most importantly, Muhammad Yasir Ali, Sajid Ali, Muhammad Umair Amin, Dr. Jarmila Jedelská, Dr. Jana Brüßler, Uzma Ali, Ghazala Ambreen for their outstanding support, sensible advice and willingness to help.

I would like to acknowledge the help of Mrs. Eva Maria Mohr who has supported me and motivated me with her background knowledge and expertise throughout my research work.

Sincere thanks to my colleagues at the research group Bakowsky especially Dr. Gihan Mahmoud, Dr. Konrad Engelhardt, Mohamad Alawak, Lili Duse, Alice Abu Dayyih, Nathalie Goergen for helping me out in my studies.

Special thanks to Julia Michaelis for her patience and guidance in every official and administrative work.

I am grateful to overseas scholarship committee of University of the Punjab for providing Ph.D. scholarship and make it possible for me to get higher education.

Nobody has been more important to me in the pursuit of this project than the members of my family. I would like to thank my parents, whose love and guidance are with me in whatever I pursue. They are the ultimate role models. Most importantly, I wish to thank my loving and supportive wife, Shamsa Imran and my two wonderful children, Muhammad Arbaz Imran and Eman Imran, for their patience and to provide unending inspiration.

Die vorliegende Arbeit entstand auf Anregung und unter Leitung von

Herrn Prof. Dr. Udo Bakowsky

am Institut für Pharmazeutische Technologie und Biopharmazie

der Philipps-Universität Marburg

TABLE OF CONTENTS

Chapter I: Introduction.....	1
1.1 Gene therapy.....	2
1.2 Viral Vectors.....	2
1.3 Non-viral vectors.....	3
1.3.1 Plasmid based non-viral vectors.....	3
1.3.2 Polymer based gene delivery.....	3
1.3.3 Liposomes based gene delivery.....	5
1.3.4 Lipodendriplexes.....	5
1.4 Multidrug resistance and RNA interference.....	7
1.5 Aims and Objectives.....	8
Chapter II: Materials and Methods.....	10
2.1 Materials.....	11
List of materials.....	11
2.1.1 Polymers.....	17
2.1.1.1 Polyamidoamine (PAMAM).....	17
2.1.2 Nucleic acids.....	17
2.1.2.1 Plasmid DNA.....	17
2.1.2.1.1 pCMV-luc.....	17
2.1.2.1.2 pCMV-GFP.....	18
2.1.2.2 Oligonucleotides.....	18
2.1.3 Lipids.....	18
2.1.3.1 DPPC.....	18

2.1.3.2 DOTAP.....	19
2.1.3.3 DOPE.....	19
2.1.3.4 MPEG5000-DPPE.....	20
2.1.3.5 DPPG.....	20
2.1.3.6 Cholesterol.....	21
2.1.4 Imatinib Mesylate.....	21
2.2 Methods.....	22
2.2.1 Formulations.....	22
2.2.1.1 Preparation of liposomes.....	22
2.2.1.2 Preparation of dendriplexes.....	22
2.2.1.3 Preparation of lipodendriplexes.....	23
2.2.2 Physicochemical characterization.....	23
2.2.2.1 Dynamic light scattering.....	23
2.2.2.2 Laser Doppler anemometry.....	23
2.2.3 Complex stability studies.....	23
2.2.3.1 Gel retardation assay.....	23
2.2.3.2 Fluorescence quenching assay.....	24
2.2.4 Surface morphology.....	24
2.2.4.1 Atomic force microscopy.....	24
2.2.5 <i>In vitro</i> cell culture experiments	25
2.2.5.1 Maintenance of cells.....	25
2.2.5.2 pDNA transfection studies.....	25
2.2.5.3 Transgene luciferase expression analysis.....	25
2.2.5.4 Protein quantification assay.....	26
2.2.5.5 Cellular uptake studies.....	26

2.2.6 Cytotoxicity studies.....	27
2.2.6.1 MTT assay.....	27
2.2.6.2 Determination of reactive oxygen species	27
2.2.6.3 Lysosomal disruption and actin polymerization.....	28
2.2.6.4 DNA damage assay.....	28
2.2.7 Biocompatibility studies	29
2.2.7.1 <i>Ex vivo</i> hemolysis assay.....	29
2.2.7.2 Heparin competition assay.....	29
2.2.8 RNA interference experiments.....	30
2.2.8.1 Luciferase knockdown assay.....	30
2.2.8.2 GFP silencing.....	30
2.2.8.3 MDR1 silencing.....	30
2.2.8.3.1 RNA isolation, reverse transcription and RT-qPCR.....	31
2.2.9 Cell migration studies.....	31
2.2.9.1 Scratch closure assay.....	31
2.2.9.2 Transwell migration assay	31
2.2.9.3 Plate colony formation assay.....	32
2.2.9.4 Formation of 3D tumor spheroids and ring bioprinting.....	32
2.2.9.4.1 3D tumor spheroids cell migration assay.....	34
2.2.9.4.2 Cytoskeleton staining of spheroids.....	34
2.2.9.5 3D tumor ring closure assay.....	35
2.2.10 Apoptosis assay by flow cytometry.....	35
2.2.11 Apoptosis determination in spheroids by live dead viability assay.....	36
2.2.12 Cell cycle analysis by flow cytometry.....	36
2.2.13 <i>In ovo</i> chorioallantoic membrane assay.....	36

2.2.14 <i>In vivo</i> experiments.....	37
2.2.14.1 Animals.....	37
2.2.14.2 Acute <i>in vivo</i> toxicity.....	37
2.2.14.2.1 Serum biochemistry and hemotological analysis.....	38
2.2.14.2.2 Organ to body ratio.....	38
2.2.14.2.3 Erythrocytes aggregation assay.....	38
2.2.14.2.4 Histopathology of vital organs.....	39
2.2.14.3 <i>In vivo</i> biodistribution and imaging experiments.....	39
2.2.14.4 Frozen tissue GFP distribution analysis.....	39
2.2.15 Statistical analysis.....	39
Chapter III: Results and discussion.....	40
3.1 Physicochemical characterization and optimization of dendriplexes.....	41
3.2 Physicochemical characterization and optimization of lipodendriplexes.....	44
3.3 DNA transfection experiments.....	47
3.3.1 pDNA transfection experiments of lipodendriplexes.....	47
3.3.2 Cellular uptake studies.....	48
3.4 Cytotoxicity studies.....	50
3.4.1 MTT assay.....	50
3.4.2 ROS generation assay.....	51
3.4.3 Lysosomal disruption and actin polymerization.....	53
3.4.4 DNA damage assay.....	54
3.5 Biocompatibility studies.....	55
3.5.1 <i>Ex vivo</i> hemolysis analysis.....	55
3.5.2 Heparin competition assay.....	56
3.6 RNA interference experiments.....	57

3.6.1 Luciferase gene knockdown assay.....	57
3.6.2 GFP silencing studies.....	58
3.6.3 MDR1 silencing and RT-qPCR assay.....	59
3.7 Cell migration studies.....	59
3.7.1 Scratch closure assay.....	59
3.7.2 Transwell migration assay.....	61
3.7.3 Plate colony formation assay	61
3.7.4 3D tumor spheroid cell migration.....	62
3.7.5 Cytoskeleton staining of spheroids.....	64
3.7.6 3D tumor ring closure assay.....	65
3.7.7 3D tumor ring closure assay by mobile device.....	67
3.8 Apoptosis by flow cytometry.....	68
3.9 Apoptosis determination of spheroids by live dead viability assay.....	70
3.10 Cell cycle analysis and accumulation of Sub-G1 phase.....	72
3.11 <i>In ovo</i> chorioallantoic membrane assay.....	73
3.12 <i>In vivo</i> experiments.....	74
3.12.1 Acute <i>in vivo</i> toxicity	74
3.12.1.1 Body weight and behaviour monitoring.....	74
3.12.1.2 Organ to body ratio.....	75
3.12.1.3 Serum biochemistry analysis.....	76
3.12.1.4 Hemotological evaluation.....	79
3.12.1.5 Erythrocytes aggregation assay.....	80
3.12.1.6 Histopathology of vital organs.....	80
3.12.2 <i>In vivo</i> biodistribution and imaging analysis	82
3.12.3 Freeze tissue GFP distribution analysis	84

Chapter IV: Summary and outlook.....	85
4.1 Summary and outlook	86
4.2 Zusammenfassung und Ausblick	89
Chapter V: Appendix.....	92
5.1 References	93
5.2 Research output	105
5.3 Presentations	106
5.4 Curriculum vitae	107

LIST OF FIGURES

Figure 1. Schematic representation of PAMAM based dendriplex formation.....	4
Figure 2. Schematic illustration of lipodendriplex formation and its cellular internalization.	6
Figure 3. MDR1 gene knockdown mechanism and their contribution to drug induced apoptosis.....	8
Figure 4. Chemical structure of DPPC.....	19
Figure 5. Chemical structure of DOTAP.....	19
Figure 6. Chemical structure of DOPE.....	20
Figure 7. Chemical structure of MPEG5000-DPPE	20
Figure 8. Chemical structure of DPPG.....	21
Figure 9. Chemical structure of cholesterol.....	21
Figure 10. Chemical structure of imatinib mesylate.....	22
Figure 11. Schematic representation of 3D tumor spheroid and 3D tumor ring bioprinting formation by magnetic levitation method.....	33
Figure 12. Gel retardation assay of dendriplexes at various N/P ratios.....	41
Figure 13. Fluorescence quenching assay of dendriplexes at different N/P ratios.....	42
Figure 14. Size and zeta-potential of dendriplexes at different N/P ratios.....	42
Figure 15. pDNA transfection studies of dendriplexes at different N/P ratios in HEK-293 cell line.....	43
Figure 16. Cytotoxicity studies of dendriplexes at different N/P ratios in HEK-293 cell line.	44
Figure 17. Size and zeta potentials of different liposome to PAMAM dendrimer mass ratios of DPPC:CH-PAMAM lipodendriplexes (N/P ratio 12)	45

Figure 18. AFM micrographs with lock in amplitude, height measured and lock in phase view of DPPC:CH (85:15) liposome and DPPC:CH-PAMAM lipodendriplexes (liposome to PAMAM dendrimer mass ratio 0.5; N/P ratio 12)	46
Figure 19. pDNA transfection studies in SKOV-3 cell line with different liposome to PAMAM mass ratios (0.1-1) of DPPC:CH-PAMAM lipodendriplexes (N/P ratio 12)	47
Figure 20. pDNA transfection studies in SKOV-3 cell line of lipodendriplexes of different liposome formulations (liposome to PAMAM dendrimer mass ratio 0.5; N/P ratio 12)	48
Figure 21. Fluorescence micrographs with DAPI, GFP and Merged channels. GFP expression in HEK-293 and SKOV-3 cell lines with optimized dendriplexes and DPPC:CH-PAMAM lipodendriplexes (liposome to PAMAM dendrimer mass ratio 0.5; N/P ratio 12)	49
Figure 22. Cell viability studies in SKOV-3 cell line with different liposome to PAMAM mass ratios (0.1-1) of DPPC:CH-PAMAM lipodendriplexes (N/P ratio 12)	50
Figure 23. Cell viability studies in SKOV-3 cell line of lipodendriplexes of different liposomal formulations (liposome to PAMAM dendrimer mass ratio 0.5; N/P ratio 12)	51
Figure 24. Fluorescence micrograph and relative fluorescence units of intracellular ROS generation in HEK-293 and SKOV-3 cell lines, respectively after the addition of optimized dendriplexes, DPPC:CH-PAMAM lipodendriplexes (liposome to PAMAM dendrimer mass ratio 0.5; N/P ratio 12) and TBHP.....	52
Figure 25. Lysosomal disruption and actin polymerization assay in SKOV-3 cell line of optimized dendriplexes and DPPC:CH-PAMAM lipodendriplexes (liposome to PAMAM dendrimer mass ratio 0.5; N/P ratio 12)	53
Figure 26. DNA damage assay in SKOV-3 cell line of optimized dendriplexes and DPPC:CH-PAMAM lipodendriplexes (liposome to PAMAM dendrimer mass ratio 0.5; N/P ratio 12).....	55

Figure 27. <i>Ex vivo</i> hemolysis assay of pDNA (0.25 µg) containing optimized dendriplexes and DPPC:CH-PAMAM lipodendriplexes (liposome to PAMAM dendrimer mass ratio 0.5; N/P ratio 12)	56
Figure 28. pDNA stability studies of optimized dendriplexes and DPPC:CH-PAMAM lipodendriplexes (liposome to PAMAM dendrimer mass ratio 0.5; N/P ratio 12)	57
Figure 29. Luciferase knockdown efficiency in HeLa LG cell line of optimized dendriplexes and DPPC:CH-PAMAM lipodendriplexes (liposome to PAMAM dendrimer mass ratio 0.5; N/P ratio 12)	57
Figure 30. GFP silencing in HeLa LG cell line of optimized dendriplexes and DPPC:CH-PAMAM lipodendriplexes (liposome to PAMAM dendrimer mass ratio 0.5; N/P ratio 12).....	58
Figure 31. MDR1 silencing in Caco-2 cell line of optimized dendriplexes and DPPC:CH-PAMAM lipodendriplexes (liposome to PAMAM dendrimer mass ratio 0.5; N/P ratio 12)	59
Figure 32. Scratch closure assay in Caco-2 cell line of optimized dendriplexes and DPPC:CH-PAMAM lipodendriplexes (liposome to PAMAM dendrimer mass ratio 0.5; N/P ratio 12) using Ibidi inserts.....	60
Figure 33. Transwell cell migration assay in Caco-2 cell line of optimized dendriplexes and DPPC:CH-PAMAM lipodendriplexes (liposome to PAMAM dendrimer mass ratio 0.5; N/P ratio 12)	61
Figure 34. Colony formation assay in Caco-2 cell line of optimized dendriplexes and DPPC:CH-PAMAM lipodendriplexes (liposome to PAMAM dendrimer mass ratio 0.5; N/P ratio 12).....	62
Figure 35. 3D tumor spheroid cell migration assay in Caco-2 cell line of optimized dendriplexes and DPPC:CH-PAMAM lipodendriplexes (liposome to PAMAM dendrimer mass ratio 0.5; N/P ratio 12)	63

Figure 36. Steps involved in staining and transferring the 3D tumor spheroid on the glass slides.....	64
Figure 37. Cytoskeleton staining of spheroids of Caco-2 cell line of optimized dendriplexes and DPPC:CH-PAMAM lipodendriplexes (liposome to PAMAM dendrimer mass ratio 0.5; N/P ratio 12).....	65
Figure 38. Micrographs of 3D tumor ring closure assay in Caco-2 cell line of optimized dendriplexes and DPPC:CH-PAMAM lipodendriplexes (liposome to PAMAM dendrimer mass ratio 0.5; N/P ratio 12).	66
Figure 39. Graphical representation of 3D tumor ring closure assay in Caco-2 cell line of optimized dendriplexes and DPPC:CH-PAMAM lipodendriplexes (liposome to PAMAM dendrimer mass ratio 0.5; N/P ratio 12) at specified time intervals.....	66
Figure 40. Analysis of 3D tumor ring closure assay by mobile device in Caco-2 cell line of optimized dendriplexes and DPPC:CH-PAMAM lipodendriplexes (liposome to PAMAM dendrimer mass ratio 0.5; N/P ratio 12)	67
Figure 41. Graphical presentation of 3D tumor ring closure assay by mobile device in Caco-2 cell line of optimized dendriplexes and DPPC:CH-PAMAM lipodendriplexes (liposome to PAMAM dendrimer mass ratio 0.5; N/P ratio 12) at specified time intervals.	68
Figure 42. Apoptosis assay (FACS micrographs) in Caco-2 cell line by optimized dendriplexes and DPPC:CH-PAMAM lipodendriplexes (liposome to PAMAM dendrimer mass ratio 0.5; N/P ratio 12) without or with IM (75 μ M) treatment	69
Figure 43. Apoptosis assay (graphical representation) by flow cytometry in Caco-2 cell line by optimized dendriplexes and DPPC:CH-PAMAM lipodendriplexes (liposome to PAMAM dendrimer mass ratio 0.5; N/P ratio 12) without or with IM (75 μ M) treatment	70

Figure 44. Live dead viability assay of spheroids for apoptosis determination by fluorescence microscopy in Caco-2 cell line by optimized dendriplexes and DPPC:CH-PAMAM lipodendriplexes (liposome to PAMAM dendrimer mass ratio 0.5; N/P ratio 12) without or with IM (75 μ M) treatment.....71

Figure 45. Cell cycle analysis (FACS micrographs) by flow cytometry in Caco-2 cell line by optimized dendriplexes and DPPC:CH-PAMAM lipodendriplexes (liposome to PAMAM dendrimer mass ratio 0.5; N/P ratio 12) without or with IM (75 μ M) treatment72

Figure 46. Cell cycle analysis (graphical representation) by flow cytometry in Caco-2 cell line by optimized dendriplexes and DPPC:CH-PAMAM lipodendriplexes (liposome to PAMAM dendrimer mass ratio 0.5; N/P ratio 12) without or with IM (75 μ M) treatment73

Figure 47. Apical view of CAM on the egg development day 11 and CLSM micrographs of GFP expression in CAM (epithelial cells) with optimized dendriplexes and DPPC:CH-PAMAM lipodendriplexes (liposome to PAMAM dendrimer mass ratio 0.5; N/P ratio 12)74

Figure 48. Process of: *i.v.* administration, blood collection by cardiac puncture and sacrifice of mice by cervical dislocation method, respectively and changes in body weight of mice for 7 days in untreated groups and after the administration of the complexes (dendriplexes and DPPC:CH-PAMAM lipodendriplexes; liposome to PAMAM dendrimer mass ratio 0.5 with N/P ratio 12)75

Figure 49. The organ to body index (%) of untreated and treated (dendriplexes and DPPC:CH-PAMAM lipodendriplexes; liposome to PAMAM dendrimer mass ratio 0.5 with N/P ratio 12) groups.....76

Figure 50. Typical liver function tests (LFTs) parameters including ALT, AST and ALP levels of untreated group and after *i.v.* administration of the complexes containing 10 μ g of pDNA (dendriplexes and DPPC:CH-PAMAM lipodendriplexes; liposome to PAMAM dendrimer mass ratio 0.5 with N/P ratio 12)77

Figure 51. Typical serum biochemical parameters including blood glucose, total bilirubin and total protein parameters of untreated group and after *i.v.* administration of the complexes containing 10 µg of pDNA (dendriplexes and DPPC:CH-PAMAM lipodendriplexes; liposome to PAMAM dendrimer mass ratio 0.5 with N/P ratio 12)78

Figure 52. Typical renal function tests (RFTs) parameters including blood urea nitrogen and creatinine levels of untreated group and after *i.v.* administration of the complexes containing 10 µg of pDNA (dendriplexes and DPPC:CH-PAMAM lipodendriplexes; liposome to PAMAM dendrimer mass ratio 0.5 with N/P ratio 12)78

Figure 53. *Ex vivo* erythrocytes aggregation assay after treatment of complexes (dendriplexes and DPPC:CH-PAMAM lipodendriplexes; liposome to PAMAM dendrimer mass ratio 0.5 with N/P ratio 12) with erythrocytes suspension and compared to untreated cells.....80

Figure 54. Histopathology studies: H & E stained sections of vital organs from mice (heart, lungs, liver and kidney) of untreated group and after *i.v.* administration of the complexes containing 10 µg of pDNA (dendriplexes and DPPC:CH-PAMAM lipodendriplexes; liposome to PAMAM dendrimer mass ratio 0.5 with N/P ratio 12)81

Figure 55. *Ex vivo* fluorescence images and quantitative biodistribution (fluorescence intensity a.u) of pCMV-GFP labeled DNA complexes in vital organs after *i.v.* administration of the complexes containing 10 µg of pCMV-GFP (dendriplexes and lipodendriplexes of DPPC:CH-PAMAM; liposome to PAMAM dendrimer mass ratio 0.5 with N/P ratio 12).83

Figure 56. *Ex vivo* fluorescence imaging in the frozen thin section of dissected vital organs (heart, lungs, liver, kidneys and spleen) after *i.v.* administration of the complexes containing 10 µg of pCMV-GFP (dendriplexes and DPPC:CH-PAMAM lipodendriplexes liposome to PAMAM dendrimer mass ratio 0.5 with N/P ratio 12)84

LIST OF TABLES

Table 1. Size and zeta potential (mean \pm S.D) of different liposomal formulations	44
Table 2. Hematological parameters of mice in untreated and treated (dendriplexes, lipodendriplexes of DPPC:CH-PAMAM; liposome to PAMAM dendrimer mass ratio 0.5; N/P ratio 12) groups (mean \pm S.D)	79

LIST OF ABBREVIATIONS

AFM	Atomic force microscopy
AIDS	Acquired immunodeficiency syndrome
ALP	Alkaline phosphatase
ALT	Alanine aminotransferase
AST	Aspartate aminotransferase
ATCC	American Type Culture Collection
BSA	Bovine serum albumin
Ca ²⁺	Calcium
Caco-2	Homo sapiens colorectal adenocarcinoma cell line
CAM	Chorioallantoic membrane model
CCLR	Cell culture lysis reagent
CH	Cholesterol
CML	Chronic myeloid leukemia
DAPI	4',6-diamidino-2-phenylindole
DCF	Dichlorofluorescein
DLS	Dynamic light scattering
DMEM	Dulbecco's modified Eagle's minimum essential medium
DMSO	Dimethyl sulfoxide
DOPE	1,2-dioleoyl-sn-glycero-3-phosphoethanolamine
DOTAP	1,2-dioleoyloxy-3-trimethylammonium propane
DP	Dendriplexes
DPPC	1,2-dipalmitoylphosphatidylcholine
DPPG	1,2-dipalmitoylphosphatidylglycerol
EDD	Egg development day
FACS	Fluorescence activated cell sorting
FBS	Fetal bovine serum
FDA	Food and Drug Administration
GFP	Green fluorescent protein
GIST	Gastrointestinal stromal tumors
H & E	Hematoxylin and Eosin
H ₂ DCFDA	2,7-dichlorofluorescein diacetate
Hb	Hemoglobin
XIV	

HBG buffer	20 mM HEPES buffer (pH 7.4) containing 5% glucose
HCT	Hematocrit
HEK-293	Human embryonic kidney cell line
HeLa LG	HeLa co-expressing firefly luciferase and GFP under CMV promoter cell line
HEPES	4-(2-hydroxyethyl)-1-piperazineethanesulfonic acid
IM	Imatinib mesylate
IMDM	Iscove's modified Dulbecco's medium
LDA	Laser Doppler anemometry
LDH	Lactate dehydrogenase
LDP	Lipodendriplexes
LFTs	Liver function tests
LMA	Low melting agarose
LMP	Lysosomal membrane permeabilization
MCH	Mean corpuscular haemoglobin
MCHC	Mean corpuscular hemoglobin concentration
MCV	Mean corpuscular volume
MDR	Multidrug resistance
Mg ²⁺	Magnesium
MPEG5000-DPPE	N-(methoxypolyethylene glycol 5000 carbamoyl)-1,2-dipalmitoyl-sn-glycero-3-phosphatidylethanolamine
MPV	Mean platelet volume
MTT	3-(4,5-dimethylthiazolyl-2)-2,5-diphenyltetrazolium Bromide
N/P ratios	Nitrogen to Phosphate ratio
NEA	Non-essential amino acids
NMA	Normal melting agarose
PAMAM	Polyamidoamine
PBS	Phosphate buffer
pCMV-GFP	Plasmid CMV promoter encoding green fluorescence protein
pCMV-luc	Plasmid CMV promoter encoding firefly luciferase
PDI	Polydispersity index
pDNA	Plasmid DNA
XV	

PEI	Polyethylenimine
P-gp	P-glycoproteins
PI	Propidium iodide
PLGA	Poly (DL-lactide-co-glycolide acid)
PLT	Platelets
RBCs	Red blood cells
RFTs	Renal functions tests
RISC	RNA induced silencing complex
RLU	Relative luminescence units
ROS	Reactive oxygen species
S.D	Standard deviation
si-Control	Scrambled siRNA
siRNA	Small interfering RNA
SKOV-3	Human ovarian adenocarcinoma cell line
WBCs	White blood cells
X-linked SCID	X-linked severe combined immune deficiency

Chapter I: Introduction

Chapter I: Introduction

1. Introduction

1.1 Gene therapy

Gene therapy is a promising strategy to use the genes as a therapeutic agent. It has been effectively used against various acquired and inherited diseases including cancer, acquired immunodeficiency syndrome (AIDS), cardiovascular diseases, infectious diseases, cystic fibrosis and X-linked severe combined immune deficiency (X-linked SCID).

Gene therapy can be categorized into somatic and germline gene therapy. In the case of somatic gene therapy, the modifications in the genes are not being the part of the next generation while germline therapy sustains the changes in the upcoming lot [1].

Theoretically, the gene therapy can be done by either replacing the defected gene, with a healthy copy of the gene or by completing the missing part of the gene to get the desired protein expression. However, there are several obstacles that have to be passed by therapeutic genes to reach their targeted sites.

Direct administration of free nucleic acids into the tumors or intravenous delivery can be used for efficient delivery of therapeutic gene but the insufficiency to cross the cell membrane and the intracellular enzymatic degradation limit their application [2]. Thus, the main objective of gene therapy is to develop an efficient and non-toxic carrier system that can protect the cargo from enzymatic degradation and help them to pass through the plasma membrane to their site of action [3-5].

1.2 Viral vectors

For *in vivo* gene delivery, viruses represented the first and most efficient vector system for the transfer of genetic information to the cells. For this reason, a lot of attempts has been already made to design engineered viral vectors (lentiviruses, retroviruses, adenoviruses) to transfer therapeutic genes into the diseased cells [6]. Hence, by getting the benefit from viral life cycle, one can achieve a higher gene transfection efficiency [5] but on the other hand, such system can provoke a strong immune response inside the host cellular system. Therefore, due to the safety concerns, high cost and limitations in the sequences of the inserted gene restricted its application in a biological system and urged to the development of a safe and cheap alternative [7-9].

1.3 Non-viral vectors

Gene therapy with non-viral vectors was considered clinically unfeasible during the early stages of their development due to their poor efficiency to deliver the cargo in comparison to viral vector systems. However, in recent years, the continuous efforts of the researcher and the advancement of the techniques have brought these vectors to clinical studies.

Non-viral vectors have several advantages over viral vectors in term of safety, non-immunogenicity, cost-effectiveness and customized functionality. Various physical methods have been devised to deliver the naked gene (such as plasmid DNA) to the targeted sites including direct injection, electroporation, gene gun and ultrasound triggered gene delivery [10]. On the other hand, the gene delivery by chemical methods involves the condensation of the naked gene with other carriers such as cationic liposomes, [11] polycationic polymers, [12] aptamers, [13] conjugates, [14] nanoparticles [15, 16] and by hybrid vector systems [17, 18].

1.3.1 Plasmid based non-viral vectors

Plasmid based non-viral vectors have some advantages over the viral vectors in terms of safety, ease of construction for large therapeutic genes and cost-effectiveness. However, the larger size and rapid enzymatic degradation can limit its cellular uptake and may result in lower gene expression [17, 19]. Therefore, a protective shielding of the plasmids can be accomplished by a stable complex formation with a positively charged non-viral vector system [20]. These stable complexes can thus efficiently cross the cell membrane and release the cargo for the desired therapeutic effects [2].

1.3.2 Polymer based gene delivery

Among the polymers used for gene delivery research, cationic polymers are gaining more attention due to their ability to condense large nucleic acid molecule (polyplexes) and mask their negative charge to facilitate their cellular uptake [21]. Cationic polymers having the different chemistry of linear, branched or dendritic structure, can make a complex with nucleic acid by their primary, tertiary or quaternary amine groups. Therefore, the flexibility, monodispersity, reproducibility and facile manufacturing of cationic polymers make them a potential candidate for gene therapy [22]. Different polyamine polymers including polylysine and its conjugates [23], polyethylenimines [24, 25] and dendrimers [26-28] have been explored

Chapter I: Introduction

due to their ability to form stable complex with nucleic acid via electrostatic interaction between the negatively charged phosphate groups of nucleic acid and terminal amino groups of the cationic polymers [29].

Among the synthetic cationic polymers, poly(amidoamine) (PAMAM) dendrimer and polyethylenimine (PEI) are “off-the-shelf polymers” and most extensively used for efficient gene delivery [30]. PAMAM dendrimers, with ethylenediamine core is a safe, non-immunogenic, well-characterized cationic system and has used for efficient therapeutic gene delivery [31, 32]. Contrary to PEI, which is a non-degradable polymer (with vinyl bonds in its backbone), PAMAM is a biodegradable polymer (with peptide bonds in its backbone) and is less cytotoxic than PEI [33, 34]. The primary amine groups of the PAMAM mostly participate in the interaction with the nucleic acid to make a stable nano-complex (dendriplexes) (Fig. 1), for subsequent transfection of the complexes into the cells while the tertiary amino groups act as a proton sponge in the endosomal environment and facilitate the release of cargo in the cytoplasm [35-38]. However, due to their polycationic nature, they may exhibit some cytotoxicity. They can also interact with oppositely charged macromolecules in plasma (like heparin) to prematurely displacement of the nucleic acid from the complex [39], leading to their enzymatic degradation and lower gene expression [14].

Some researchers have reported the unusual biodistribution of higher generation PAMAMs including high hepatic or renal clearance and short plasma circulation time [40]. They also proposed that the autophagy caused by PAMAM can be responsible for hepatocellular toxicity [41, 42], but the exact mechanism of PAMAM dendrimers induced hepatotoxicity is still unclear. On the other hand, PAMAM can also initiate the blood clot formation by disrupting the key platelet functions [43].

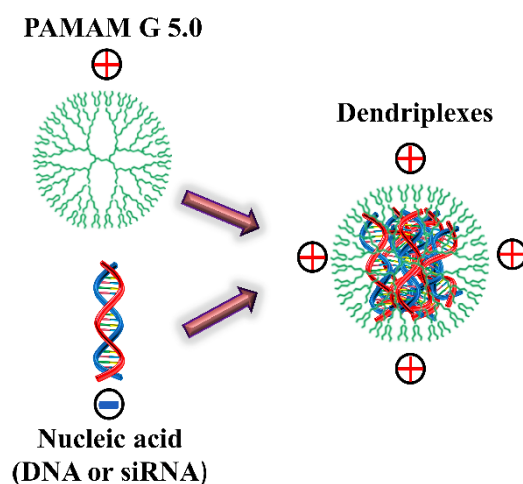


Figure 1. Schematic representation of PAMAM based dendriplex formation.

Chapter I: Introduction

Many strategies have been proposed to mask the terminal amino groups inherit toxicity of PAMAM by modifying their physicochemical properties to make them suitable for the systemic application [44-46]. To shield the cationic polymeric system, the most promising approach is the lipid modification. A non-covalent interaction of dendriplexes with the lipid membrane has been proposed as a useful tool to overcome the demerits associated with this polymeric system.

1.3.3 Liposomes based gene delivery

Liposomal formulations are well known to deliver a variety of drugs and genetic materials to the intracellular system [47-49]. A cationic lipid comprised of a hydrophobic part, containing aliphatic chains, a cationic hydrophilic head and a linker group that combines hydrophobic part with the head and played an important role in maintaining lipid's integrity [5]. Cationic lipids have been extensively used as non-viral gene vectors. They can condense large nucleic acid molecule to form stable complexes (lipoplexes) and subsequently promote transfection efficiency [9]. However, the *in vivo* use of cationic lipoplexes is hampered due to the presence of high positive charge and may lead to cytotoxicity. This may also induce some cellular changes even at the chromosomal level, like reduction in mitotic cycle number and increased vacuole formation in the cell cytoplasm [7, 49].

While neutrally or negatively charged liposomes are supposed to overcome the cytotoxicity, serum instability or rapid clearance by the reticular endothelial system which are the major hurdles for the cationic gene delivery vectors [50]. On the contrary, negative electrostatic charge repulsion of anionic liposome with the nucleic acid may also lead to poor entrapment of genetic material [51].

1.3.4 Lipodendriplexes

To overcome the associated drawbacks of these two individual systems (polymeric complexes or liposome), a new non-viral vector system was developed by hybridization the liposome with the dendriplexes to get the benefits of both moieties [52]. The hybrid of these two systems (lipodendriplexes) can thus improve their individual demerits by reducing the associated side effects with enhanced gene delivery. Lipodendriplexes are novel vesicular, spherical, supramolecular complexes, in which PAMAM-nucleic acid complexes (dendriplexes) core has encapsulated within a lipid shell by a non-covalent interaction [39, 51, 53, 54]. The inner lipid layer may confer the biocompatibility of naked dendriplexes and also decrease chances to

Chapter I: Introduction

degrade in an outer environment. The outer lipid layer provides steric stabilization and assists in the attachment to the cellular site [55]. Such triblock non-viral vectors exhibit dual interactions viz. the nucleic acid (dendriplexes formation) and also with the negatively charged surface of the cell membrane to facilitate its cellular internalization (Fig. 2) [54, 56]. By doing so, this robust platform exhibited negligible hemolytic toxicity, higher transfection efficiency with better *in vivo* tolerance, as compared to the naked dendrimeric system [57].

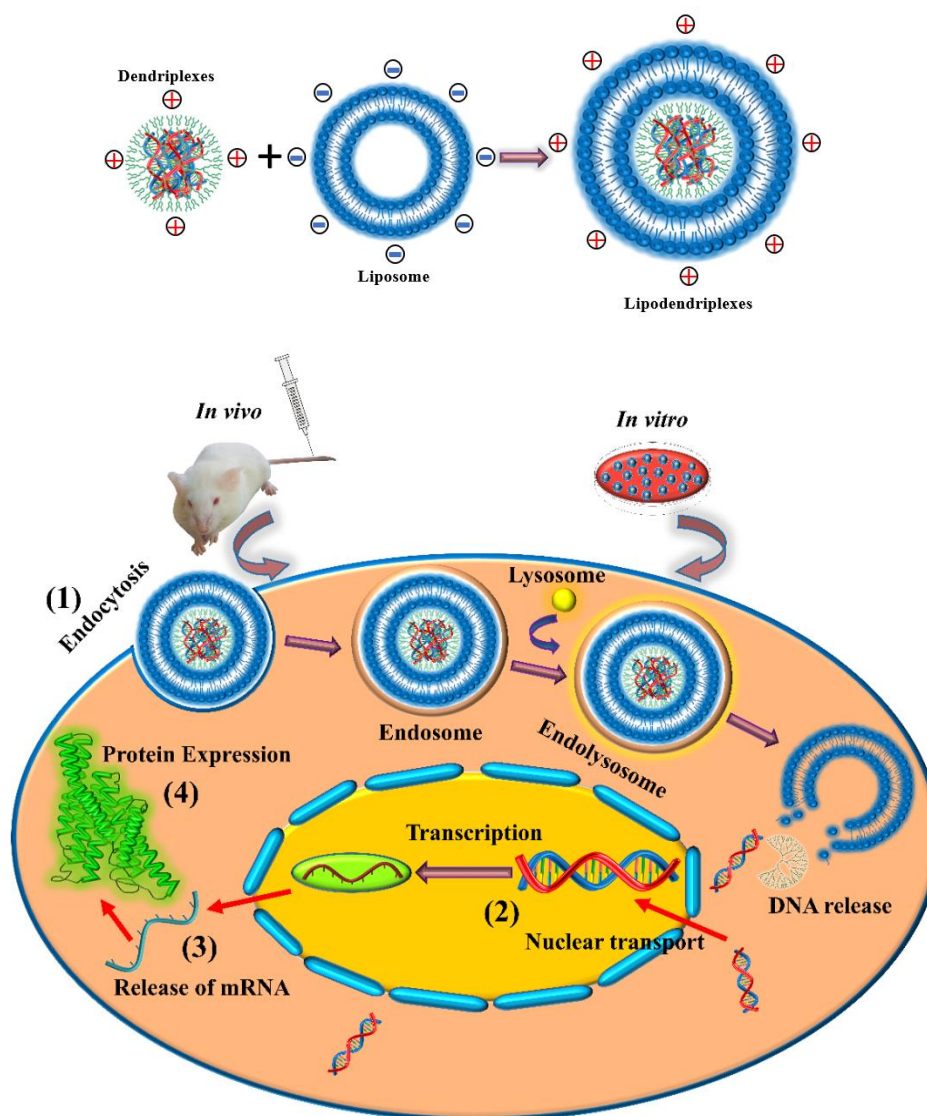


Figure 2. Schematic diagram of lipodendriplex formation and its cellular internalization. (1) Endocytosis of lipodendriplex and release of nucleic acid into the cytoplasm. (2) Gene encoded DNA is transcribed into mRNA. (3) Export of mRNA from the nucleus to cytoplasm. (4) Required protein expression.

1.4. Multidrug resistance and RNA interference

Multidrug resistance (MDR) is a phenomenon to develop a cross-resistance in tumor cells accompanied by a decreased or altered intracellular accumulation of chemotherapeutic drugs. In many cases, MDR of chemotherapeutic drugs is highly associated with the overexpression of P-glycoproteins (P-gp), encoded by the MDR1 gene. The P-gp are overexpressed on the plasma membrane of the cancerous cells, where it can trigger the ATP driven efflux of most of the anti-tumor drugs, lead to a reduced accumulation of the drug in the targeted tumor cells and failure of the chemotherapy [58, 59]. However, in some other case, amplification of BCR-ABL gene can also play a role in the development of MDR [60].

P-gp associated MDR can be tackled by the use of many P-gp inhibitors [61] or substrates [62], however, the side effects, off-targeting to tissues and interaction with many chemotherapeutic drugs limit their use for clinical purpose. Therefore, a safe alternative tool to downregulate the expression of P-gp, by silencing the MDR1 gene, can be a double-stranded small interfering RNA (siRNA) [63].

P-gp is also present in the normal healthy tissue of the body and have a crucial role to perform different vital functions. Therefore, in order to avoid off-targeting to normal cells, the si-MDR1 needs to be carefully designed to only downregulate the tumor associated P-gp [64, 65].

Imatinib mesylate (IM), a BCR-ABL tyrosine kinase inhibitor [66] has been approved by FDA in the treatment of chronic myeloid leukemia (CML) [67]. Recently, it has also been investigated against other tumors like gastrointestinal stromal tumors (GIST) [68] and colon carcinoma [69]. Imatinib mesylate is also a substrate of P-gp, therefore the overexpression of P-gp and deregulation of BCR-ABL in a cell line can elicit resistance against IM [60, 70]. However, a sequential treatment to deliver si-MDR1 (MDR modulation) and imatinib mesylate (apoptotic inducer) can be a promising strategy against MDR cancer therapy [29, 71, 72]. Downregulation of P-gp by si-MDR1 can re-sensitize the tumor resistant cell and contributes to apoptotic induction of IM by increasing its intracellular accumulation (Fig. 3) [73, 74].

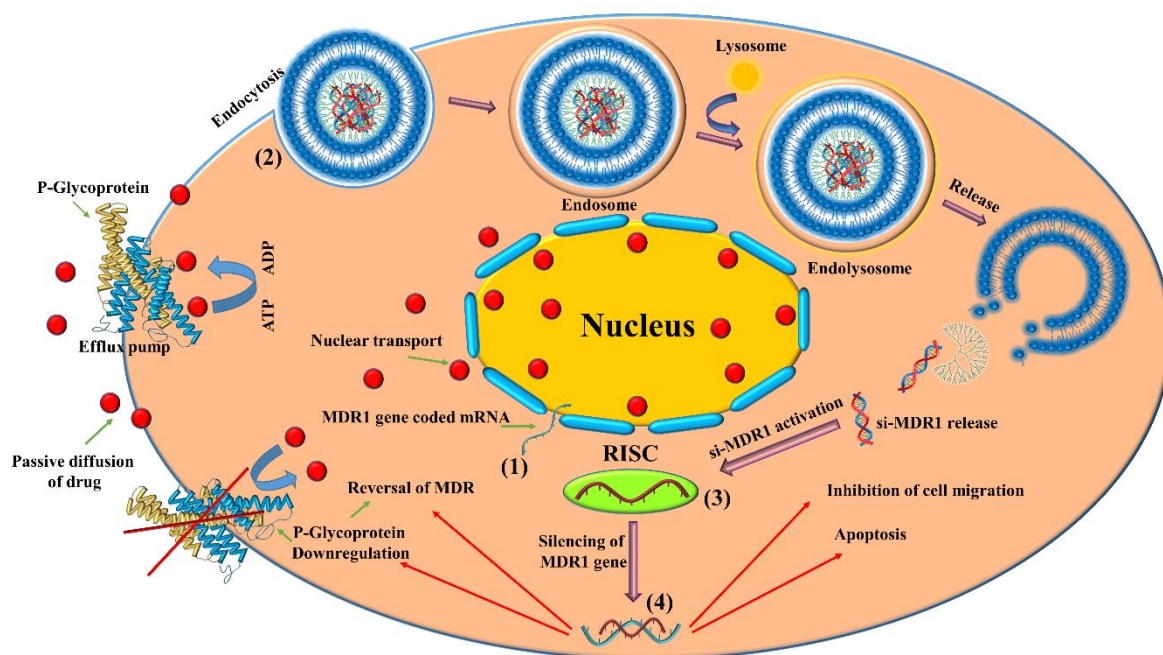


Figure 3. MDR1 gene knockdown contribution to tyrosine kinase inhibitor (imatinib mesylate) induced apoptosis: (1) Generation of MDR1 gene carrier mRNA. (2) Endocytosis of si-MDR1 complexes and release of si-MDR1 into the cytoplasm. (3) Formation of RNA induced silencing complex (RISC). (4) Selective silencing of MDR1 gene after binding with complementary mRNAs followed by P-gp downregulation leading to reversal of MDR by increasing the intracellular accumulation of IM and subsequent apoptosis [75].

1.5 Aims and objectives

The aim of the study was to establish an optimized lipodendriplexes system, using a broad range of lipid combination with polymeric system, to get the full benefit of liposome (enhanced cellular uptake and low toxicity) and PAMAM dendrimer (optimum nucleic acid complexation, facilitated endosomal release) for enhanced gene delivery with minimal toxicity profile. The formulations were characterized using dynamic light scattering, laser Doppler anemometry and atomic force microscopy. *In vitro* studies were performed to establish the transfection efficiency using luciferase and GFP expression assays. MTT, ROS, lysosomal disruption, DNA damage and hemocompatibility studies were performed to investigate the biocompatibility of the formulations.

Chapter I: Introduction

After establishing a safe and efficient nano carrier system, the next step was to investigate the efficacy of the complexes for RNA interference to silence the MDR1 gene using Caco-2 cell line (having overexpression of P-gp). By using our optimized system, we were expecting to (i) increased intracellular uptake of si-MDR by endocytosis mechanism, (ii) downregulation of P-gp expression after knockdown of MDR1 gene (iii) inhibition in MDR1 regulated cell migration (iv) reversal of MDR and (v) subsequently enhanced apoptosis. Therefore, a sequential therapy was planned, involving an efficient delivery of si-MDR1 to knockdown the MDR1 gene (responsible for the drug efflux mechanism) followed by the delivery of a tyrosine kinase inhibitor (IM), to investigate the contribution of MDR1 gene silencing for enhanced intracellular accumulation of drug.

After investigating the gene silencing effects in 2D culture, a similar analysis was planned in 3D cell culture that portrays an *in vivo* like situation, using tumor spheroid and ring bioprinting model, to further establish the efficacy of the optimized complexes.

After establishing the *in vitro* safety profile of the optimized complexes, the next strategy was to evaluate them in preclinical environment. However, in order to reduce the exposure of complexes on the animal models, *in ovo* studies were first carried out to study the behaviour of formulations in CAM model.

Afterward, the efficient and safe non-viral vectors were tested in animal models. The comprehensive biodistribution and acute toxicity profile of optimized complexes were studied *in vivo* using female BALB/c mice. The *in vitro* and *in ovo* profile was then correlated with *in vivo* results to get the full benefit of optimized lipid triblock nanocarrier system.

Chapter II: Materials and Methods

Chapter II: Materials and Methods

2.1 Materials

List of materials

Materials and Instruments

Sources

A

AFM Probe; NSC14/AI BS

Micromasch, Tallinn, Estonia

Ampicillin

Sigma Aldrich Chemie GmbH, Taufkirchen,
Germany

Anti-luc siRNA

GE Dharmacon, Lafayette, USA

Atomic force microscope; Nanowizard® 3

JPK Instruments AG, Berlin, Germany

Autoclave, Tuttinauer 3850 ELC

Tuttinauer GmbH, Linden, Germany

B

Bath sonicator; Transonic Digital S

Elmasonic P30H Schmidbauer GmbH,
Singen, Germany

Beetle luciferin

Synchem UG & Co. KG, Felsberg, Germany

C

Caco-2 cell line

A kind gift from Institute for Lung Research,
University of Marburg, Germany

Cell counter R1

Olympus Corporation, Tokyo, Japan

Cell counting slides R1-SLI

Olympus Corporation, Tokyo, Japan

Cell Culture Lysis Reagent

Promega GmbH, Mannheim, Germany

Centrifugation machine II

Centurion Scientific, Chichester, UK

Cholesterol

Sigma Aldrich Chemie GmbH, Taufkirchen,
Germany

CO₂ incubator, HeraCell

Heraus GmbH & Co. KG, Hanau, Germany

Confocal laser scanning microscope;

Carl Zeiss Microscopy GmbH, Jena, Germany

LSM 700

Constant power supply LKB 2197

LKB Bromma, Bromma, Sweden

Chapter II: Materials and Methods

D

DAPI	Sigma Aldrich Chemie GmbH, Taufkirchen, Germany
Disposable folded capillary cell; DTS1060	Malvern Instruments Ltd, Malvern, UK
DMEM	Capricorn Scientific, Ebsdorfergrund, Germany
DMSO; $\geq 99\%$	Carl Roth GmbH & Co. KG, Karlsruhe, Germany
DOPE, DOTAP, DPPC and DPPG	Gift samples from Lipoid AG, Steinhausen, Switzerland.

E

Ethanol	Carl Roth GmbH & Co. KG, Karlsruhe, Germany
Extruder; Avanti Mini	Avanti Polar Lipids Inc., Alabaster, USA

F

Female BALB/c, mice	National Institute of Health, Islamabad, Pakistan
Fetal bovine serum	Capricorn Scientific, Ebsdorfergrund, Germany
Fertilized eggs	Mastkükenbrüterei Brommann, Rheda- Wiedenbruck, Germany
Formaldehyde	Carl Roth GmbH & Co. KG, Karlsruhe, Germany
Fluorescence microscope I CKX-53	Olympus Corporation, Pennsylvania, USA
Fluorescence microscope II	EVOS FL cell imaging system, Thermo Scientific, San Diego, CA, USA

G

Gene JET Plasmid Miniprep kit	Thermo Fischer Scientific, Dreieich, Germany
Guava [®] easyCyte [™]	Millipore Sigma, USA

H

H ₂ DCFDA	Sigma Aldrich Chemie GmbH, Taufkirchen, Germany
----------------------	--

Chapter II: Materials and Methods

Hatching incubator; Ehret KMB 6	Dipl. Ing. W. Ehret GmbH, Emmendingen, Germany
HEK-293 cell line	ATCC®, Manassas, USA
HeLa LG cell line	GenTarget Inc., San Diego, USA
Hematology analyser	Icon-3, Norma Instruments, Budapest, Hungary
Heparin sodium salt	Thermo Fischer Scientific, Dreieich, Germany
HEPES	Sigma Aldrich Chemie GmbH, Taufkirchen, Germany
High Capacity cDNA Reverse Transcription Kit	Thermo Fischer Scientific, Dreieich, Germany
I	
IMDM	Capricorn Scientific, Ebsdorfergrund, Germany
J	
Jet prime® transfection reagent	Polyplus, Illkirch, France
K	
Kanamycin	Sigma Aldrich Chemie GmbH, Taufkirchen, Germany
L	
Laminar Flow Hood; Labogene	LMS GmbH & Co. KG, Brigachtal, Germany
Liquid CO ₂	Praxair Deutschland GmbH, Düsseldorf, Germany
Live / Dead assay staining kit	Invitrogen™, Oregon, USA
Low melting agarose	Carl Roth GmbH & Co. KG, Karlsruhe, Germany
Luminometer; FLUOstar® Optima	BMG Labtech, Ortenberg, Germany
Lyso® tracker red DND-99	Thermo Fischer Scientific, Dreieich, Germany

Chapter II: Materials and Methods

M

Magnetic Stirrer; MCS 66	CAT Scientific, Paso Robles, USA
Megafuge 1.0 R	Thermo Fischer Scientific, Dreieich, Germany
Mounting medium; FluorSave™	Calbiochem Corporation, San Diego, USA
MTT dye	Sigma Aldrich Chemie GmbH, Taufkirchen, Germany
Microscopy Slides	Carl Roth GmbH & Co. KG, Karlsruhe, Germany
Micro-Dish with inserts	Ibidi, Martius, Germany
MPEG5000-DPPE	A gift sample from Lipoid AG, Steinhausen, Switzerland
Magpen	Greiner Bio-One GmbH, Frickenhausen, Germany

N

Nano-100 Micro-Spectrophotometer	Hangzhou Allsheng Instruments Co., Ltd, Hangzhou, China
Nano3D Biosciences NanoShuttle™-PL	Greiner Bio-One GmbH, Frickenhausen, Germany
Normal Melting Agarose	Carl Roth GmbH & Co. KG, Karlsruhe, Germany

P

PAMAM dendrimer, ethylenediamine core, generation 5.0 solution	Sigma Aldrich Chemie GmbH, Taufkirchen, Germany
pCMV-luc	Plasmid Factory GmbH & Co. KG, Bielefeld, Germany
pCMV-GFP	Plasmid Factory GmbH & Co. KG, Bielefeld, Germany
Petri Dishes; Tissue Culture grade	Sarstedt AG & Co., Nümbrecht, Germany
Phalloidin FITC	Sigma Aldrich Chemie GmbH, Taufkirchen, Germany
Pierce BCA assay kit	Thermo Fischer Scientific, Dreieich, Germany

Chapter II: Materials and Methods

Pneumatic egg puncher

Schuett Biotech, GmbH, Göttingen, Germany

Polycarbonate membranes

Whatman™ plc, Buckinghamshire, UK

PowerUp™ SYBR® Green

Thermo Fischer Scientific, Dreieich, Germany

Master Mix

PURELAB flex II dispenser

ELGA LabWater, High Wycombe, UK

Q

QuantStudio® 3 RT-PCR System

Applied Biosystems, Foster City, CA, USA

R

RNase free water

GE Dharmacon, Lafayette, USA

RNA dilution buffer

GE Dharmacon, Lafayette, USA

RNeasy mini kit

Qiagen, Hilden, Germany

Rotary Evaporator; Laborota efficient

Heidolph Instruments GmbH & Co. KG,

4000

Schwabach, Germany

S

Scrambled siRNA I

GE Dharmacon, Lafayette, USA

Scrambled siRNA II

Eurogentec, Seraing, Belgium

Serum biochemical marker analyser

Micro lab 300, Merck, Germany

Shaking Incubator; IKA KS4000 IC

IKA Werke & Co. KG, Staufen, Germany

si-GFP

GE Dharmacon, Lafayette, USA

si-MDR1

Eurogentec, Seraing, Belgium

SKOV-3 cell cline

ATCC®, Manassas, USA

Stereomicroscope

Stemi 2000-C, Carl Zeiss GmbH, Germany

SYBR® Safe DNA gel stain

Thermo Fischer Scientific, Dreieich, Germany

T

Thermo Hybaid Electro 4 gel system

Thermo Electron Corporation, Ulm, Germany

Trans-Illuminator; BioDoc Analyse Ti5

Whatman™ Biometra GmbH, Göttingen,
Germany

Chapter II: Materials and Methods

Transwell chamber, 8µm pore size,
polyester membrane (PET)

Corning, New York, USA

Tris

Merck KGaA, Darmstadt, Germany

Triton™ X-100

Sigma Aldrich Chemie GmbH, Taufkirchen,
Germany

U

UVP iBox® Explorer2™

Analytik Jena US LLC, Jena, Germany

V

Vacuum Pump; SC 920

KNF Neuberger GmbH, Freiburg, Germany

W

Water Bath

Kottermann GmbH & Co. KG, Hänigsen,
Germany

White opaque 96-well plates

Brand GmbH & Co. KG, Wertheim, Germany

Z

Zetasizer Nano ZS

Malvern Instruments Ltd, Malvern, UK

Others

0.2 µm PES syringe filters

Sarstedt AG & Co. KG, Nümbrecht, Germany

15 mm cover slips

Gerhard Menzel B.V. & Co. KG, Braunschweig,
Germany

6-well plates; TC Standard. F

Sarstedt AG & Co. KG, Nümbrecht, Germany

6-well ultra-low attachment plates

Greiner Bio-One GmbH, Frickenhausen,
Germany

12-well plates; Nunclon Delta

Nunc GmbH & Co. KG, Wiesbaden, Germany

24-well plates, TC Standard. F

Nunc GmbH & Co. KG, Wiesbaden, Germany

96-well microtiter plates, Nunclon Delta

Thermo Fischer Scientific, Dreieich, Germany

96-well ultra-low attachment plates

Greiner Bio-One GmbH, Frickenhausen,
Germany

Chapter II: Materials and Methods

2.1.1 Polymer

2.1.1.1 Polyamidoamine (PAMAM)

Dendrimers are highly branched molecular entities of a specific size, shape and functionality. They are synthesized by a repetitive sequential reaction, radiating from a central core, to generate a monodisperse polymeric system. These macromolecules comprise of three structural components including a central core, interior branches and exterior branches possessing surface groups [76].

PAMAM dendrimers are the first well-characterized dendrimeric system. These dendrimers consist of an ethylenediamine core with a repeating amidoamine branching system which upon controlled addition of monomer units can give rise to different generations of PAMAM [77, 78].

In this work, we have used PAMAM dendrimer of generation 5.0 solution (5 weight % in methanol) with a molecular weight of 28,824.81 g/mol. They are polycationic in nature due to the presence of 128 terminal amino groups. At neutral pH, all the terminal primary amino groups are protonated to react with negatively charged nucleic acids. A stock solution of 1 mg/ml was prepared in purified water and its pH was adjusted to 7.4 with 0.1 N HCl. The solution was sterilized using a 0.2 μm syringe filter (WhatmanTM) and aliquots were stored at -20 °C till further use.

2.1.2 Nucleic acids

2.1.2.1 Plasmid DNA

2.1.2.1.1 pCMV-luc

Luciferase encoding pCMV-luc (6233 base pairs) was obtained from Plasmid Factory (Bielefeld, Germany). pCMV-luc was amplified in *Escherichia coli* (DH5 α strain) using ampicillin resistant antibiotic and purified using a Gene JET Plasmid Miniprep kit, according to the manufacturer's protocol. The concentration and purity of nucleic acids were determined by $A_{260/280}$ using Nano-100 (Allsheng, China). The Integrity of plasmids was confirmed by 0.9% agarose gel electrophoresis and was stored at -20 °C for further experiments.

Chapter II: Materials and Methods

2.1.2.1.2 pCMV-GFP

Green fluorescence protein encoding pCMV-GFP plasmids (3487 base pairs) was obtained from Plasmid Factory (Bielefeld, Germany). Isolation and amplification of pCMV-GFP were similar to pCMV-luc, except the difference in antibiotic used i.e. kanamycin.

2.1.2.2 Oligonucleotides

siRNA duplexes against MDR1 gene (si-MDR1) (sense 5'-GAUGAUGUCUCCAAGAUU AdTdT-3'; sense 5'-GUCACUGCCUAAUAAAUAUdTdT-3'; sense 5'-GAUCGCUACUGA AGCAAUAdTdT-3'), a non-specific scrambled siRNA with no gene silencing effects on mouse, rat and human genes and gene-specific primers (forward 5'-TTCAGGTGGCTCTGGATAAG-3' and reverse 5'-TCAGCATTACGAACTGTAGACA-3') were purchased from Eurogentec (Seraing, Belgium). While the siRNA duplexes against the green fluorescent protein (sense 5'-GACGUAAACGGCCACAAGUUC-3') and firefly luciferase gene (sense 5'-GCCAUUCUAUCCUCUAGAGGAUG-3') were obtained from Dharmacon (Lafayette, USA).

2.1.3 Lipids

2.1.3.1 DPPC

DPPC (1,2-dipalmitoyl-sn-glycero-3-phosphocholine) is a saturated phospholipid which is composed of phosphatidylcholine head-group having two palmitic acid groups with a molecular weight of 734.039 g/mol. The presence of negatively charged phosphate groups and positively charged quaternary ammonium groups make its zwitterion chemistry. Fully hydrated DPPC phospholipid bilayers undergo four distinct phases including sub-gel, gel, ripple and fluid [79]. At 41 °C lipid bilayers of DPPC get a phase transition from a gel state to fluidic state. In our work, we used DPPC lipid (a gift sample from Lipoid AG, Steinhausen, Switzerland) with a purity of more than 99%. A stock solution of 10 mg/ml was prepared by dissolving the lipid contents in chloroform: methanol solution (2:1; v/v) and stored at -20 °C till further use.

Chapter II: Materials and Methods

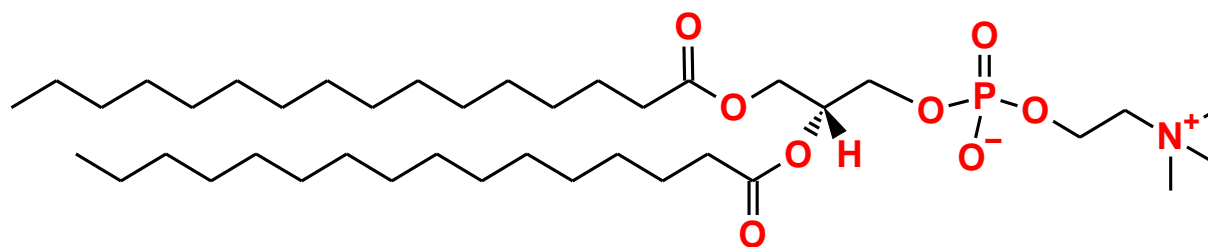


Figure 4. Chemical structure of DPPC.

2.1.3.2 DOTAP

DOTAP (1,2-dioleoyloxy-3-trimethylammonium propane) is an unsaturated lipid consists of a quaternary amine head group with two oleoyl chains to make its backbone, with a molecular weight of 698.542 g/mol. Due to its cationic nature, it can be used as a promising carrier for an efficient stable transfection of the nucleic acids (including DNA, RNA and other oligonucleotides) into the mammalian cells. However, strong affinity with the nucleic acid may hamper the release of cargo from the cationic carrier. Therefore, DOTAP is mostly used with the aid of helper lipids (i.e. DOPE) for effective gene delivery [80]. In our work, we used DOTAP lipid (a gift sample from Lipoid AG, Steinhausen, Switzerland) with a purity of more than 99%. A stock solution of 10 mg/ml was prepared by dissolving the lipid contents in chloroform: methanol solution (2:1; v/v) and stored at -20 °C till further use.

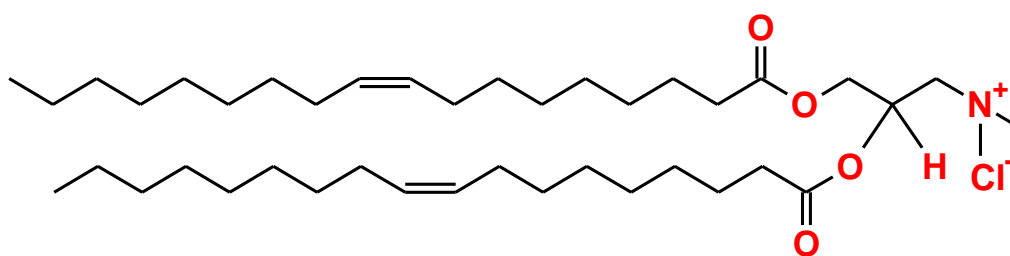


Figure 5. Chemical structure of DOTAP.

2.1.3.3 DOPE

DOPE (1,2-dioleoyl-*sn*-glycero-3-phosphoethanolamine) is a neutral unsaturated phospholipid having a transition temperature of -16 °C with molecular weight of 744.034 g/mol. It has been mostly used as co-lipid or helper lipid with other lipid combinations [81]. It can exhibit structural transitions upon a change in different environmental pH. At alkaline pH, they can form micelles while at acidic pH they can transformed into an inverted hexagonal structure. The

Chapter II: Materials and Methods

hexagonal chemistry allows the destabilization of endosomal membrane and results in an efficient escape of nucleic acid from the carrier [82]. In our work, we used DOPE lipid (a gift sample from Lipoid AG, Steinhausen, Switzerland) with a purity of more than 99%. A stock solution of 10 mg/ml was prepared by dissolving the lipid contents in chloroform: methanol solution (2:1; v/v) and stored at -20 °C till further use.

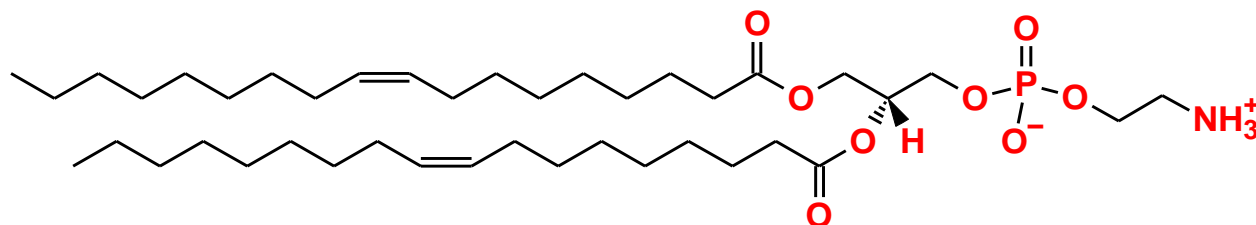


Figure 6. Chemical structure of DOPE.

2.1.3.4 MPEG5000-DPPE

MPEG5000-DPPE (N-(methoxypolyethylene glycol 5000 carbamoyl)-1,2-dipalmitoyl-sn-glycero-3-phosphatidylethanolamine) is a saturated phospholipid having a covalent linkage with the linear polyethylene glycol (PEG) molecule. PEG modified lipids are supposed to improve the blood circulation times of liposomal formulation to deliver various drugs (doxorubicin, paclitaxel, mitoxantrone) and proteins (insulin, streptokinase). MPEG5000-DPPE has a transition temperature of 63 °C with molecular weight of 5736 g/mol. In our work, we used MPEG5000-DPPE lipid (a gift sample from Lipoid AG, Steinhausen, Switzerland) with a purity of more than 99%. A stock solution of 10 mg/ml was prepared by dissolving the lipid contents in chloroform: methanol solution (2:1; v/v) and stored at -20 °C till further use.

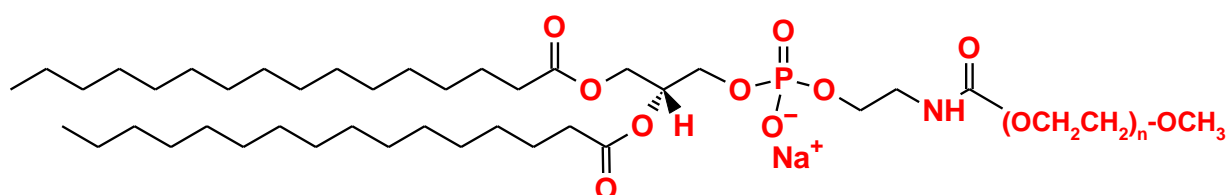


Figure 7. Chemical structure of MPEG5000-DPPE.

2.1.3.5 DPPG

DPPG (1,2-dipalmitoylphosphatidylglycerol) is a saturated lipid consisting of phosphorylglycerol acylated chain with palmitic acids. It has a molecular weight of 744.952 g/mol with a transition temperature of 41°C. In our work, we used a DPPG lipid (a gift sample

Chapter II: Materials and Methods

from Lipoid AG, Steinhausen, Switzerland) with a purity of more than 99%. A stock solution of 10 mg/ml was prepared by dissolving the lipid contents in chloroform: methanol solution (2:1; v/v) and stored at -20 °C till further use.

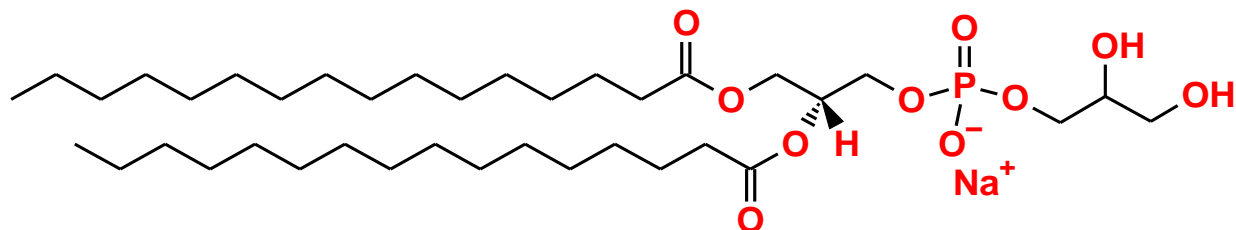


Figure 8. Chemical structure of DPPG.

2.1.3.6 Cholesterol

Cholesterol is a natural lipid consist of a sterol rings having a double bond at the 5,6-position as well as a 3 beta-hydroxyl group, with a molecular weight of 386.65 g/mol. The addition of cholesterol in liposomal formulations modify their membrane in term of stability and flexibility. Furthermore, it also reduces the leakage of water soluble entities from the lipid bilayer and strengthens its stability in the presence of biological fluids [83]. A stock solution of 10 mg/ml was prepared by dissolving the lipid contents in chloroform: methanol solution (2:1; v/v) and stored at -20 °C till further use.

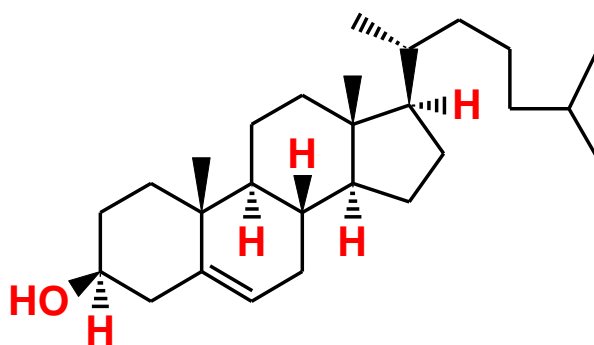


Figure 9. Chemical structure of cholesterol.

2.1.4 Imatinib mesylate

Imatinib methanesulfonic acid (4-[(4-methylpiperazin-1-yl) methyl]-N-[4-methyl-3-[(4-pyridin-3-yl)pyrimidin-2-yl) amino] phenyl] benzamide) is a monomesylate salt of imatinib with a molecular weight of 589.7 g/mol. It is a selective inhibitor of the BCR-ABL tyrosine kinase, where it block the ATP binding pocket to prevent the phosphorylation process and different

Chapter II: Materials and Methods

signal transduction pathways, responsible for tumour metastasis. A stock solution of 1 mg/ml was prepared by dissolving the drug in purified water and stored at -20 °C till further use.

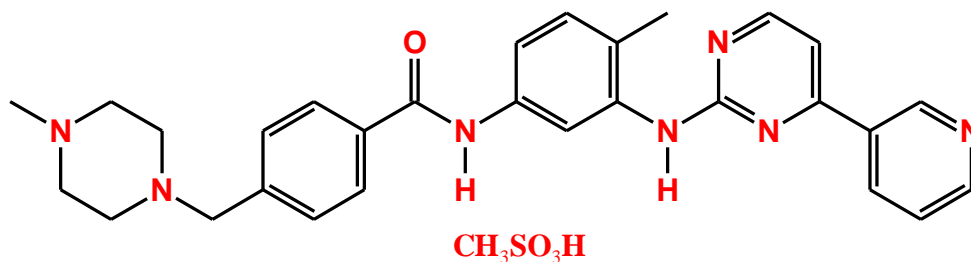


Figure 10. Chemical structure of imatinib mesylate.

2.2 Methods

2.2.1 Formulations

2.2.1.1 Preparation of liposomes

For the preparation of liposomal formulations, lipids with different molar ratios were dissolved in chloroform: methanol (2:1, v/v) solution. The organic phase was removed by using a rotary evaporator (Heidolph, Germany) and the resulting thin lipid film was rehydrated using 20 mM HEPES buffer (pH 7.4) containing 5% glucose (HBG buffer). The pre-formed liposomal suspension was sonicated for 10 min in an ultrasonic water bath (Elmasonic P30H, Elma Schmidbauer GmbH, Singen, Germany) to obtain a homogenous suspension. The multilamellar liposomes were then slowly extruded (15x) through a 100 nm polycarbonate membrane, using a pre-heated Avanti mini extruder (Avanti Polar Lipids, Alabaster, USA) to obtain unilamellar vesicles. Prior to use, the liposomal formulations were passed through 0.2 μm syringe filters [84].

2.2.1.2 Preparation of dendriplexes

Dendriplexes were formulated at different N/P ratios (the ratio of terminal amino groups in the PAMAM dendrimer to the phosphate groups of the nucleic acid). For the dendriplex formation, equal volumes of pDNA or siRNA and PAMAM dendrimer in HBG buffer were mixed with vigorous pipetting and incubated for 30 min under a laminar airflow hood at room temperature.

Chapter II: Materials and Methods

2.2.1.3 Preparation of lipodendriplexes

For the preparation of lipodendriplexes, a fine dispersion of liposomes at different liposome to PAMAM dendrimer mass ratios (0.1-1) were pipetted with dendriplexes solution (equal volumes) and incubated under the laminar airflow hood for 1 h at room temperature [85].

2.2.2 Physicochemical characterization

2.2.2.1 Dynamic light scattering (DLS)

The hydrodynamic diameter of the liposomes and of the complexes was measured by dynamic light scattering (DLS) technique using Zetasizer Nano ZS (Malvern Instruments, Malvern, UK). Detection of light scattering was measured at the angle of 173° by an automatically positioned laser attenuator (10 mW HeNe), using a clear disposable folded capillary cell (DTS1060, Malvern Instruments). The samples were diluted (1:100 ratio) using purified water prior to measurement. The average size was calculated with the data of three independent formulations (mean \pm standard deviation). The results were expressed as size distribution by intensity.

2.2.2.2 Laser Doppler anemometry (LDA)

The zeta potential of the liposomes and of different complexes was measured with laser Doppler anemometry (LDA) at a scattering angle of 17° on a Zetasizer Nano ZS. Depending upon the intensity signals of the sample, the instrument automatically performs 15-100 runs per measurement. The average value of the zeta potential was calculated with data of three individual formulations (mean \pm standard deviation).

2.2.3 Complex stability assay

2.2.3.1 Gel retardation assay

To check the complex forming ability of pDNA with PAMAM dendrimer, the dendriplexes with various N/P ratios were subjected to gel electrophoresis using 0.9% agarose gel containing SYBR[®] safe DNA dye (1: 10,000 in the 1x TAE buffer). Dendriplexes containing 0.5 μ g of pDNA with varying PAMAM dendrimer ratios (0.5-20) were transferred onto the gel. The gels

Chapter II: Materials and Methods

were subjected to electrophoresis using a Thermo Hybaid Electro 4 gel system (Thermo Electron Corporation, Ulm, Germany) connected to a constant power supply (LKB Bromma, Bromma, Sweden) at 80 V for 1 h. The pDNA localization was visualized on a UV transilluminator (WhatmanTM Biometra, Gottingen, Germany) at a wavelength of 312 nm.

2.2.3.2 Fluorescence quenching assay

The intercalation of the pDNA with dendrimer was also evaluated by fluorescence quenching assay. The quenching of the fluorescence of SYBR[®] safe DNA dye from pDNA, resulting from the complexation with positively charged PAMAM dendrimer, was the signal of the dendriplex formation [86]. Complexes containing 0.5 µg pDNA with SYBR[®] Safe DNA dye (1: 10,000 in 1x TAE buffer) were prepared at different N/P ratios. A microplate reader (FLUOstar Optima, BMG Labtech, Offenburg, Germany) was used for fluorescence measurements at an excitation and emission wavelengths of 502 nm and 520 nm, respectively. The fluorescence measurement of the pDNA complex with SYBR[®] safe DNA dye without PAMAM dendrimer was considered as 100%. The fluorescence measurement of the complexes was estimated using the following equation [51].

$$F_R = \frac{F_{OBS} - F_D}{F_0 - F_D} \times 100 \dots \text{Eq. (1)}$$

F_R depicts relative fluorescence measurement, F_{OBS} is the observed fluorescence of the given sample, F_D is the fluorescence of SYBR[®] Safe dye without pDNA in HBG buffer, and F_0 is the initial fluorescence without PAMAM dendrimer.

2.2.4 Surface morphology

2.2.4.1 Atomic force microscopy (AFM)

Atomic force microscopy was performed with a NanoWizard[®] 3 NanoScience (JPK Instruments, Berlin, Germany). 20 µl of the sample dispersions were placed onto a silicon wafer, fixed on a glass slide, and allowed them to settled on the surface for 10 min. After this, the supernatant was removed and the sample was allowed to dry. Cantilever tips (NSC 14 AlBS, Micromash, Tallinn, Estonia) having a length of 125 mm with a resonance frequency of about 160 kHz and nominal force constant of 5 N/m were used. The measurements were carried

Chapter II: Materials and Methods

out in intermittent contact mode (tapping mode) at a scan rate between 0.5 to 1.5 Hz, to avoid the damaging of samples.

2.2.5 *In vitro* cell culture experiments

2.2.5.1 Maintenance of cells

A wild-type human ovarian adenocarcinoma (SKOV-3) cell line and human embryonic kidney (HEK-293) cell line were purchased from American Type Culture Collection (ATCC®, Manassas, USA). HeLa co-expressing firefly luciferase and GFP under CMV promoter (HeLa LG) were purchased from GenTarget Inc (San Diego, USA). Homosapiens colorectal adenocarcinoma (Caco-2) cell line was a kind gift from Institute for Lung Research, University of Marburg, Germany. SKOV-3 cell line was cultured in IMDM (containing 10% FBS) at 37 °C and 7% CO₂ under humid conditions. HeLa LG, Caco-2 and HEK-293 cell lines were cultured in DMEM (containing 10% FBS supplemented with 10% NEA) at 37 °C and 8.5% CO₂ under humid conditions. All cells were cultivated as monolayers and passaged upon reaching 80% confluency.

2.2.5.2 pDNA transfection studies

For gene transfection studies, HEK-293 and SKOV-3 cells were seeded at a seeding density of 10,000 cells per well in a 96-well microtiter plate and were allowed to grow overnight before transfection. The complexes containing 0.25 µg pDNA (25 µl) were added in each well containing 75 µl of medium. The additional 100 µl medium was added after 4 h and plates were evaluated 48 h after transfection.

2.2.5.3 Transgene luciferase expression analysis

After 48 h incubation period, the complexes were removed and cells were washed twice with 200 µl of phosphate buffer pH 7.4 (PBS) containing calcium (Ca²⁺) and magnesium (Mg²⁺). The buffer was then replaced by 50 µl cell culture lysis reagent (CCLR) (Promega, Mannheim, Germany). 20 µl of lysate was then transferred to a 96-well white plate for luciferase reporter gene expression assay. 50 µl of luciferase assay reagents (Synchem OHG, Felsberg, Germany)

Chapter II: Materials and Methods

were pumped into each well by the automatic injection system of FLUOstar Optima microplate reader and luminescence was recorded after a 10 s integration time [87].

2.2.5.4 Protein quantification assay

For protein quantification, Pierce protein BCA assay kit was used, according to the manufacturer's protocol. A portion of 20 μ l lysate was transferred to an opaque 96-well microtiter plate and 180 μ l of BCA mixture was added to each well. The lysates were incubated at 37 °C for 30 min. The absorbance was measured at 570 nm using a microplate reader (FLUOstar Optima) and the values were compared against the bovine serum albumin (BSA) standard curve. The results obtained from these two experiments were expressed as relative luminescence units (RLU) / mg protein.

2.2.5.5 Cellular uptake studies

For the cellular uptake analysis, HEK-293 and SKOV-3 cells were seeded in 12-well cell culture plates (Nunc Delta, Nunc GmbH & Co. KG, Wiesbaden, Germany) containing coverslips (15 mm diameter) at the seeding density of 90,000 cells per well. After 24 h, the complexes containing 2 μ g of pCMV-GFP (200 μ l) were added dropwise into each well containing 800 μ l of medium and incubated for 4 h. After incubation, an additional 1 ml of medium was added to the wells and incubated up to 48 h. The cells were washed thrice with 300 μ l ice-cold PBS containing Ca^{2+} and Mg^{2+} . The cells were then fixed with 300 μ l of 4% formaldehyde solution, followed by incubation for further 20 min at room temperature. The cells nuclei were then counterstained with 300 μ l of DAPI (0.1 μ g/ml). The cells were then washed with 300 μ l PBS containing Ca^{2+} and Mg^{2+} and the coverslips were placed onto a clear glass slide and sealed with fluorescence-free glycerol-based mounting medium (FluorSave™, Calbiochem, San Diego, USA). Finally, the cells were analysed under a microscope (CKX-53 Olympus, USA), equipped with fluorescence detection filters for GFP (ex.505 nm - em.530 nm) and DAPI (ex.385 nm - em.470 nm).

Chapter II: Materials and Methods

2.2.6 Cytotoxicity studies

2.2.6.1 MTT assay

For *in vitro* cell viability assay, HEK-293 and SKOV-3 cells were seeded at a seeding density of 10,000 cells per well in a 96-well microtiter plate and were incubated overnight. On the following day, the complexes containing 0.25 µg pDNA (25 µl) were added in each well containing 75 µl of medium for 4 h. 1% TritonTM X-100 was used as a positive control. Additional 100 µl medium was added after 4 h and incubated for further 24 h. The medium was replaced with MTT dye (2 mg/ml) containing medium (200 µl) and incubated for further 4 h. After the incubation, 200 µl of DMSO was added to dissolve the formazan crystals formed by the metabolism of the MTT dye by viable cells. The plate was incubated on a shaking incubator (IKA KS4000 IC, Staufen, Germany) for 15 min. The absorbance of formazan was measured at 570 nm (FLUOstar Optima). The cell viability of the cells was expressed as a percentage of viability in comparison to untreated cells [88].

2.2.6.2 Determination of reactive oxygen species (ROS)

For reactive oxygen species generation studies, HEK-293 and SKOV-3 cells were seeded at the seeding density of 25,000 cells per well in a 96-well microtiter plate (black plate with clear bottom) and were incubated overnight before the experiment. For the measurement of ROS production, cellular ROS protocol by Abcam (Cambridge, UK) was used, with slight modification. Briefly, 100 µl of 25 µM cell permeant reagent 2,7-dichlorofluorescein diacetate (H₂DCFDA) was added to the cells 1 hour before adding the complexes. After washing with PBS, the complexes containing 0.25 µg pDNA (25 µl) were added in each well containing 75 µl of medium for 1 h, using 50 µM TBHP as a positive control. The cells were washed again with PBS and detectable green fluorescence of dichlorofluorescein (DCF) was recorded using excitation and emission wavelength of 485 nm and 520 nm, respectively (FLUOstar Optima). The intracellular fluorescence visualization was analysed using a microscope (CKX-53 Olympus, USA), equipped with GFP fluorescence detection filters (ex.505 nm - em.530 nm) [89, 90].

Chapter II: Materials and Methods

2.2.6.3 Lysosomal disruption and actin polymerization

SKOV-3 cells were seeded at the seeding density of 90,000 cells per well in a 12-well cell culture plate containing coverslips (15 mm diameter). After 24 h incubation, the old culture medium was replaced with the 800 μ l fresh medium and incubated with the complexes containing 2 μ g pDNA (200 μ l). Cells were incubated with the complexes for 4 h followed by incubation with 100 nM of LysoTracker[®] red DND-99 for 30 min at 37 °C to stain the lysosome. The cells were then washed with 300 μ l PBS containing Ca²⁺ and Mg²⁺ before fixing with 300 μ l of 4% formaldehyde solution [91]. Thereafter, cells nuclei were stained with 300 μ l of DAPI (0.1 μ g/ml) followed by cytoskeleton staining with 300 μ l of Phalloidin-FITC (50 μ g/ml). The coverslip was placed on a clear glass slide and sealed with fluorescence-free glycerol-based mounting medium (FluorSave[™], Calbiochem, San Diego, USA) before being analysed under a confocal laser scanning microscope (Zeiss LSM 700, Carl Zeiss GmbH, Jena, Germany). The untreated cells were considered as blank.

2.2.6.4 DNA damage assay

DNA damage was analysed by the comet assay. Briefly, SKOV-3 cells were seeded at the seeding density of 90,000 cells per well in a 12-well cell culture plate and incubated overnight. After incubation, old culture medium was replaced with the 800 μ l fresh medium and incubated with the complexes containing 2 μ g pDNA (200 μ l) for 4 h. After incubation, additional 1 ml of medium was added to the wells and incubated up to 48 h. The cells were washed thrice with 300 μ l ice-cold PBS containing Ca²⁺ and Mg²⁺. The cells were then trypsinized and suspended (8,000 cells in 25 μ l of PBS) in 75 μ l of low melting agarose 1% (LMA) and placed on pre-coated microscopic slides (Super frost microscopic slides were coated with 1% normal melting point agarose (NMA) and the lower surface was wiped before the settling of gel). The gel was covered with glass coverslips and allowed to set on an ice block. The coverslips were carefully removed and the settled gel was sandwiched by addition layer of LMA. The slides were then gently placed in ice cold lysis buffer (2.5 M NaCl, 100 mM EDTA, 10 mM Tris, 1% Triton[™] X-100; pH 10) and incubated overnight at 4 °C under dark condition. Afterward, the microscopic slides were placed in alkaline electrophoresis solution (300 mM NaOH, 1 mM EDTA; pH > 13) for 20 min to start the DNA unwinding process. Gel electrophoresis was performed under refrigerating condition at 25 V and 250 mA for 30 min. The level of the electrophoresis solution should not be more than 5 mm above the gel. Subsequently, the slides

Chapter II: Materials and Methods

were removed from electrophoresis chamber and rinsed with ice cold neutralizing buffer (400 mM Tris buffer; pH 7.5) for 5 min to remove the alkaline traces. The slides were dried and fixed with 70% ethanol for 15 min. Thereafter, slides were stained with SYBR[®] safe DNA gel stain for 20 min in dark condition. The cells were analysed by scoring 50 comets per slide using a microscope (CKX-53 Olympus, USA), equipped with GFP fluorescence detection filters (ex.505 nm - em.530 nm). The comets were analysed using Comet IV software (Instem, Staffordshire, UK).

2.2.7 Biocompatibility assay

2.2.7.1 *Ex vivo* hemolysis assay

To determine the hemolytic effect of the complex in blood, human erythrocytes were isolated from fresh blood [92]. The blood was transferred into tubes containing EDTA to avoid coagulation and centrifuged to separate the plasma fraction. The erythrocyte pellet was washed thrice with PBS and diluted to 1:50 with PBS. 180 μ l of erythrocytes dispersion were mixed with 20 μ l complexes, containing 0.25 μ g pDNA in a V-bottomed 96-well plate and incubated for 1 h at 37 °C in a shaking incubator (IKA KS4000 IC). The plates were then centrifuged and the supernatant was collected to measure the absorbance at 540 nm (FLUOstar Optima). PBS, NaCl 0.9% solution, untreated erythrocytes and 1% Triton[™] X-100 were used as controls. The absorbance value of 1% Triton[™] X-100 was considered as 100% hemolysis [89, 93].

2.2.7.2 Heparin competition assay

The nucleic acid stability of the dendriplexes and lipodendriplexes, against the natural polyanion (heparin) was evaluated by heparin competition assay. The complexes containing 0.25 μ g pDNA were used for analysis and incubated for 30 min with increasing amounts of heparin. The complexes were then loaded onto 0.9% agarose gel containing SYBR[®] safe DNA dye and subjected to electrophoresis for 1 h at 80 V and visualized using a UV trans-illuminator (Whatman[™] Biometra) at 312 nm [51, 94].

Chapter II: Materials and Methods

2.2.8 RNA interference experiments

2.2.8.1 Luciferase knockdown assay

For luciferase gene knockdown assay, stably transfected HeLa LG cells were seeded at a seeding density of 10,000 cells per well in a 96-well microtiter plate and were allowed to grow overnight. The complexes were added to the cell at the si-Luc concentration of 36 nM (7.2 pmol si-Luc in 200 μ l) and incubated for 48 h. Luciferase expression was determined in the same manner described in section 2.2.5.3. The knockdown produced by si-Luc complexes was expressed as a percentage of luciferase expression by control siRNA (si-Control).

2.2.8.2 GFP silencing

GFP reporter gene knockdown experiments were performed in stably transfected HeLa LG cell line. Briefly, 50,000 cells per well were seeded overnight in 24-well cell culture plates (Nunc Delta, Nunc GmbH & Co. KG, Wiesbaden, Germany). The complexes were added to the cell at the si-GFP concentration of 36 nM (36 pmol in 1 ml) and incubated for 48 h. After incubation, the cells were washed thrice with 300 μ l ice-cold PBS containing Ca^{2+} and Mg^{2+} . The cells were then fixed with 300 μ l of 4% formaldehyde solution and then washed again with PBS containing Ca^{2+} and Mg^{2+} . Thereafter, the cells were analysed for GFP silencing under a microscope (CKX-53 Olympus, USA), equipped with GFP fluorescence detection filters (ex.505 nm - em.530 nm).

2.2.8.3 MDR1 silencing

Knockdown of MDR1 gene experiment was conducted in MDR1 gene expressing Caco-2 cell line. Cells were seeded in 6-well cell culture plates (Sarstedt AG & Co. KG, Nümbrecht, Germany) at the seeding density of 1,00,0000 cells per well. After overnight incubation, the cells were transfected with complexes at the si-MDR1 concentration of 36 nM (108 pmol in 3 ml) and incubated for 48 h. After incubation, the cells were washed with PBS followed by the trypsinization of the cells. The cells were collected and re-suspend in PBS and subjected to RNA isolation.

Chapter II: Materials and Methods

2.2.8.3.1 RNA isolation, reverse transcription and real time quantitative PCR

Total RNA was isolated using the RNeasy Mini Kit, according to the manufacturer's instruction. After measuring the amount of isolated RNA, cDNA was synthesized using a High Capacity cDNA Reverse Transcription Kit, according to the manufacturer's instructions. 20 μ l reactions mixture was subjected to a thermal cycler program as follows, 25 °C for 10 min, 37 °C for 120 min, 85 °C for 5 min and then held at 4 °C. Quantitative real time PCR was performed with Quant studio 3 RT-PCR System (Applied Biosystems, Foster City, CA) using PowerUp™ SYBR® Green Master Mix, according to manufacturer's protocol. 10 μ l of the reaction mixture was used for RT-qPCR containing 15 ng of cDNA and 0.4 μ l of 10 mM gene specific primers. GPDH (house-keeper gene) was used as positive control and Ct values were used to calculate the relative mRNA expression level.

2.2.9 Cell Migration studies

2.2.9.1 Scratch closure assay

Caco-2 cells were seeded at the seeding density of 1,00,0000 cells per well in a 6-well cell culture plate. After overnight incubation, the cells were transfected with complexes at the si-MDR1 concentration of 36 nM (108 pmol in 3 ml) and incubated for 48 h. After 48 h of transfection period, the cells were trypsinized and washed with culture medium. Thereafter, 25,000 cells with a seeding volume of 70 μ l were transferred into each chamber of culture insert of μ -Dish (Ibidi, Martius, Germany) and incubated overnight for their confluency. After incubation, culture inserts were removed and additional medium (3 ml) was added in μ -Dish. Scratch closure was photographed to investigate the wound recovery at different time points (0, 16, 24, 48 h), using a microscope (CKX-53 Olympus, USA). Scratch closure area was calculated according to the gap filled by migrated cells in comparison to the scratch area at 0 h. Image J analysis software was used to calculate scratch closure.

2.2.9.2 Transwell migration assay

Caco-2 cells were grown in 6-well cell culture plates at a seeding density of 1,00,0000 cells per well. The cells were transfected with complexes at the si-MDR1 concentration of 36 nM (108 pmol in 3 ml) and incubated for 48 h. After 48 h of transfection period, the cells were

Chapter II: Materials and Methods

trypsinized and washed with serum free culture medium. Thereafter, 2,50,000 cells with a seeding volume of 200 μ l were transferred to the upper chamber of transwell insert (8 μ m pore size, PET membrane; Corning, New York, USA). 500 μ l of culture medium with 20% FBS was added to lower chamber and incubated the plate for 48 h. After incubation, the old medium was aspirated from the upper chamber of the insert and unmigrated cells were removed by the help of wet cotton swab. The migrated cells attached to the lower part of the chamber were fixed with 70% ethanol and stained with 0.1% crystal violet dye. The cell migration was observed in five randomly selected stained area under a bright field microscope and analysed using Wimasis image analysis software.

2.2.9.3 Plate colony formation assay

Caco-2 cells were grown in 6-well cell culture plates at a seeding density of 1,00,0000 cells per well. The cells were transfected with complexes at the si-MDR1 concentration of 36 nM (108 pmol in 3 ml) and incubated for 48 h. After 48 h of transfection period, the cells were trypsinized and resuspended in the new medium. Thereafter, 1,000 cells were transferred into a well of 6-well cell culture plate and allowed to grow for the period of 14 days. The cells were then fixed with 70% ethanol followed by washing with PBS. The cells were then stained with 0.1% crystal violet dye to detect the formation of colonies in the wells. The colony containing more than 50 cells was counted manually.

2.2.9.4 Formation of 3D tumor spheroid and 3D ring bioprinting

In two dimensional (2D) cell culture assays, the cells vasculatures are not in direct contact with the biochemical components of the media. On the other hand, it is also difficult to regulate the extracellular matrix (ECM) for the diffusion of extracellular compounds in 2D environment. To overcome these challenges, the 3D magnetic bioprinting can play a novel role to pattern a 3D cell culture structure by magnetizing the cells with biocompatible magnetic nanoparticles. The process of magnetic levitation initiates the cell aggregation and generates the ECM among the cells. Afterward, the induction of the magnetic field rapidly patterns the cells into a spheroidal or ring shape (Fig. 11). After the removal of the magnetic field, the cells tried to proliferate or migrate through ECM [95, 96].

Chapter II: Materials and Methods

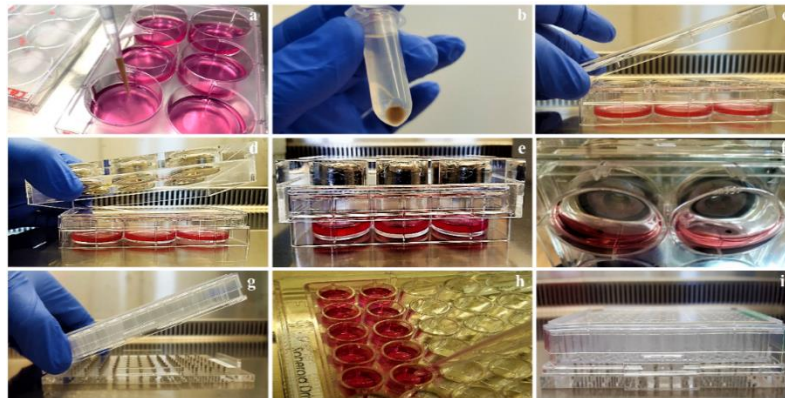
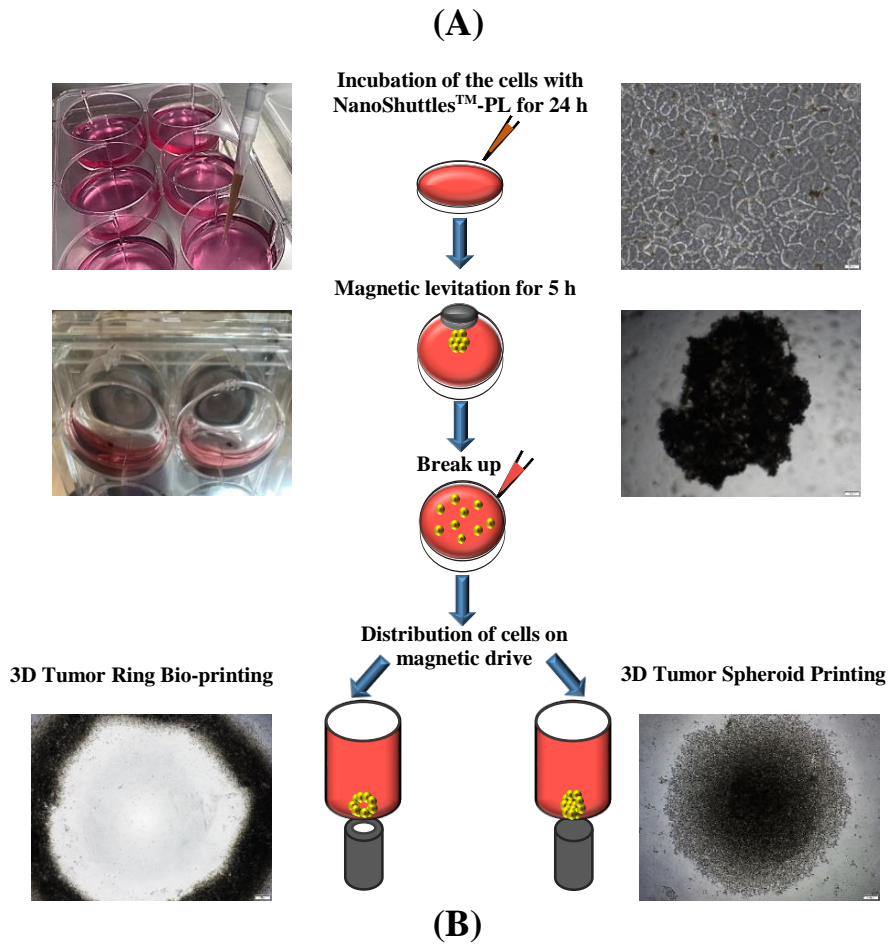


Figure 11. (A) Schematic representation of 3D tumor spheroid and 3D tumor ring bioprinting formation by magnetic levitation method. (B) Steps involved in spheroid formation: (a) Addition of NanoShuttles™-PL in the cells. (b) Trypsinization and washing of cells. (c) Addition of cells in 6-well ultra-low attachments plate and placement of the lid. (d) Placement of levitating drive. (e) Incubation for 5 h to generate the ECM among the cells. (f) Formation of cells aggregate and break down. (g) Placement of 96-well ultra-low attachment plate on spheroid magnetic drive. (h) Addition of cells under the influence of magnetic field. (i) Incubate the plate for 15 minutes to print spheroids.

Chapter II: Materials and Methods

2.2.9.4.1 3D tumor spheroids cell migration

3D tumor spheroids were prepared by magnetic levitation method using the 96-well Bio assay™ kit (Greiner Bio-One GmbH, Frickenhausen, Germany). Caco-2 cells were seeded in a 6-well cell culture plate at the seeding density of 1,00,0000 cells per well. After overnight growth, the cells were transfected with complexes at the si-MDR1 concentration of 36 nM (108 pmol in 3 ml) and incubated for 48 h. Afterward, the cells were incubated overnight with Nano3D Biosciences NanoShuttle™-PL (Greiner Bio-One GmbH, Frickenhausen, Germany) (8 µl/cm² of cell culture area) to crosslink the nanoparticles with the cells. On the following day, the cells were washed, trypsinized and resuspended in the media. 2 ml of cell suspension was then distributed in the 6-well ultra-low attachment plate (Greiner Bio-One GmbH, Frickenhausen, Germany) at the cell density of 2,50,000 cells per ml. The plates were then covered with the lid and the levitating drive was placed at the top of the lid. The plates were then rotated 3-4 times and observed under the microscope to check the initiation of the levitating process. The plate was then incubated for 5 h to generate the extra cellular matrix (ECM) among the levitating cells. The levitating cells were then broken by pipetting action. Afterward, a 96-well ultra-low attachment plate (Greiner Bio-One GmbH, Frickenhausen, Germany) was placed on the magnetic spheroid drive and broken cells were distributed at the cell density of 50,000 cells per well. The cells were then allowed to print on the magnetic spheroid drive for 15 min to obtain a loose connected spheroidal structure. The magnetic spheroid drive was then removed from the bottom and plate was incubated overnight to grow the tumor spheroid. The migration of cells through the ECM was then recorded for 48 h and the percentage of cell migration was calculated according to the following formula:

$$\text{Cell migration (\%)} = \frac{\text{Area covered by migrating cells (\mu\text{m})}}{\text{Total area covered by bioprinted region (\mu\text{m})}} \times 100 \dots \text{Eq. (2)}$$

2.2.9.4.2 Cytoskeleton staining of spheroids

Spheroid formation was done in the same manner discussed in section 2.2.9.4.1. After the 48 h of incubation, the spheroids were washed with PBS containing Ca²⁺ and Mg²⁺ and fixed with 4% formaldehyde solution for 1 h. The spheroids were then washed twice with PBS and counterstained with DAPI followed by Phalloidin-FITC for nuclei and cytoskeleton visualization, respectively. For every step, the spheroids were anchored by a magnetic spheroid drive in order to maintain the structural integrity. The magnetic spheroids were then

Chapter II: Materials and Methods

carefully pulled out using a Magpen (Greiner Bio-One GmbH, Frickenhausen, Germany) and placed on a clear glass slide under the influence of magnetic field. A coverslip was then placed over the spheroids and sealed with fluorescence-free glycerol-based mounting medium. The spheroids were then analysed under a microscope (CKX-53 Olympus, USA), equipped with fluorescence filters.

2.2.9.5 3D tumor ring closure assay

Levitation of the cells was performed in the same manner mentioned in subsection 2.2.9.4.1. The levitating cells were then broken by pipetting action. Afterward, a 96-well ultra-low attachment plate was placed on the magnetic ring drive and broken cells were distributed at the cell density of 100,000 cells per well. The cells were then allowed to print on magnetic ring drive for 15 min to obtain a loosely connected ring structure. The magnetic ring drive was then removed from the bottom and plates were incubated overnight to grow the tumor ring. Ring closure area was recorded for 48 h and compared with the si-Control. The % of ring closure area was determined using the following formula:

$$\text{Ring closure area (\%)} = \frac{\text{Inner diameter (\mu m) of ring after specified time interval}}{\text{Initial inner diameter (\mu m) of the ring}} \times 100 \dots \text{Eq. (3)}$$

2.2.10 Apoptosis assay by flow cytometry

Cell apoptosis was investigated, according to the sequential treatment protocol, by flow cytometry (FACS) technique. Briefly, 90,000 Caco-2 cells per well were seeded overnight in 12-well cell culture plates. The cells were transfected with complexes at the si-MDR1 concentration of 36 nM (72 pmol in 2 ml) and incubated for 48 h. After incubation, the media was replaced by 75 μ M of IM (2 ml drug solution in medium) and incubated for further 24 h. The controlled cells were incubated without any addition of the drug. Afterward, the cells were collected, washed with cold PBS and resuspended in 1 x binding buffer. 50 μ l of binding buffer supplemented with 1 μ l (10 μ g/ml) of APC Annexin V were gently mixed with equal volume of cell suspension and incubated at room temperature for 15 min under dark condition. Afterward, 300 μ l of binding buffer containing 0.4 μ l (5 mg/ml) of propidium iodide (PI) was added and placed on ice for 5 min before analyse by flow cytometer (Guava[®]easyCyte[™], Millipore Sigma, USA). The data was processed by flowjo 10 software.

Chapter II: Materials and Methods

2.2.11 Apoptosis determination in spheroids by live dead viability assay

Tumor spheroids were formed in the manner discussed in section 2.2.9.4.1. After the 24 h of spheroids formation, the media was replaced by 200 μ l of IM (75 μ M) and incubated for 24 h. The controlled spheroids were incubated without any addition of the drug. The spheroids were then washed with PBS before staining with a solution containing 3 μ M syto 9 and 7.5 μ M PI for live dead viability assay, using Live/Dead viability kit (InvitrogenTM, Oregon, USA). The spheroids were then again washed with PBS and analysed under a microscope (CKX-53 Olympus, USA) equipped with fluorescence filters.

2.2.12 Cell cycle analysis by flow cytometry

For cell cycle analysis, briefly, 1,00,000 Caco-2 cells per well were seeded overnight in 6-well cell culture plates. The cells were transfected with complexes at the si-MDR1 concentration of 36 nM (108 pmol in 3 ml) and incubated for 48 h. After incubation, the media were replaced by 75 μ M of IM (3 ml drug solution in medium) and further incubated for further 24 h. The controlled cells were incubated without any addition of the drug. Afterward, the cells were trypsinized and washed with ice-cold PBS. The cells were then fixed by a dropwise addition of 70% ice-cold ethanol and stored at -20 °C for at least one hour. At the time of analysis, the cells pellet was washed twice with ice-cold PBS and suspended in 1 ml of PI / 0.1% TritonTM X-100 staining solution (PI 20 μ g and RNase 50 μ g in 1 ml of 0.1% TritonTM X-100 solution). Keep the cell suspension in the dark condition at the room temperature for 30 min. Just before the analysis, the cells suspension was vortexed and filtered using a polystyrene round bottom tube equipped with a cell strainer cap. The cell suspension was poured in the cap and centrifuged for a short period of time. The cell cycle distribution was then analysed using a PE-A channel with a flow cytometer (BD Biosciences LSR II FACS, San Francisco, USA). A minimum of 20,000 events were measured per sample and data was analyzed using ModFit LT V 5.0 software (with special updated file for Sub-G1 phase calculation).

2.2.13 *In ovo* chorioallantoic membrane (CAM) assay

Fertilized eggs were purchased from Mastkukenbruterei Brommann (Rheda-Wiedenbruck, Germany). The eggs were disinfected with 70% ethanol and incubated in an egg hatching incubator, equipped with an automatic rotator (rotation after every 4 h) at a temperature of

Chapter II: Materials and Methods

37 °C with a relative humidity of about 60%. On the egg development day (EDD) 4, a hole of 30 mm diameter was made into eggshell using a pneumatic egg punch (Schuett Biotech, Germany), to expose the CAM surface. The exposed part of the egg was then covered with a small Petri dish and placed back into the incubator. On the EDD 11, 50 µl of dendriplexes or lipodendriplexes containing 0.5 µg of pCMV-GFP were injected under the stereomicroscope (Stemi 2000-C, Carl Zeiss GmbH, Germany) into the mesoderm of CAM with the help of glass cannulas. The eggs were further incubated for 48 h. On EDD 13, about 1 cm of the CAM was dissected and placed on a clear glass slide after washing with 0.9% NaCl. Finally, the GFP expression was observed under a confocal laser scanning microscope (Zeiss LSM 700, Carl Zeiss GmbH, Jena, Germany).

2.2.14 *In vivo* experiments

2.2.14.1 Animals

7-8 weeks old, female BALB/c, mice were purchased from the National Institute of Health, Islamabad, Pakistan and handled according to the protocols approved by the Ethical committee of Punjab University College of Pharmacy, University of the Punjab (Protocol No. AEC/PUCP/1085 dated 03.09.2018). Total 15 animals were used in study and divided into 5 groups (each having 3 animals per cage). The animals were maintained in a controlled environment (between 20 °C to 25 °C), with standard condition of food and water (ad libitum).

2.2.14.2 Acute *in vivo* toxicity

For *in vivo* acute toxicity studies, the untreated mice were served as negative control (group 1), while the groups of the mice injected with the dendriplexes and lipodendriplexes (containing 10 µg pDNA) by tail vein were categorized into group 2 and group 3, respectively. The first dose of the complexes was administered at day 1 while the second dose was given at day 4. The mice were kept under observation for 7 days to monitor any change in weight, behaviour and physical alteration to assess any kind of illness. The following parameters were evaluated for acute *in vivo* toxicity determination:

Chapter II: Materials and Methods

2.2.14.2.1 Serum biochemistry and hematological analysis

To check the biocompatibility of the complexes, the blood was collected under anaesthesia by cardiac puncture method at day 7, for serum biochemistry and hematological analysis. The serum was separated by centrifugation of the blood at 1200 g for 10 min, using a centrifuge (Centurion Scientific, Chichester, UK). The supernatant was collected and stored at -20 °C for further experiments. Serum biochemical parameters like liver function tests (LFTs), renal functions tests (RFTs), total bilirubin, blood glucose and total protein levels were evaluated using serum biochemical marker analyser (Micro lab 300, Merck, Germany).

Hematology parameters, included the red blood cells count (RBCs), hemoglobin (Hb), hematocrit (HCT), white blood cells count (WBCs), mean corpuscular volume (MCV), neutrophils, eosinophils, lymphocytes, monocytes, platelets count (PLT), mean corpuscular hemoglobin (MCH), mean corpuscular hemoglobin concentration (MCHC), and mean platelet volume (MPV) were measured using a hematology analyser (Icon-3, Norma Instruments, Budapest, Hungary).

2.2.14.2.2 Organ to body ratio

The relative organ to body ratio was considered as a tool to evaluate any toxic effect of the complexes on mice organ after their repeated administration. The animals were sacrificed by cervical dislocation method and vital organs (liver, lungs, heart, kidney and spleen) were removed carefully. The organs were washed with normal saline and weighed individually for the organ to body index calculation, which is the percentage of the organ weight to the total body weight ratios.

2.2.14.2.3 Erythrocyte aggregation assay

For the erythrocytes aggregation assay, erythrocytes of the mice were washed three times with PBS by centrifugation at 5,000 g for 5 min. The erythrocytes pellet was then re-suspended with PBS to make a final stock suspension of 2% (v/v). A 100 µl of the erythrocyte suspension was mixed with 100 µl of the complexes containing 1 µg pDNA and incubated for 2 h at room temperature. A 10 µl sample of the mixture was placed on a glass slide and observed under bright field microscopy.

Chapter II: Materials and Methods

2.2.14.2.4 Histopathology of vital organs

The macroscopic necropsies were evaluated in the organ tissues of sacrificed mice. The vital organs like heart, lungs, liver and kidneys were collected for tissue histopathology and fixed in 10% formalin solution before embedding into a paraffin block. Thin tissue sections (0.5 μm) were then obtained with the help of rotary microtome (Hunan Kaida scientific instruments, Changsha, China) and were stained using hematoxylin and eosin (H & E staining) dyes for microscopic evaluation (Olympus BX51M, Tokyo, Japan).

2.2.14.3 *In vivo* biodistribution and imaging experiments

For the *in vivo* biodistribution analysis, the mice were *i.v.* injected with the complexes (dendriplexes; group 4 and lipodendriplexes; group 5) containing pCMV-GFP (10 μg) by tail vein route. The mice were sacrificed after 24 h post injection and the vital organs were collected for *ex vivo* imaging. A UVP iBox[®] Explorer2[™] (Analytik Jena US LLC, Jena, Germany) small animal imaging system, having customized wavelength filters for green fluorescence (ex.455 nm - 495 nm, em.503 nm - 523 nm) was used for the measurement of the GFP expression in vital organs. The results were analysed by using VisionWorks[®] LS software.

2.2.14.4 Frozen tissues GFP distribution analysis

The organs of the mice were stored in 10% formalin solution for the fixation of the cells and freezed at -20 °C. GFP expression was then observed in the thin sections of frozen tissues under the fluorescence microscope (EVOS FL Cell Imaging System, Thermo Scientific, San Diego, CA, USA).

2.2.15 Statistical analysis

All the experimental evaluations were performed in triplicates and the values were given as a mean \pm standard deviation. One-way ANOVA was performed to identify statistically significant differences using IBM SPSS software (Ver. 22). Dunnett's test was used for multi-comparison between the results and control, whereas multi-comparison among the different groups was made using Tukey's test. Probability values less than 0.05 were considered significant. Statistical significances are denoted as * $p < 0.05$, ** $p < 0.01$, *** $p < 0.001$.

Chapter III: Results and Discussion

Chapter III: Results and Discussion

3.1 Physicochemical characterization and optimization of dendriplexes

The characterization of dendriplexes is the prerequisite of lipodendriplexes preparation. It has been reported that PAMAM dendrimer of generation 5.0, has all of its 128 primary amines in the protonated form at physiological pH, and thus can electrostatically interact with the negatively charged nucleic acid to form dendriplexes [97]. To check the stable complex formation of PAMAM dendrimer with pDNA, N/P ratios from 0.5 to 20 were selected and analysed using gel electrophoresis and fluorescence quenching assay. Gel electrophoresis reveals that at N/P ratio 2, stable complex formation occurs, showing no DNA band on the gel (Fig. 12). Similar findings were observed by Movassaghian et al. [53].

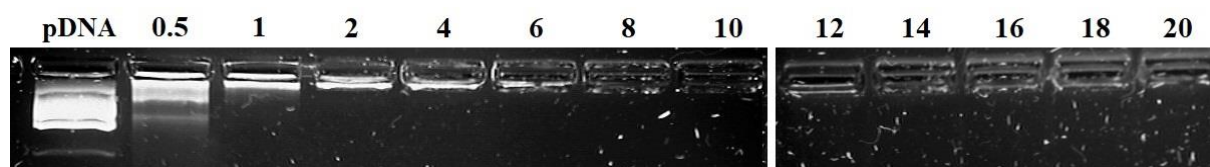


Figure 12. Gel retardation assay of dendriplexes at various N/P ratios from 0.5 to 20, showing complex formation at N/P ratio 2 with no band on the gel. Free pDNA was used as a control.

Further analysis with fluorescence quenching assay, indicated similar results. The quenching in relative fluorescence was observed upon the increase in N/P ratios (Fig. 13). The results suggested the complexation at N/P ratio 2 which is indicated by the reduction in fluorescence intensity. This also suggests that the PAMAM dendrimer's binding on pDNA was very strong and that the dendrimer cannot be displaced by the addition of the dye. A saturation point was then attained indicating a state of equilibrium [40].

Chapter III: Results and Discussion

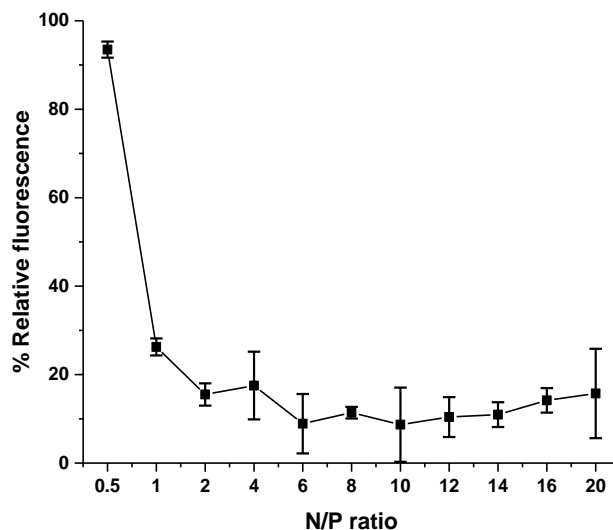


Figure 13. Fluorescence quenching assay of dendriplexes at different N/P ratios showed a decrease in fluorescence with the increase in N/P ratio. About 85% fluorescence was reduced at N/P ratio 2 indicating the complex formation. Values are represented as means \pm S.D (n=3).

The size and zeta potential of the dendriplexes were measured by DLS and LDA, respectively. It was observed that with an increase in N/P ratio from 0.5 to 2, the size of the complexes decreased and the zeta potential changed from negative to positive, due to the decrease in pDNA mobility (as mentioned above). At greater N/P ratios, a state of equilibrium was observed (Fig. 14). Results showed that dendriplexes have a tendency to form aggregates at a zeta potential close to zero, but stabilized at the higher positive zeta potential. Therefore, the sufficiently high zeta potential was crucial for the stability of dendriplexes.

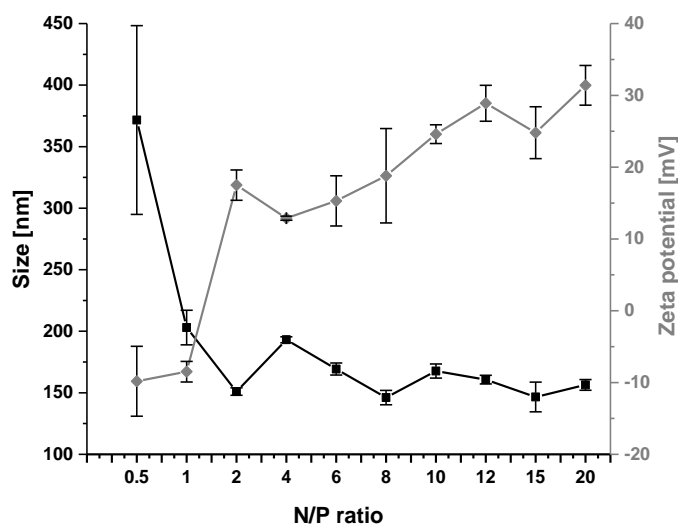


Figure 14. Size and zeta-potential of dendriplexes at different N/P ratios prepared in HBG buffer (pH 7.4) after 30 min of incubation. Values are represented as means \pm S.D (n=3).

Chapter III: Results and Discussion

For the optimization of dendriplexes, pDNA transfection and cell viability experiments were performed on HEK-293 cell line [98] using different N/P ratios (Fig. 15 and 16). It was observed that by increasing the charge ratio, the transfection efficiency was increased, due to an increase in charge interaction between the complexes and the negatively charged surface of the cell membrane. Maximum pDNA transfection was observed at N/P ratio 12 as compared to lower N/P ratios. With a further increase in N/P ratio, transfection efficiency dropped because the induction of very high positive charge on the complexes can lead to enhanced cell membrane disruption and lower transfection efficiency [38]. The cytotoxicity assay also showed a 50% drop in the viability of the cells at N/P ratio 8 and a further increase in toxicity with increasing N/P ratios.

Therefore, dendriplexes with N/P ratio 12, having a size of 160.7 ± 3.5 nm with a zeta potential of 28.9 ± 2.5 mV (suitable for incorporation into liposomes) and the highest transfection efficiency with least toxicity among the three best transfecting N/P ratios were selected for further studies to optimize lipodendriplexes.

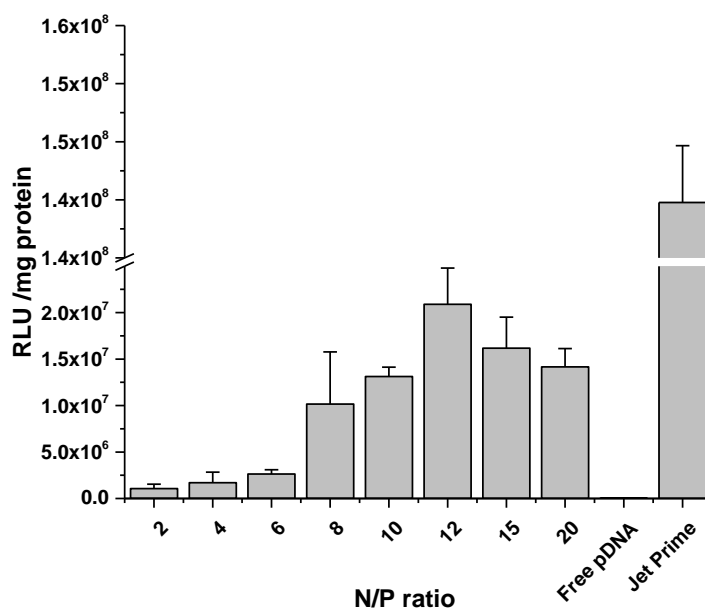


Figure 15. pDNA transfection studies of dendriplexes at different N/P ratios in HEK-293 cell line using Jet Prime[®] as positive control. Untransfected cells were considered as negative control. Values are represented as means \pm S.D (n=3).

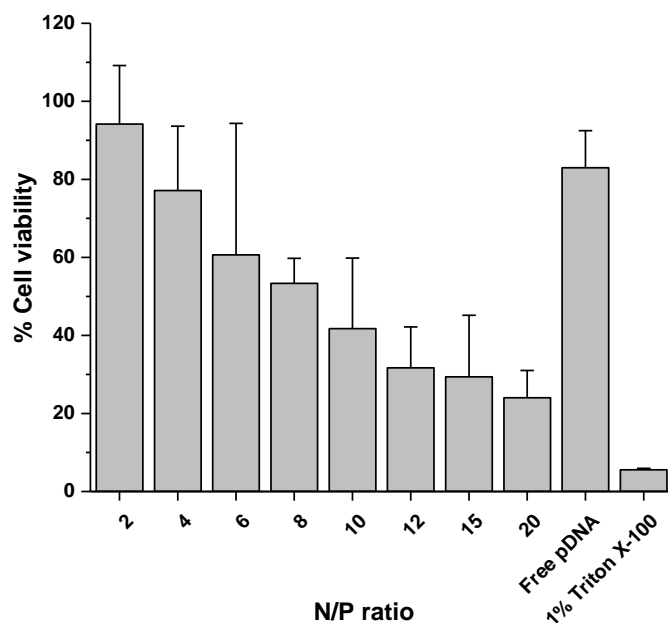


Figure 16. Cytotoxicity studies of dendriplexes at different N/P ratios in HEK-293 cell line, using 1% Triton™ X-100 as positive control. Values are represented as means \pm S.D (n=3).

3.2 Physicochemical characterization of lipodendriplexes

To find an optimal lipid composition for lipodendriplex formation, different lipids with various molar ratios were investigated. The physicochemical properties of a broad range of liposomal formulations were determined. All the extruded liposomes were in the size range of 87.8 nm to 128.7 nm, with a narrow and monodisperse size distribution, having a polydispersity index (PDI) of approximately 0.1, except for pegylated liposomes, having a PDI of about 0.2 (Table 1). The zeta potential of the liposomal formulations was in the negative range except for the positively charged DPPC:DOTAP (95:5) liposomes.

Table 1. Size and zeta potential (mean \pm S.D) of different liposomal formulations (n=3).

Formulations (mol:mol)	Size \pm S.D [nm] (PDI)	Zeta potential \pm S.D [mV]
DPPC:CH (85:15)	105.2 \pm 17.3 (0.12)	-7.5 \pm 0.7
DPPC:CH:MPEG5000-DPPE (85:14:1)	128.7 \pm 59.8 (0.23)	-17.9 \pm 11.2
DPPC:DPPG (92:8)	107.1 \pm 32.8 (0.15)	-14.0 \pm 2.5
DPPC:DOTAP (95:5)	87.8 \pm 12.7 (0.15)	35.8 \pm 5.8
DPPC:DOPE:CH (45:40:15)	109.2 \pm 22.2 (0.19)	-12.6 \pm 2.0
DPPC:MPEG5000-DPPE (95:5)	125.6 \pm 68.5 (0.21)	-22.5 \pm 2.2

Chapter III: Results and Discussion

In order to optimize the stoichiometry of lipodendriplexes, the DPPC:CH (85:15) formulation was initially selected, to complex with optimized dendriplexes. Different liposome to PAMAM dendrimer mass ratios from 0.1 to 1 were tested for lipodendriplexes formation. As shown in Fig. 17, the size of the resulting lipodendriplexes was increased compared to parent dendriplexes. It was also observed that by increasing the liposome mass ratio from 0.1 to 0.5, zeta potential of the lipodendriplexes decreased from +16.9 to +8.8 mV, showing the maximum liposome shielding over the dendriplexes at the mass ratio of 0.5. The maximum shielding is very important to minimize the PAMAM associated cytotoxicity and unwanted interaction of these complexes with the blood components [99]. With a further increase in liposome mass ratio, a slight increase in zeta potential of the complexes was observed, which was due to possible charge competition between negatively charged liposomes and pDNA for the binding sites on the positively charged PAMAM. These changes can cause a slight destabilisation of dendriplexes and expose some of the amino groups to the outer site. The additional positive charge may also lead to lower transfection efficiency with an increase in cytotoxicity, as depicted in Fig. 19 and 22.

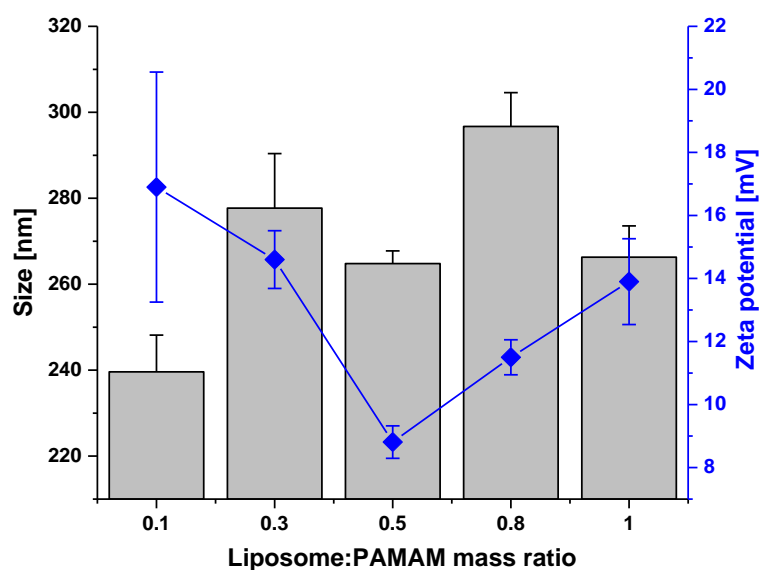


Figure 17. Size (bar graph) and zeta potentials (line graph) of different liposome to PAMAM dendrimer mass ratios (0.1-1) of DPPC:CH-PAMAM lipodendriplexes (N/P ratio 12). Values are represented as mean \pm S.D (n=3).

The results of size analysis were in good correlation with the AFM findings. AFM images showed that the pure liposomes of DPPC:CH (85:15) were spherical and their size (110.3 ± 7.2 nm) was similar to the hydrodynamic diameter obtained from DLS analysis (Fig. 18 A-C). While the lipodendriplexes settled on the silica surface showed a size of

Chapter III: Results and Discussion

259.6 ± 5.3 nm and a slight change in shape from spherical to oval. The non-covalent interaction of liposome with dendriplexes and the adsorption of lipid layer on the silica surface results in the broadening of the lipodendriplexes (Fig. 18 D-F) [100]. Fig. 18 E also showed the spreading of some lipid layer, with a height of 4 nm, representing a lipid bilayer.

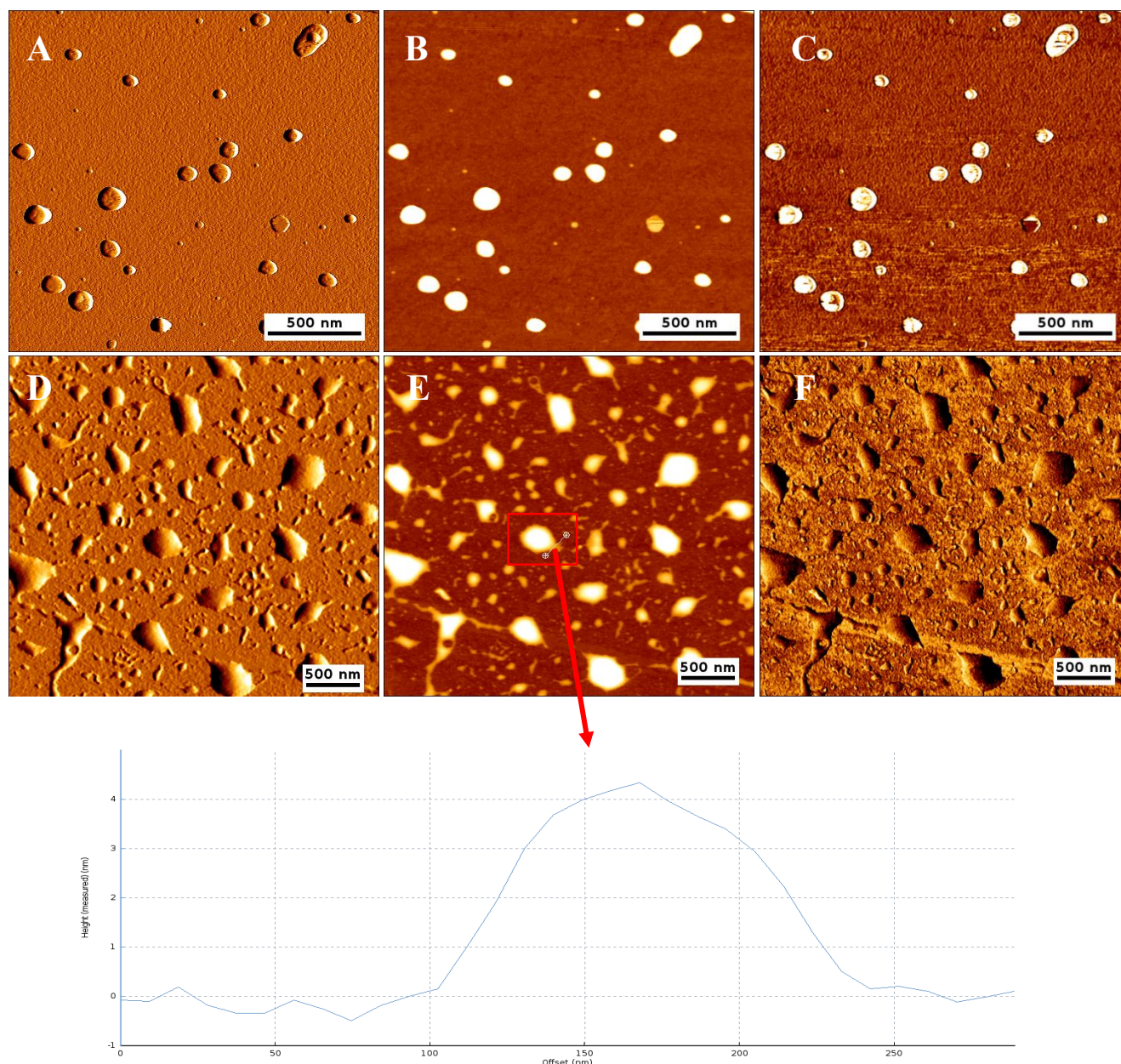


Figure 18. AFM micrographs with lock in amplitude, height measured and lock in phase view of DPPC:CH (85:15) liposome (A-C) and DPPC:CH-PAMAM lipodendriplexes (liposome to PAMAM dendrimer mass ratio 0.5; N/P ratio 12) (D-F), respectively. Cross section view of spreading lipid layer (indicated by red arrow) showing a height of 4 nm, representing a lipid bilayer. Scale bar represents 500 nm.

Chapter III: Results and Discussion

3.3 DNA transfection experiments

3.3.1 pDNA transfection experiments of lipodendriplexes

After the establishment of optimized dendriplexes, the transfection efficiency of lipodendriplexes of DPPC:CH (85:15) using different liposomes to PAMAM dendrimer mass ratios (0.1 to 1) was tested in SKOV-3 cell line. It was observed that the liposome to PAMAM dendrimer mass ratio 0.5 showed the best transfection results (Fig. 19). Thereby, this ratio was further tested with lipodendriplexes of different liposomal formulations, in order to optimize the best transfecting formulation (Fig. 20). Lipodendriplexes of DPPC:CH (85:15), DPPC:CH:MPEG5000-DPPE (85:14:1) and also of positively charged DPPC:DOTAP (95:5) showed good transfection efficiencies. In contrast, lipodendriplexes of DPPC:CH (85:15) showed a significant improvement in transfection efficiency as compared to lipodendriplexes of DPPC:DPPG (92:8), DPPC:DOPE:CH (45:40:15) and DPPC:MPEG5000-DPPE (95:5) and of its parent dendriplexes. Surprisingly, DOPE containing lipodendriplexes exhibited lower transfection efficiency, which might be due to a change in the physicochemical properties of the resulting complex, while the large PEG chain containing liposome (DPPC:MPEG5000-DPPE, 95:5) remarkably reduced the transfection efficiency, depicting a lower cellular internalization. This finding was in accordance to the work done by Schäfer et al. [101].

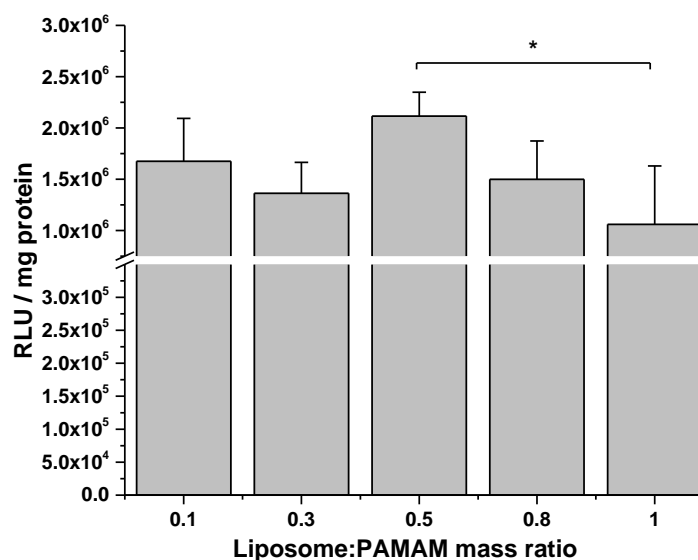


Figure 19. pDNA transfection studies in SKOV-3 cell line with different liposome to PAMAM mass ratios (0.1-1) of DPPC:CH-PAMAM lipodendriplexes (N/P ratio 12). Values are represented as mean \pm S.D (n=3) and statistical significance is indicated as * $p < 0.05$.

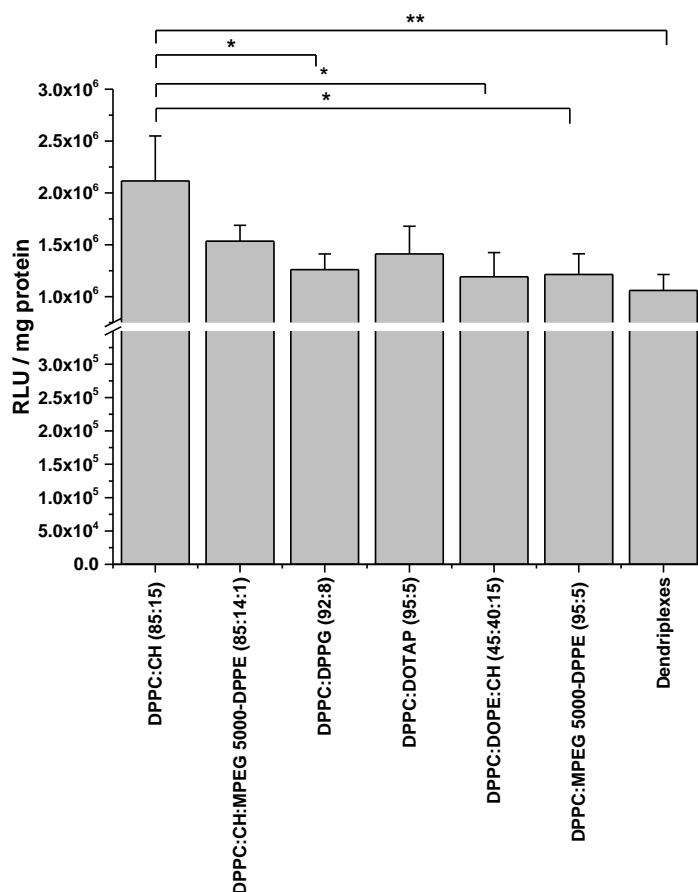


Figure 20. pDNA transfection studies in SKOV-3 cell line of lipodendriplexes of different liposome formulations (liposome to PAMAM dendrimer mass ratio 0.5) and dendriplexes (N/P ratio 12). Values are represented as mean \pm S.D (n=3) and statistical significances are indicated as * $p < 0.05$, ** $p < 0.01$.

3.3.2 Cellular uptake studies

To visualize the cellular uptake of the optimized dendriplexes and lipodendriplexes, GFP reporter gene expression assay was done. Internalization of complexes was monitored by GFP positive cells to estimate the transfection efficiency showing an overlay of DAPI treated cells coupled to the green fluorescence signal arising from the GFP expression. Cells transfected with lipodendriplexes exhibited a higher green fluorescence signal compared to dendriplexes alone. The higher cellular uptake could have contributed towards an increased plasmid GFP transfection through possible cellular events like interactions of nano-complexes with the cell membrane, cellular uptake and endosomal release which results in an efficient entry of pCMV-GFP to the cytoplasm and finally to the nucleus (Fig. 21) [87].

Chapter III: Results and Discussion

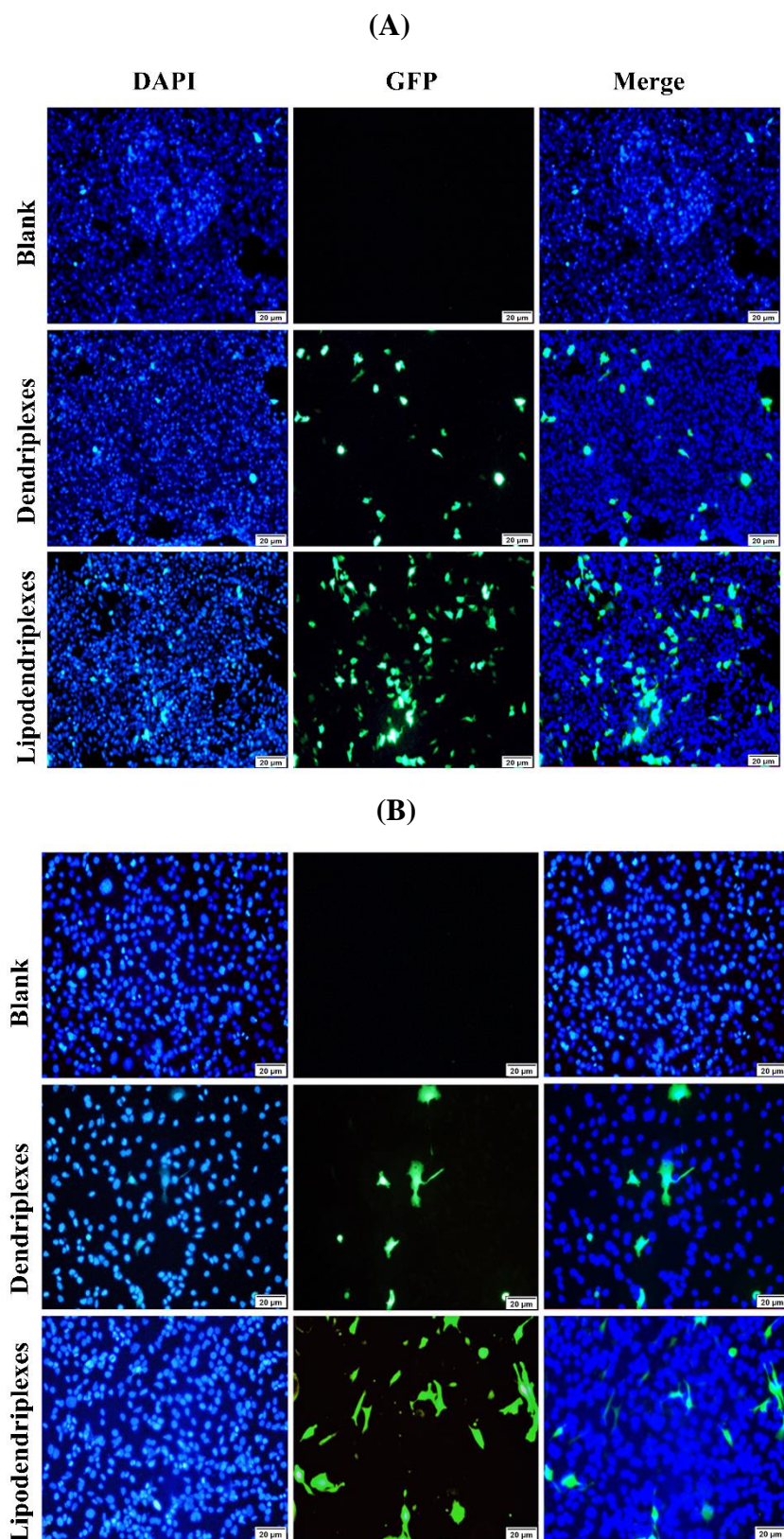


Figure 21. Fluorescence micrographs with DAPI, GFP and Merged (DAPI + GFP) channels. GFP expression in (A) HEK-293 and (B) SKOV-3 cell lines with optimized dendriplexes and DPPC:CH-PAMAM lipodendriplexes (liposome to PAMAM dendrimer mass ratio 0.5; N/P ratio 12). Untransfected cells were considered as blank. Scale bar represents 20 μm .

3.4 Cytotoxicity studies

3.4.1 MTT assay

In the case of lipodendriplexes, the liposomal layer covers the surface of the dendriplex and inhibit the binding of terminal amino groups to the surface of the cell membrane, thereby create a more favourable environment for the cells and consequently improve cell viability [53]. The lipodendriplexes of DPPC:CH (85:15) with different liposome to PAMAM dendrimer mass ratios (0.1-1), using optimized dendriplexes, were initially tested in cell viability assay. It was observed that lipodendriplexes with a liposome to PAMAM dendrimer mass ratio of 0.5 showed the highest cell viability (Fig. 22). Therefore, the liposome to PAMAM dendrimer mass ratio 0.5 was further studied with lipodendriplexes of different liposomal formulations. The lipodendriplexes of DPPC:CH (85:15) showed a significant ($p < 0.05$) improvement in cell viability as compared to its respective optimized dendriplexes. The results also depicted a good cell viability profile for lipodendriplexes of DPPC:CH:MPEG5000-DPPE (85:14:1), DPPC:DOTAP (95:5) and DPPC:DPPG (92:8). While lipodendriplexes of DPPC:DOPE:CH (45:40:15) and DPPC:MPEG5000-DPPE (95:5) exhibited a lower cell viability profile (Fig. 23).

Therefore, DPPC:CH (85:15) lipodendriplexes were considered to be the best formulation in terms of cell viability and DNA transfection efficiency, hence, they were used for all further investigations.

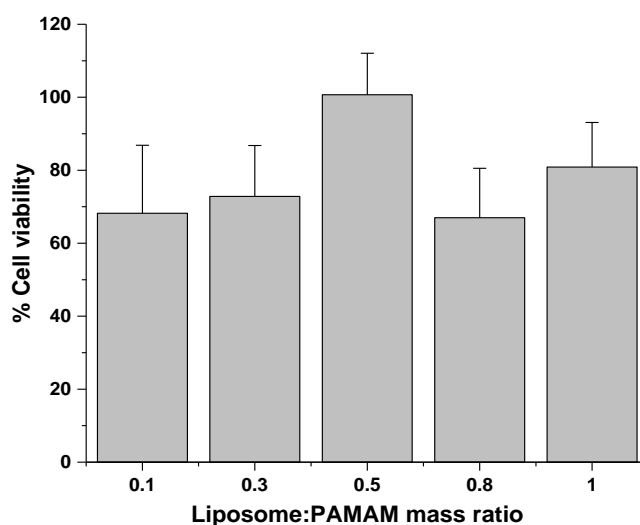


Figure 22. Cell viability studies in SKOV-3 cell line with different liposome to PAMAM mass ratios (0.1-1) of DPPC:CH-PAMAM lipodendriplexes (N/P ratio 12). Values are represented as mean \pm S.D (n=3).

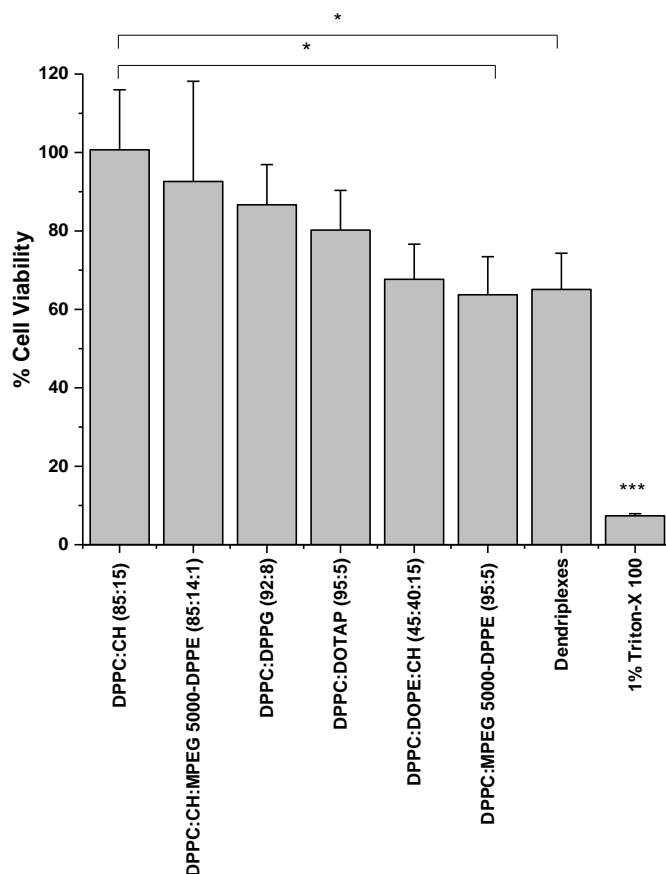
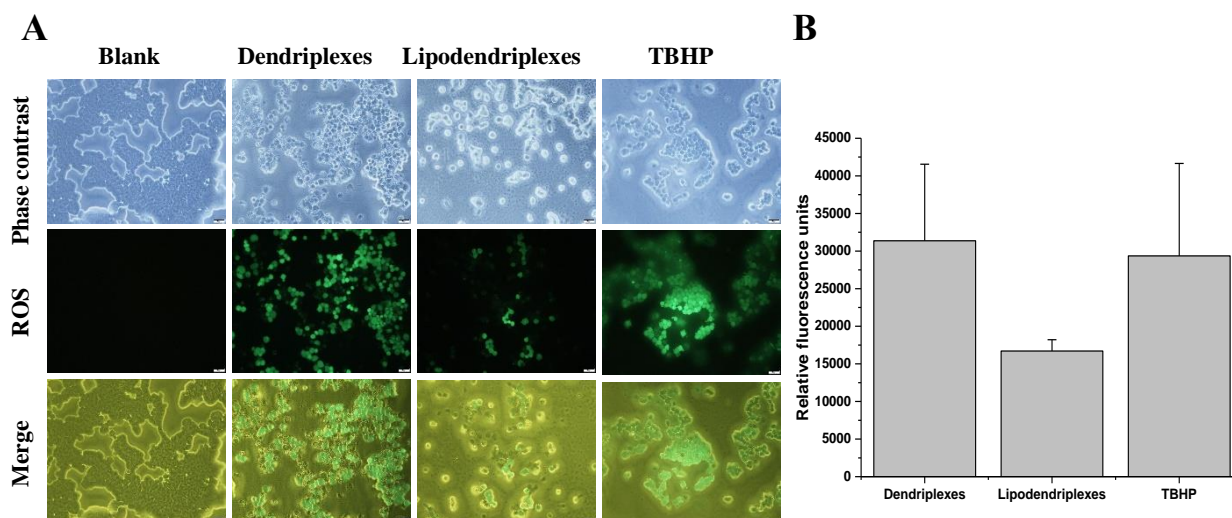


Figure 23. Cell viability studies in SKOV-3 cell line of lipodendriplexes of different liposomal formulations (liposome to PAMAM dendrimer mass ratio 0.5) and dendriplexes (N/P ratio 12) using 1% Triton™ X-100 as a positive control. Values are represented as mean ± S.D (n=3) and statistical significances are indicated as * $p < 0.05$, *** $p < 0.001$.

3.4.2 Reactive oxygen species generation assay

In the case of ROS assay, after the exposure of the complexes, the production of intracellular ROS was observed in the HEK-293 and SKOV-3 cells. It was observed that the dendriplexes, having exposed terminal amino groups, produce increased fluorescence signals of DCF as compared to lipodendriplexes (Fig. 24). This portrayed that the positively charged surface of the PAMAM dendrimers played a critical role of ROS generation, by the disruption of the mitochondrial electron transduction chain and may result in enhanced O_2 production [102].

HEK-293



SKOV-3

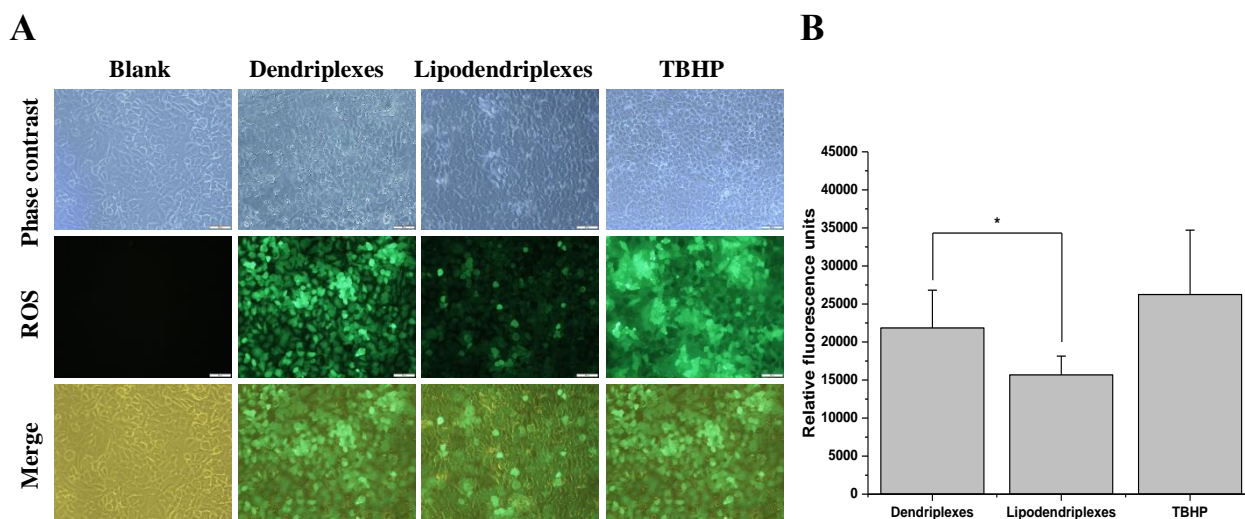


Figure 24. (A) Fluorescence micrograph and (B) relative fluorescence units of intracellular ROS generation in HEK-293 and SKOV-3 cell lines, respectively after the addition of optimized dendriplexes and DPPC:CH-PAMAM lipodendriplexes (liposome to PAMAM dendrimer mass ratio 0.5; N/P ratio 12) using TBHP as a positive control. Higher DCF (green fluorescence) was produced from H₂DCFDA after the addition of dendriplexes to the cells in comparison to lipodendriplexes. Values are represented as mean \pm S.D (n=3) and statistical significance is indicated as **p < 0.05. Blank represents cells without treatment and scale bar represents 20 μ m.

3.4.3 Lysosomal disruption and actin polymerization

For an efficient nucleic acid delivery, the cargo should be stable during the endocytic uptake to release into the cytosol [103]. It has been reported that endocytosis is the main mechanism of cellular uptake of protonated PAMAM dendrimers which trafficked to lysosomes and buffer the endolysosomal pH (proton sponge effect) and can cause lysosomal rupturing by lysosomal membrane permeabilization (LMP) mechanism [104, 105]. Cell death associated with LMP is highly associated with mitochondrial membrane permeabilization that can result in enhanced reactive oxygen species (ROS) generation, cytosolic acidification and cellular necrosis [106].

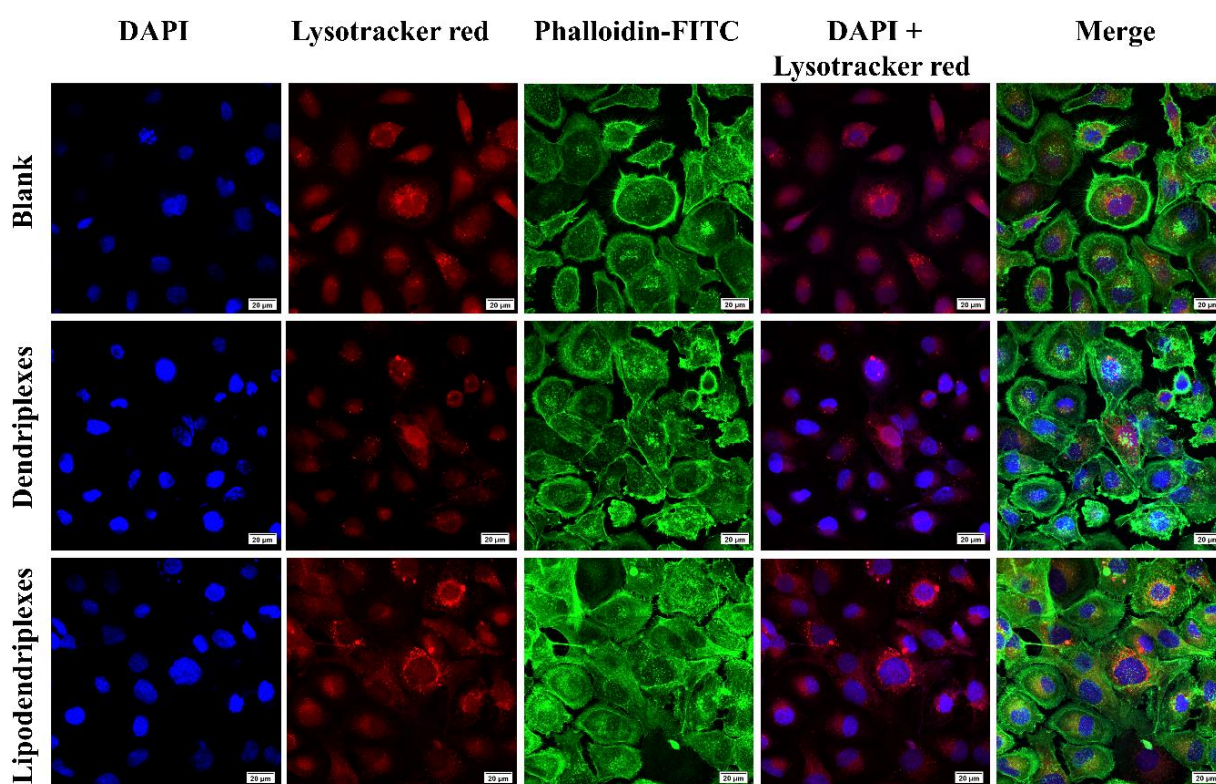


Figure 25. Lysosomal disruption and actin polymerization assay in SKOV-3 cell line of optimized dendriplexes and DPPC:CH-PAMAM lipodendriplexes (liposome to PAMAM dendrimer mass ratio 0.5; N/P ratio 12). DAPI (blue) correspond to the nuclei staining while LysoTracker red (red) represents lysosomal staining. Phalloidin FITC (green) representing the cytoskeleton staining to monitor actin polymerization. Untreated cells representing as blank. Scale bar represents 20 μm.

Chapter III: Results and Discussion

It has also reported that the PAMAM dendrimer can interact with the cytoskeleton in a biphasic manner. At low concentration, they retard the actin polymerization by acting as G-binding actin protein while at higher concentration they behave as a nucleating protein to cause actin polymerization [107, 108]. Therefore, in order to investigate the intracellular trafficking of PAMAM based complexes, LysoTracker[®] red DND-99 (lysosomal marker) and Phalloidin FITC were used. Fig. 25 depicted that after the incubation period of 4 h, the cells treated with lipodendriplexes showed a higher fluorescence intensity of LysoTracker red as compared to dendriplexes suggesting a lower damaging of lysosomes by lipid modified system. It was further observed that the concentration of PAMAM used in the complexes does not alter the structure of cytoskeleton and inhibited the actin polymerization process.

3.4.4 DNA damage assay

It has been evaluated from section 3.4.2 and 3.4.3, the naked dendriplexes were responsible for enhanced oxidative stress and mitochondrial membrane permeabilization which are the key determinants of cellular toxicity. The free radical formation was further responsible for the damage of many biological components including cellular proteins and DNA, which may lead to apoptosis and cellular necrosis [109]. The alkaline comet assay, also called a single cell gel electrophoresis method, is a fast and reliable method for the determination of DNA damage. If there is some damage or fragments present in a negatively charged DNA, the broken part may migrate towards the anode to resolve into DNA head and tail, similar to a broken comet.

The results of comet assay showed that the lipodendriplexes exhibited an olive tail moment of 0.7 ± 0.8 while in the case of dendriplexes it was significantly ($p < 0.01$) high i.e. 6.2 ± 4.2 indicating the damaging of DNA by naked dendriplexes system (Fig. 26).

Therefore, the exposed terminal amino groups on the surface of naked dendriplexes were considered to be responsible for ROS generation, mitochondrial damage, cytotoxicity and DNA damage.

Chapter III: Results and Discussion

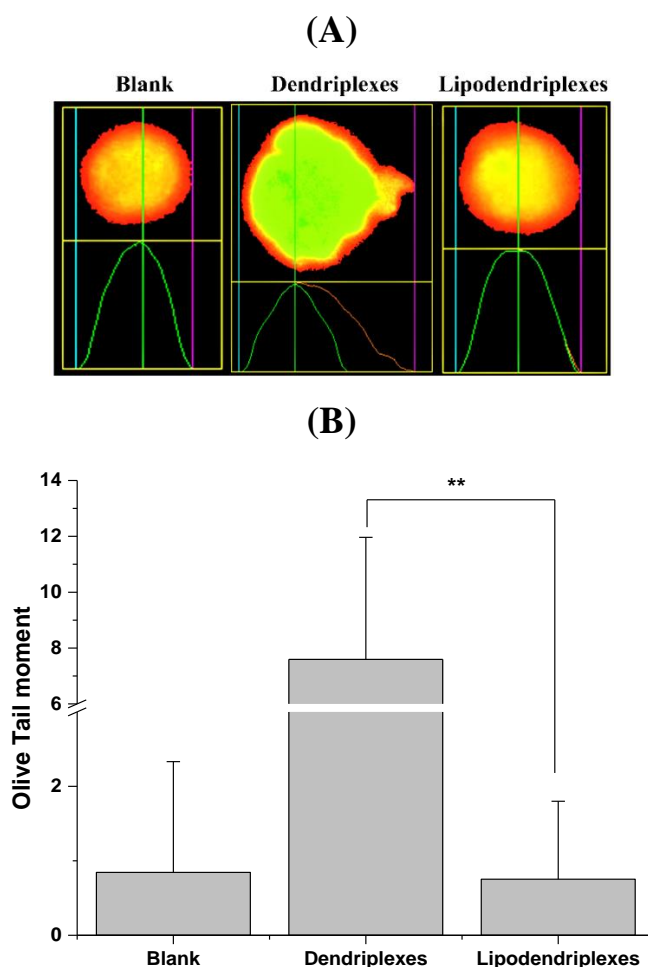


Figure 26. DNA damage assay in SKOV-3 cell line of optimized dendriplexes and DPPC:CH-PAMAM lipodendriplexes (liposome to PAMAM dendrimer mass ratio 0.5; N/P ratio12). (A) Comet IV software generated graphs and (B) olive tail moment representing the extent of DNA damage. Untreated cells represents as blank. Values are represented as mean \pm S.D (n=50) and statistical significance is indicated as **p < 0.01.

3.5 Biocompatibility studies

3.5.1 *Ex vivo* hemolysis assay

The free terminal amino groups of PAMAM contributed to the concentration-dependent hemolytic effect on red blood cells [110], consequently, by increasing the charge ratio of dendriplexes, a constant increase in toxicity was recorded. Therefore, the most efficient and less toxic non-viral vectors from pDNA transfection and *in vitro* cytotoxicity experiments were chosen for the hemolysis assay. Optimized lipodendriplexes were very stable and

Chapter III: Results and Discussion

showed hemolysis of about 7.3%, which was less than the hemolysis induced by dendriplexes alone (Fig. 27).

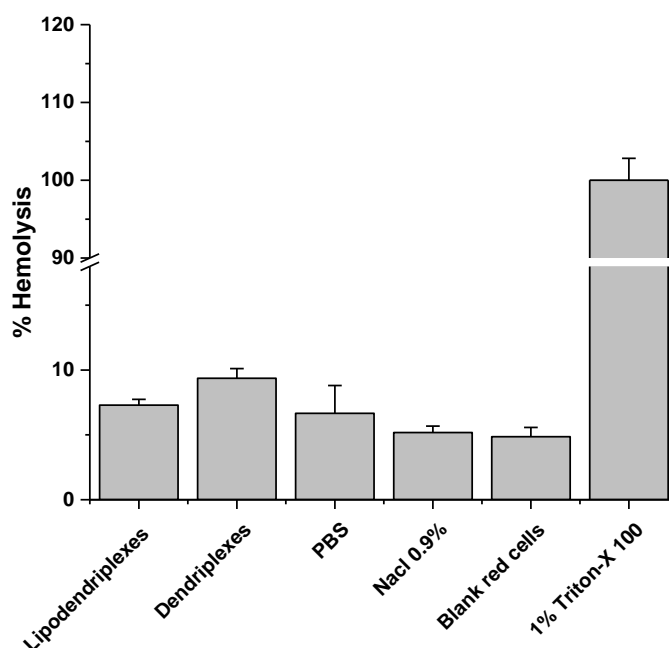


Figure 27. *Ex vivo* hemolysis assay of pDNA (0.25 μ g) containing optimized dendriplexes and DPPC:CH-PAMAM lipodendriplexes (liposome to PAMAM dendrimer mass ratio 0.5; N/P 12) using 1% TritonTM X-100 as a positive control. PBS, 0.9% NaCl and untreated erythrocytes were used as negative controls. Values are represented as mean \pm S.D (n=3).

3.5.2 Heparin competition assay

pDNA stability of the charged complexes is the key factor to evaluate the integrity of the non-viral gene carrier system. The stability of the complexes can be affected by the increasing concentrations of natural polyanions (heparin) that can competitively interact with the oppositely charged PAMAM dendrimer and may result in the initial release of pDNA. Therefore, the stability of the complexes was tested by *in vitro* pDNA stability assay, using heparin as a model molecule. It was observed that the optimized dendriplexes showed stability against heparin up to a concentration of 20 I.U./ 100ml (1mg=100 I.U.), while lipodendriplexes exhibited stability up to a concentration of 30 I.U./ 100 ml. The concentration of heparin in a healthy adult ranges from 5 - 15 I.U./ 100 ml [111]. Therefore, the optimized complexes were considered biocompatible. However, in comparison to dendriplexes, lipodendriplexes exhibited more resistance against natural polyanions (Fig. 28).

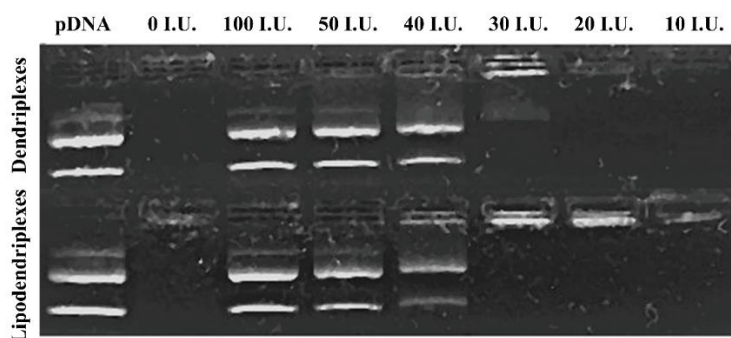


Figure 28. pDNA stability studies of optimized dendriplexes and DPPC:CH-PAMAM lipodendriplexes (liposome to PAMAM dendrimer mass ratio 0.5; N/P ratio 12) using different heparin concentrations (I.U./ 100 ml). 0 I.U. represents complexes without heparin treatment.

3.6 RNA interference experiments

3.6.1 Luciferase gene knockdown assay

Knockdown experiments were performed to determine the gene silencing effect of the formulations. Based on the best transfection efficiency profile, lipodendriplexes of DPPC:CH (85:15) were selected for luciferase gene knockdown experiments. Lipodendriplexes showed a significant knockdown of luciferase gene in comparison to si-Control while an improved (insignificant) gene silencing was also observed as compared to dendriplexes group (Fig. 29).

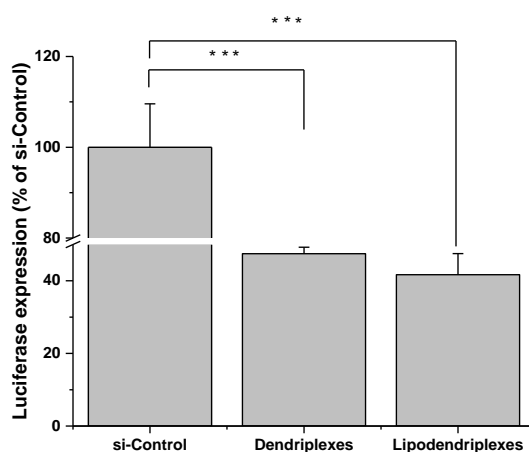


Figure 29. Luciferase knockdown efficiency in HeLa LG cell line of optimized dendriplexes and DPPC:CH-PAMAM lipodendriplexes (liposome to PAMAM dendrimer mass ratio 0.5; N/P ratio 12). Luciferase gene knockdown of the complexes is expressed as the percentage of non-specific scrambled siRNA (si-Control). Values are represented as mean \pm S.D (n=3) and statistical significance is indicated as *** $p < 0.001$.

Chapter III: Results and Discussion

3.6.2 GFP silencing

Gene silencing efficiency mediated by si-GFP complexes was studied in GFP-expressing HeLa LG cell line, using fluorescence microscopy. Results of Fig. 30 depicted the higher knockdown efficiency, with good cells viability profile by lipodendriplexes as compared to unmodified dendriplexes. While the cells treated with a lipodendriplexes containing scrambled siRNA did not produce gene knockdown, confirming the silencing specificity by si-GFP.

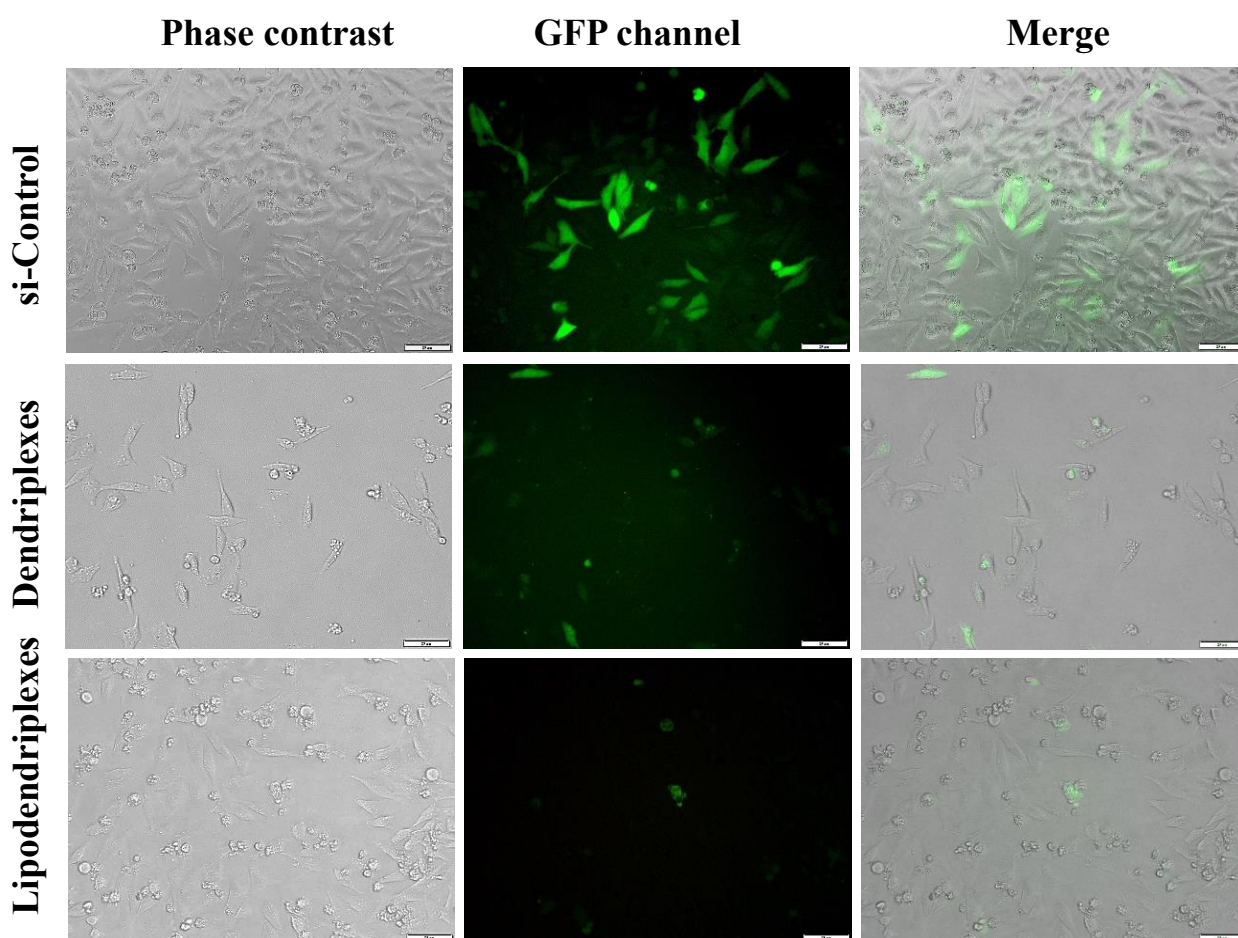


Figure 30. GFP silencing in HeLa LG cell line of optimized dendriplexes and DPPC:CH-PAMAM lipodendriplexes (liposome to PAMAM dendrimer mass ratio 0.5; N/P ratio 12). Cells treated with lipodendriplexes containing non-specific scrambled siRNA were used as si-Control. GFP channel (green) represents GFP expression in the cells. Scale bar represents 20 μm .

Chapter III: Results and Discussion

3.6.3 MDR1 silencing and RT-qPCR assay

RT-qPCR assay was performed to measure the gene silencing mediated by si-MDR complexes. It was observed that lipid modified complexes exhibited 70% MDR1 gene silencing ($p < 0.001$) which was 1.7 higher than naked dendriplexes ($p < 0.01$) i.e. 41% knockdown, as shown in Fig. 31.

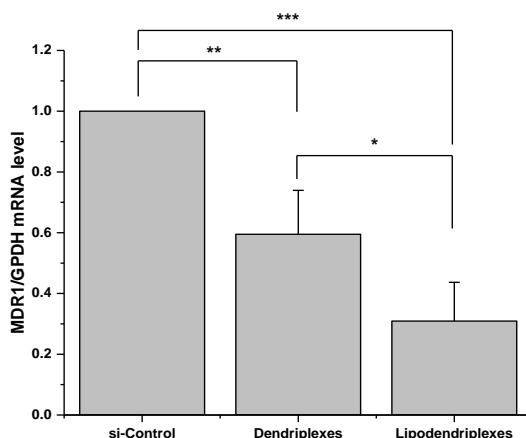


Figure 31. MDR1 silencing in Caco-2 cell line of optimized dendriplexes and DPPC:CH-PAMAM lipodendriplexes (liposome to PAMAM dendrimer mass ratio 0.5; N/P ratio 12). Cells treated with lipodendriplexes containing non-specific scrambled siRNA were used as si-Control. Values are represented as mean \pm S.D ($n=3$) and statistical significances are indicated as * $p < 0.05$ ** $p < 0.01$ *** $p < 0.001$.

3.7 Cell Migration studies

3.7.1 Scratch closure assay

Cancer metastasis is the primary cause of morbidity and mortality and responsible for about 90% of cancer deaths. The disseminated tumor cells play a major role in tumor metastasis, which is not a static process and can invade the nearby organs [112-114]. P-glycoproteins (P-gp), encoded by the MDR1 gene, are not only involved in the drug efflux mechanism, but they can also play a major role in the promotion of tumor metastasis and provide protection of tumor cells against caspase dependent apoptosis [115, 116]. To investigate the role of MDR1 gene in tumor metastasis, Caco-2 cells were transfected with si-MDR1 complexes and tumor progression was evaluated by scratch closure assay using Ibidi culture inserts. It was observed that the knockdown of MDR1 gene by lipodendriplexes exhibited less scratch closure as compared to dendriplexes and si-Control groups (Fig. 32). Results showed that in comparison

Chapter III: Results and Discussion

to si-Control, the percentage of the scratch closure in lipodendriplexes and dendriplexes treated cells were 23% ($p < 0.001$) and 47% ($p < 0.01$), respectively. Therefore, it is evident from the findings, the enhanced downregulation of MDR1 by lipodendriplexes contribute to inhibition of metastatic progression.

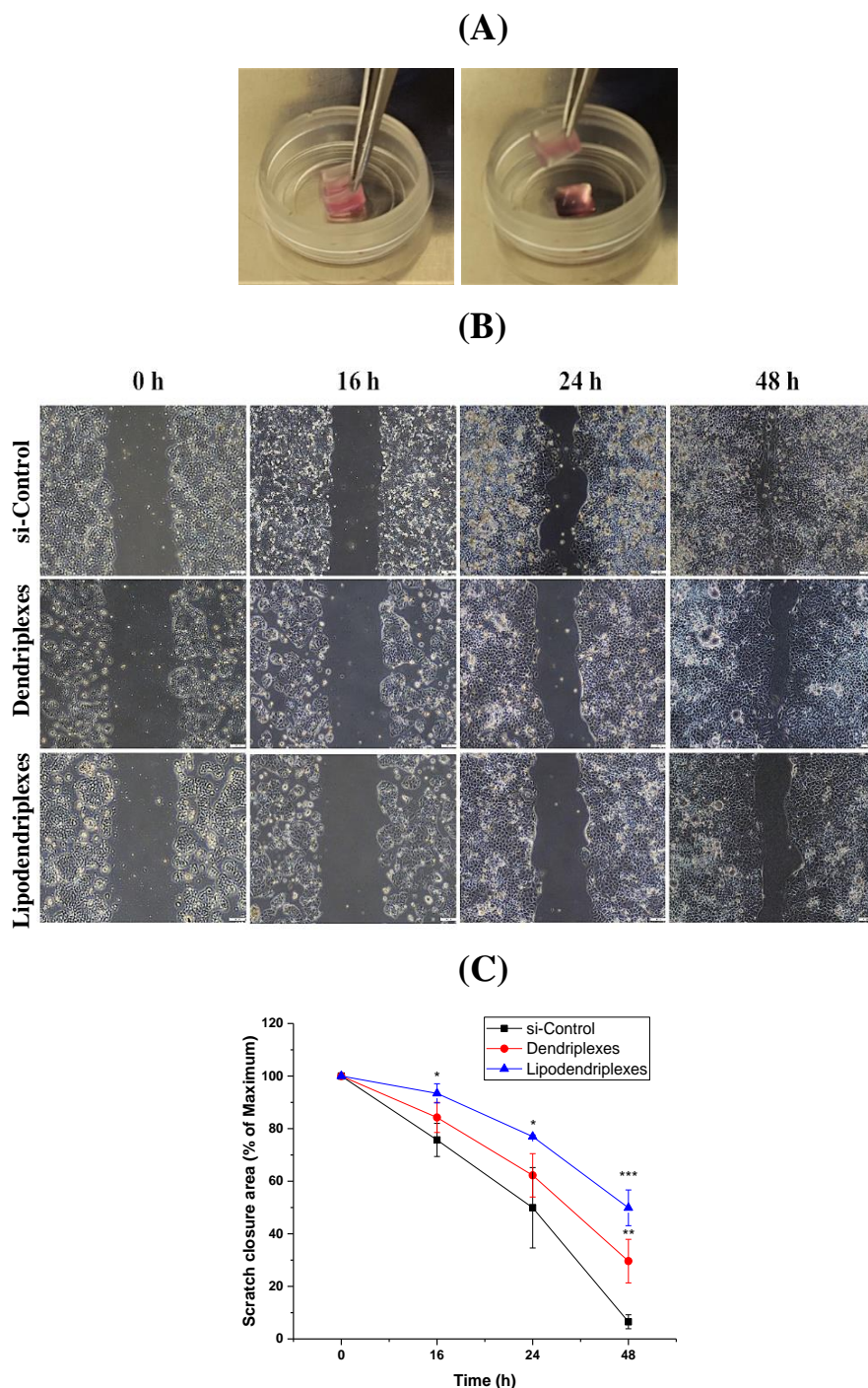


Figure 32. Scratch closure assay in Caco-2 cell line of optimized dendriplexes and DPPC:CH-PAMAM lipodendriplexes (liposome to PAMAM dendrimer mass ratio 0.5; N/P ratio 12) using Ibidi culture inserts. (A) Process of scratch formation. (B) Scratch closure over the time period of 48 h. (C) Graphical presentation of scratch closure area over a time period of 48 h i.e. the

Chapter III: Results and Discussion

percentage of maximum area at 0 h. Cells treated with lipodendriplexes containing non-specific scrambled siRNA were considered as si-Control. Scale bar represents 100 μm . Values are represented as mean \pm S.D (n=3) and statistical significances are indicated as * $p < 0.05$, ** $p < 0.01$, *** $p < 0.001$.

3.7.2 Transwell migration assay

Cell migration was also investigated by transwell migration assay. It has been observed that in comparison to si-Control the lipodendriplexes treated cells exhibited a significant reduction ($p < 0.001$) in cell migration (approximately 41% decreased) while 20% reduction ($p < 0.01$) was observed in the case of dendriplexes treated group (Fig. 33). Therefore, the results of transwell migration assay were in good correlation with the results obtained in scratch closure assay.

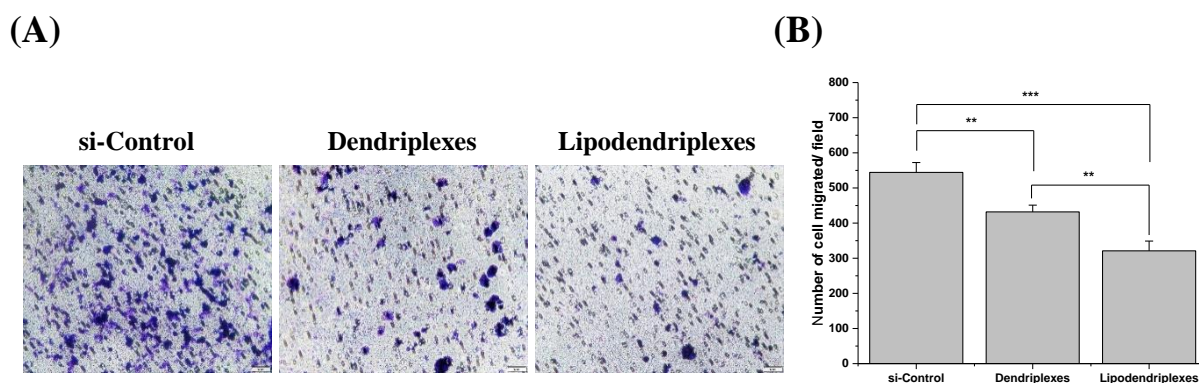


Figure 33. Transwell cell migration assay in Caco-2 cell line of optimized dendriplexes and DPPC:CH-PAMAM lipodendriplexes (N/P ratio 12). (A) Phase contrast micrographs of the cells stained with 0.1% crystal violet. (B) Graphical presentation of number of cells migrated per field. Cells treated with lipodendriplexes containing non-specific scrambled siRNA were considered as si-Control. Scale bar represents 20 μm . Values are represented as mean \pm S.D (n=3) and statistical significances are indicated as ** $p < 0.01$, *** $p < 0.001$.

3.7.3 Plate colony formation assay

Downregulation of MDR1 is also responsible for the reduction of cell proliferation and colonization [116]. To confirm this role of MDR1 in colon cancer, colony formation assay was performed in Caco-2 cell line. It was observed that after knockdown of MDR1 with lipodendriplexes, the number of colony formation was significantly ($p < 0.001$) reduced to 63% in comparison to the si-Control group. Similar effects were recorded in dendriplexes

Chapter III: Results and Discussion

treated group with an inhibition effect of about 48% ($p < 0.001$). Nevertheless, the knockdown produced by lipodendriplexes exhibited more significant ($p < 0.01$) results as compared to the parent dendriplexes group (Fig. 34). These results depicted that MDR1 knockdown played an obvious role in the inhibition of cell proliferation and colonization of Caco-2 cells.

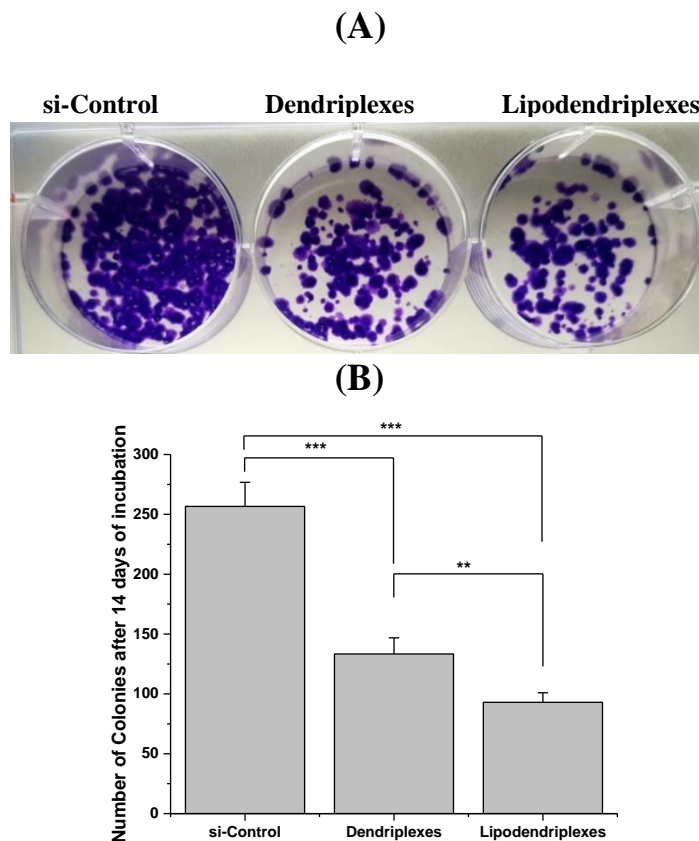


Figure 34. Colony formation assay in Caco-2 cell line of optimized dendriplexes and DPPC: CH-PAMAM lipodendriplexes (liposome to PAMAM dendrimer mass ratio 0.5; N/P ratio 12). (A) Photographs of the cells colony stained with 0.1% crystal violet. (B) Graphical presentation of number of colony formation after 14 days of incubation. Cells treated with lipodendriplexes containing non-specific scrambled siRNA were considered as si-Control. Values are represented as mean \pm S.D ($n=3$) and statistical significances are indicated as ** $p < 0.01$, *** $p < 0.001$.

3.7.4 3D tumor spheroid cell migration

Cell migration plays a vital role in tumor metastasis from their site of origin. Therefore, in order to investigate the cell metastasis in Caco-2 cells, magnetically levitated cells were patterned into a 3D tumor spheroidal model to establish a similar *in vivo* tumor like environment [117]. This 3D tumor model determines the impact of MDR1 silencing on tumor progression. The

Chapter III: Results and Discussion

cells treated with complexes containing si-MDR1 were pattern into 3D spheroidal structure and the cell migration through ECM, away from the original bioprinted area, over the incubation period of 48 h was recorded. The results showed that in the case of si-Control treated cells the percentage of cells migration was 28% while a significant reduction in cell migration was found in case of dendriplexes ($p < 0.05$) and lipodendriplexes ($p < 0.01$) i.e. 18% and 13%, respectively (Fig. 35).

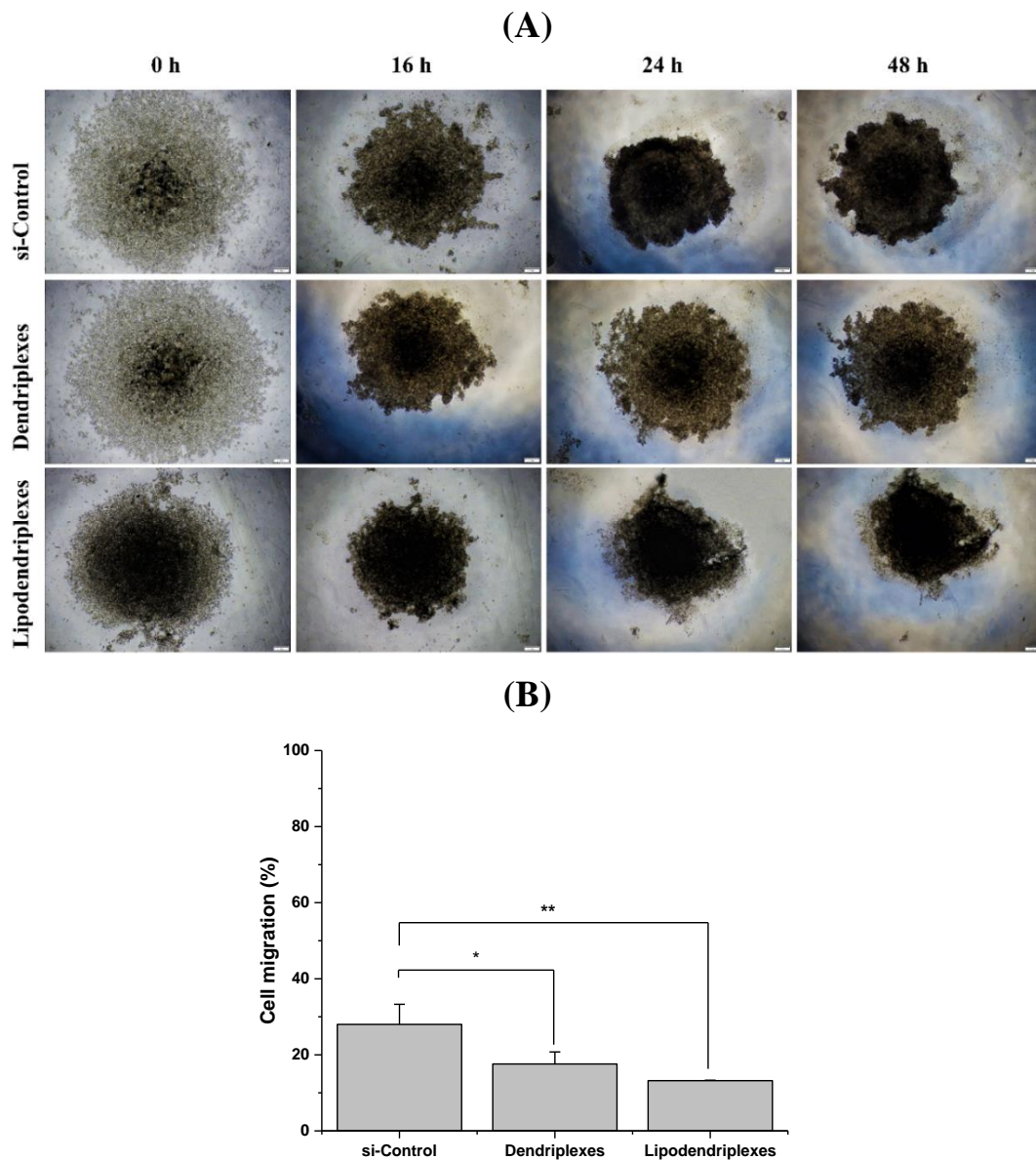


Figure 35. (A) 3D tumor spheroid cell migration assay in Caco-2 cell line of optimized dendriplexes and DPPC:CH-PAMAM lipodendriplexes (liposome to PAMAM dendrimer mass ratio 0.5; N/P ratio 12). (B) Graphical presentation of percentage of cells migration from original bioprinted area. Cells treated with lipodendriplexes containing non-specific scrambled siRNA were considered as si-Control. Scale bar represents 200 μm . Values are represented as mean \pm S.D ($n=3$) and statistical significances are indicated as * $p < 0.05$, ** $p < 0.01$.

Chapter III: Results and Discussion

3.7.5 Cytoskeleton staining of spheroids

It is difficult to handle the spheroids during the staining process. Therefore, in the case of magnetically printed spheroid for every step, including washing, fixing and staining the spheroid, magnetic drive was placed under the plate to maintain the integrity of the spheroids. The Magpen was used to lift the stained spheroid and to place them on the slide for analysis (Fig. 36).

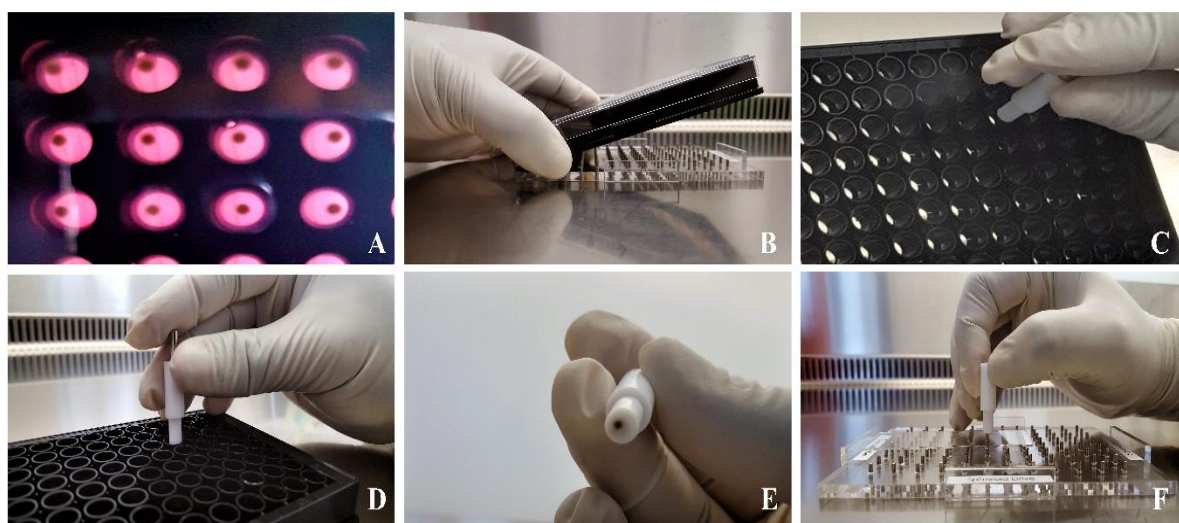


Figure 36. Steps involved in staining and transferring the 3D tumor spheroid on the glass slides. (A) Overview of spheroids in 96-well ultra-low attachment plate. (B) Placement of plate on spheroid magnetic drive to hold the spheroids during washing, fixing and staining. (C) Move the Magpen to a well of 96-well plate to pick up a spheroid. (D) Removal of Magpen out of well (with magnet) (E) A typical spheroid attached at the underside of the pen. (F) Move the Magpen (without magnet) on the glass slide to place the spheroid, under the influence of magnetic field.

The visualization of actin, in 2D culture of Caco-2 cells, was analysed in section 3.4.4 to investigate the process of actin polymerization. Similarly, the staining of actin was conducted in 3D culture to observe the distribution of cytoskeleton, responsible for cell matrix adhesion and of their shape as well. Fig. 37 illustrated that that spheroids treated with si-Control showed a loose cellular distribution due to their ability to migrate in outer media as discussed in section 3.7.4. In lipodendriplexes, after the knockdown of MDR1 gene, the intracellular layer was strongly adhered to the extracellular matrix and anchored the spheroids, responsible for the reduction in cell migration.

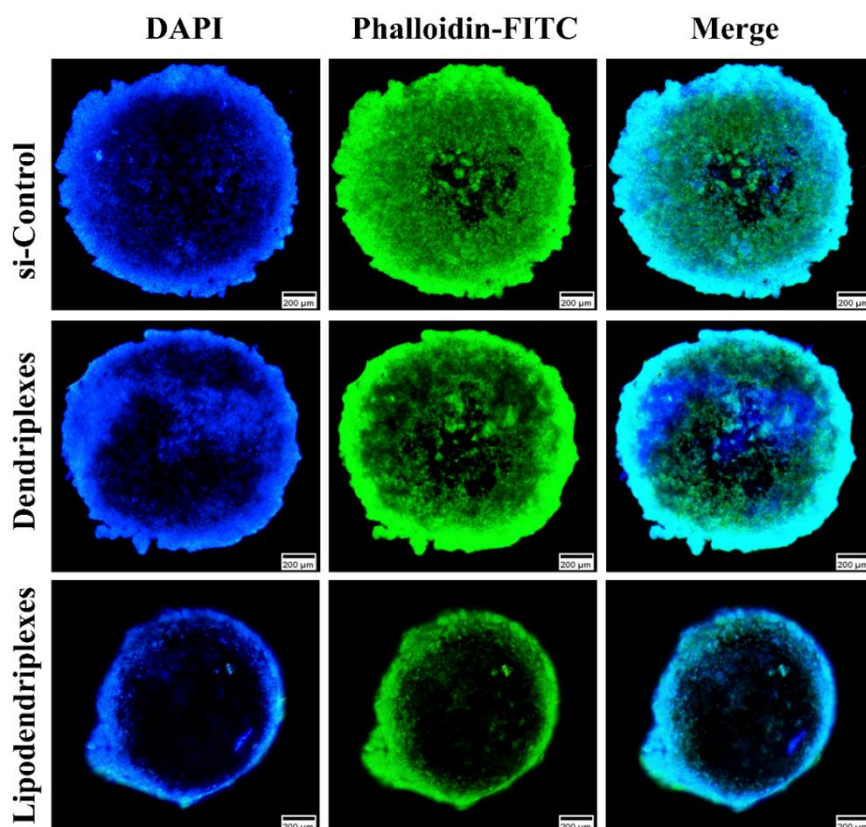


Figure 37. Cytoskeleton staining of spheroids of Caco-2 cell line of optimized dendriplexes and DPPC:CH-PAMAM lipodendriplexes (liposome to PAMAM dendrimer mass ratio 0.5; N/P ratio 12). DAPI (blue) correspond to the nuclei staining while Phalloidin FITC (green) representing the cytoskeleton staining to monitor actin polymerization. Cells treated with lipodendriplexes containing non-specific scrambled siRNA were used as si-Control. Scale bar represents 200 μm .

3.7.6 3D tumor ring closure assay

Ring closure assay is similar to a scratch closure assay in which the void circular space tends to close in 3D fashion over the specific time period [118]. Ring closure assay was performed on the magnetically levitated cells to investigate the role of MDR1 gene in cell migration using 3D bioprinted cells. The cells treated with complexes containing si-MDR1 were patterned into 3D ring structure and the ring closure was recorded for 48 h to evaluate the gene silencing effect. The rate of ring closure was determined by measuring the inner diameter of the ring at specific time intervals (0, 16, 24, 36, 48 h). The results showed that the cells treated with lipodendriplexes slower the ring closure as compared to dendriplexes and si-Control treated cells (Fig. 38). After 48 h incubation, the cells treated with si-Control shrink the ring to 92%

Chapter III: Results and Discussion

while in comparison to si-Control, a significant reduction in ring closure was found in the case of dendriplexes ($p < 0.01$) and lipodendriplexes ($p < 0.001$) with a reduction in the inner diameter of 47% and 21%, respectively (Fig. 39).

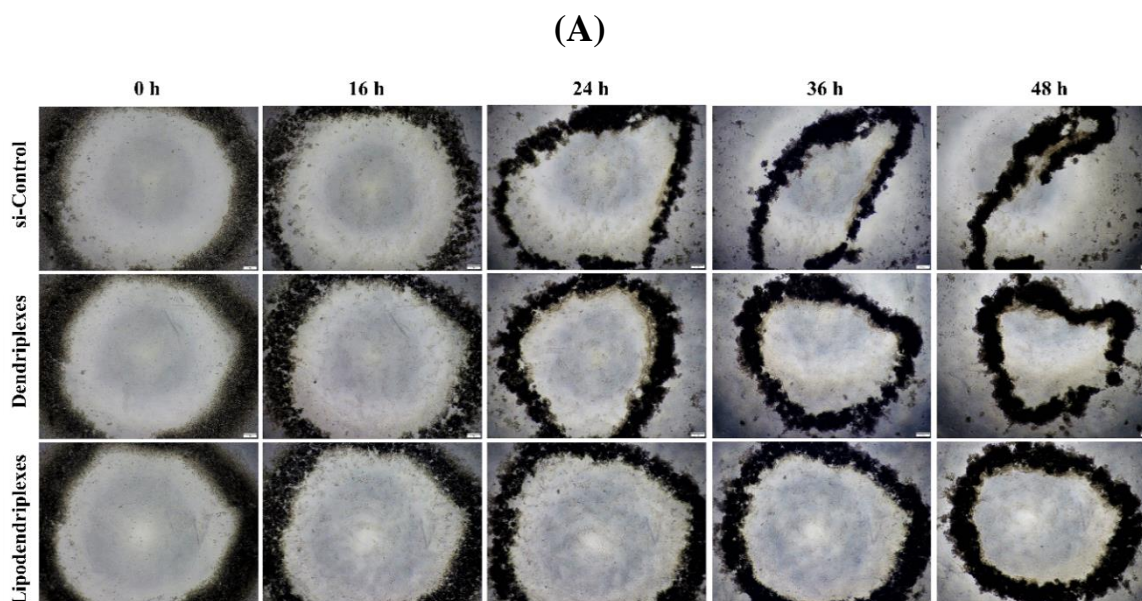


Figure 38. Micrographs of 3D tumor ring closure assay in Caco-2 cell line of optimized dendriplexes and of DPPC:CH-PAMAM lipodendriplexes (liposome to PAMAM dendrimer mass ratio 0.5; N/P ratio 12) at specified time intervals. Scale bar represents 200 μm .

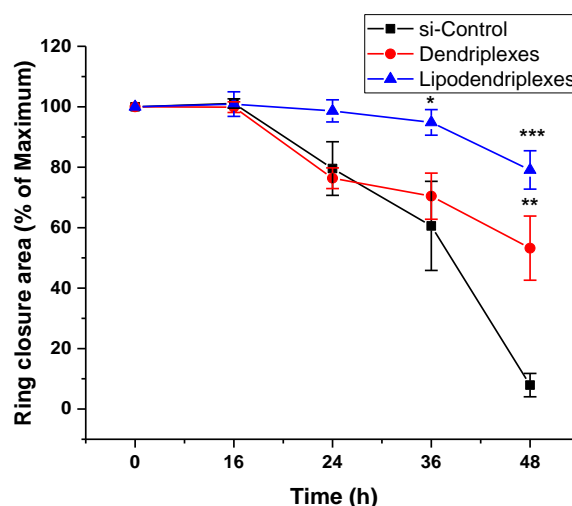


Figure 39. Graphical representation of 3D tumor ring closure assay in Caco-2 cell line of optimized dendriplexes and DPPC:CH-PAMAM lipodendriplexes (liposome to PAMAM dendrimer mass ratio 0.5; N/P ratio 12) at specified time intervals. Cells treated with lipodendriplexes containing non-specific scrambled siRNA were considered as si-Control. Values are represented as mean \pm S.D (n=3) and statistical significances are indicated as * $p < 0.05$, ** $p < 0.01$, *** $p < 0.001$.

Chapter III: Results and Discussion

3.7.7 3D tumor ring closure assay by mobile device

Ring closure area was also determined by using a less expensive mobile device in comparison to the phase contrast imaging microscope. The dark brown colouration of the ring makes it possible to capture the change in diameter in individual well on a microtiter plate (Fig. 40). It was observed that the results obtained using a mobile device were similar to the phase contrast microscope, but the lower resolution power did not provide the exact results. About 91% of ring closure was recorded in si-Control treated cells while 45% ($p < 0.01$) and 23% ($p < 0.001$) were observed in the case of dendriplexes and lipodendriplexes, respectively (Fig. 41).

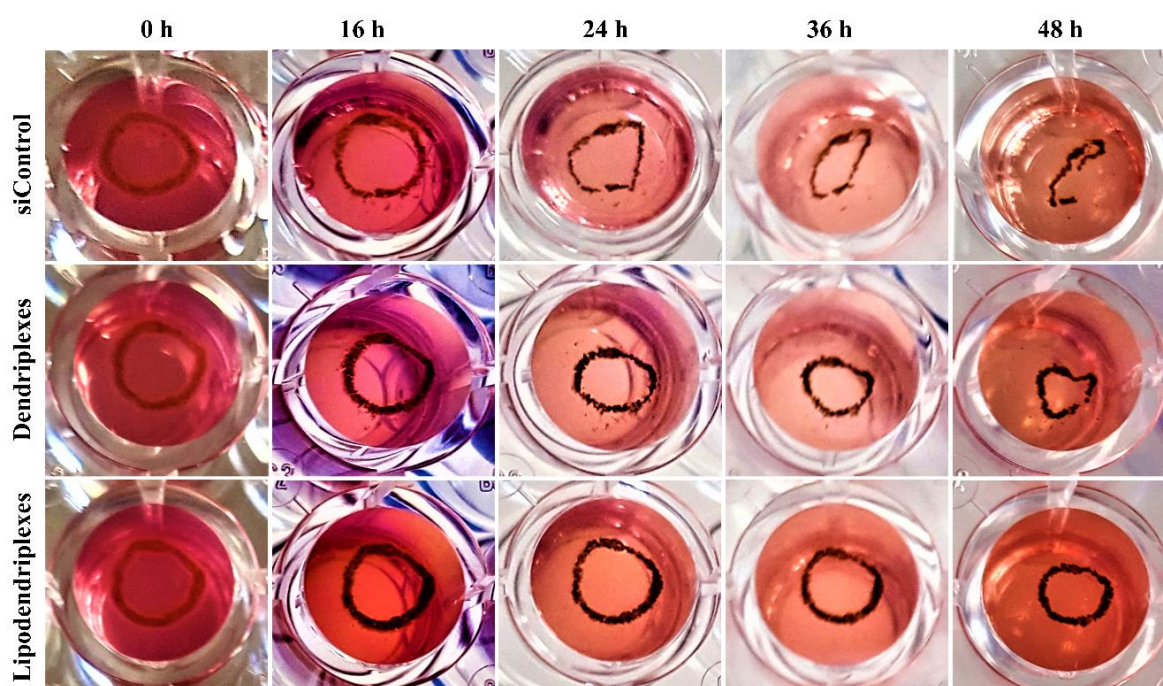


Figure 40. Analysis of 3D tumor ring closure assay by mobile device in Caco-2 cell line of optimized dendriplexes and DPPC:CH-PAMAM lipodendriplexes (liposome to PAMAM dendrimer mass ratio 0.5; N/P ratio 12) at specified time intervals. Cells treated with lipodendriplexes containing non-specific scrambled siRNA were considered as si-Control.

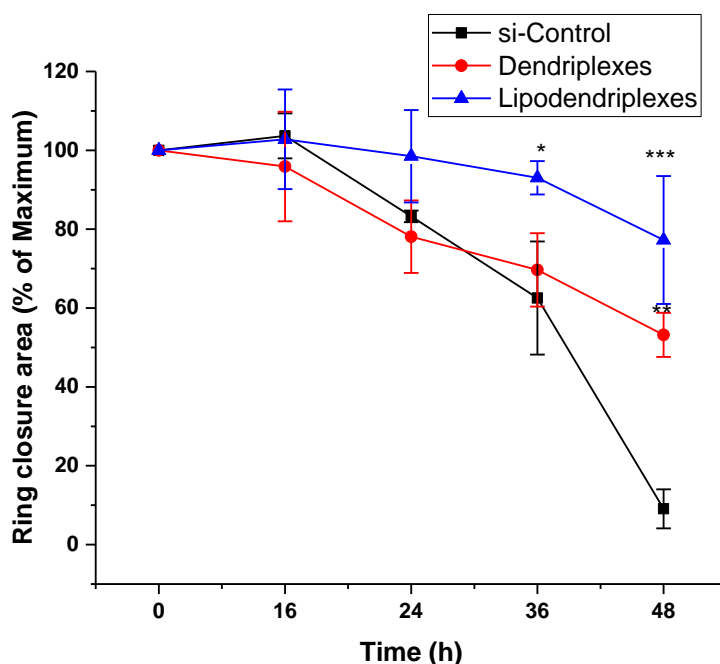


Figure 41. Graphical presentation of 3D tumor ring closure assay by mobile device in Caco-2 cell line of optimized dendriplexes and DPPC:CH-PAMAM lipodendriplexes (liposome to PAMAM dendrimer mass ratio 0.5; N/P ratio 12) at specified time intervals. Cells treated with lipodendriplexes containing non-specific scrambled siRNA were considered as si-Control. Values are represented as mean \pm S.D (n=3) and statistical significances are indicated as * $p < 0.05$, ** $p < 0.01$, *** $p < 0.001$.

3.8 Apoptosis assay by flow cytometry

A sequential treatment using RNA interference and chemotherapy provides a synergistic effect to resolve the issue of multidrug resistance [119]. The overexpression of p-glycoprotein (P-gp) on Caco-2 cells are responsible for the efflux of imatinib mesylate (IM). Therefore, the effective downregulation of P-gp can enhanced intracellular accumulation of the IM and subsequent apoptosis of the cells.

In order to investigate the apoptosis by flow cytometry (FACS), one group of the cells were incubated with si-Control, dendriplexes and lipodendriplexes and the other group of the cells were subjected to sequential treatment of si-Control, dendriplexes, lipodendriplexes followed by 75 μ M of IM. It has been observed that the downregulation of P-gp was accountable for the increased apoptosis of the cells (Fig. 42). The results of Fig. 43 showed that the cells which were only incubated with si-Control, dendriplexes and lipodendriplexes exhibited $23.5 \pm 5.5\%$, $25.3 \pm 5.7\%$ and $24.4 \pm 6.7\%$ cellular apoptosis (early + late apoptosis),

Chapter III: Results and Discussion

respectively. Contrary, a sequential treatment increased the subsequent cellular apoptosis. It has been observed that the lipodendriplexes aided sequential treatment significantly increased the apoptosis ($54.9 \pm 13.7\%$) in comparison to dendriplexes ($p < 0.05$) and si-Control group ($p < 0.001$) i.e. $35.7 \pm 23.1\%$ and $24.5 \pm 12.3\%$ respectively. Therefore, the downregulation of P-gp with the help of lipodendriplexes was responsible for re-sensitization of the cells for enhanced intracellular accumulation of drug (IM).

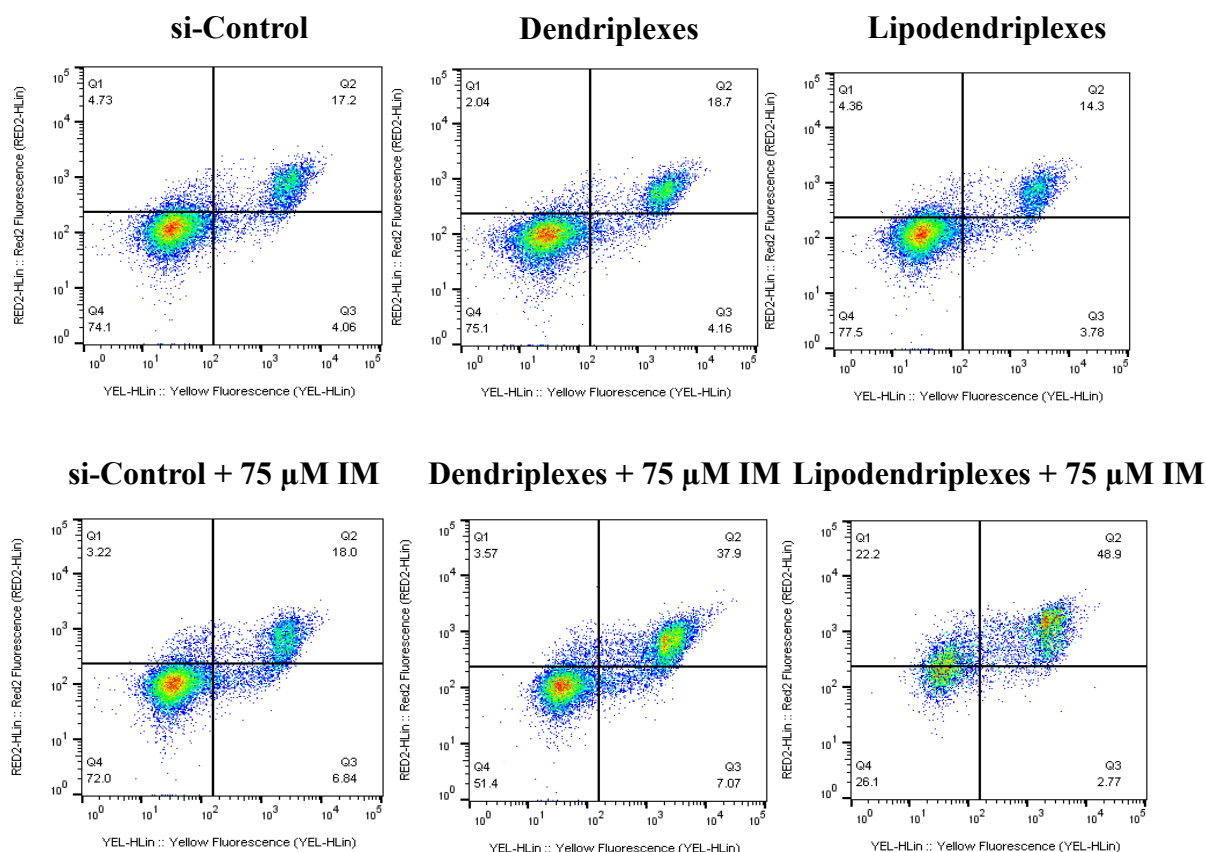


Figure 42. Apoptosis assay (FACS micrographs) in Caco-2 cell line by optimized dendriplexes and DPPC:CH-PAMAM lipodendriplexes (liposome to PAMAM dendrimer mass ratio 0.5; N/P ratio 12) without or with IM (75 μ M) treatment. Left bottom= healthy cells, right bottom= dead cells, left top= early apoptotic cells, right top= late apoptotic cells. Cells treated with lipodendriplexes containing non-specific scrambled siRNA were considered as si-Control.

Chapter III: Results and Discussion

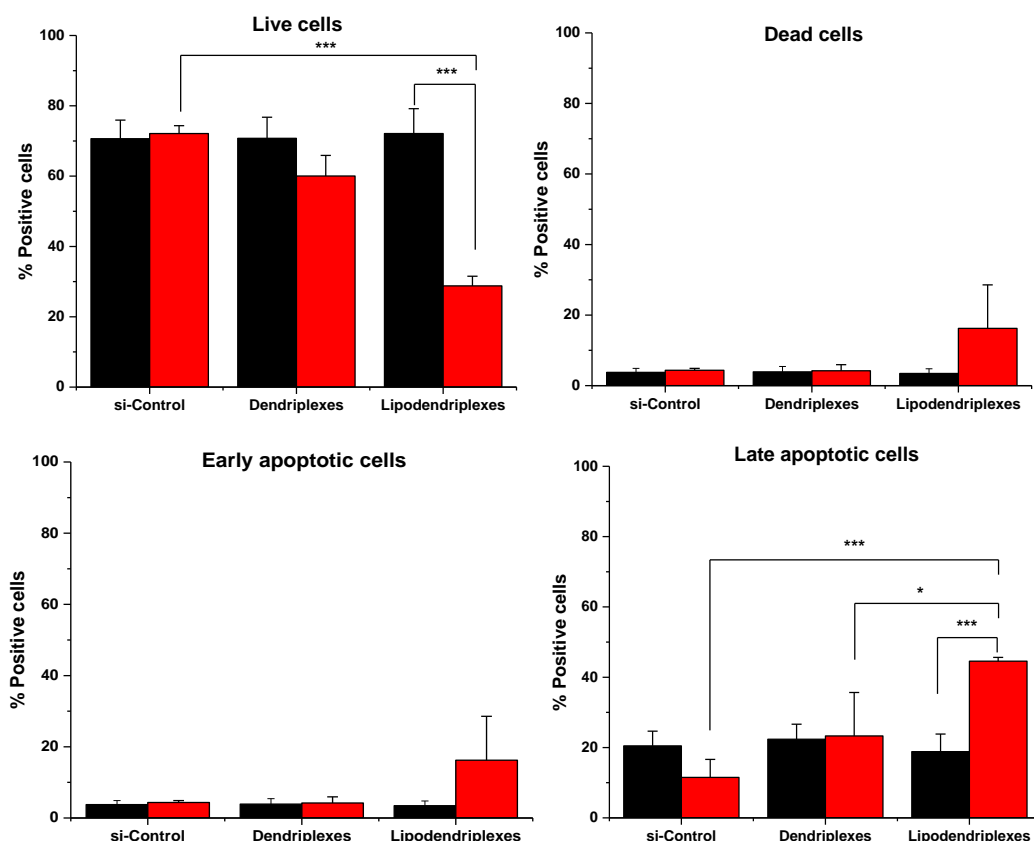


Figure 43. Apoptosis assay (graphical representation) by flow cytometry in Caco-2 cell line by optimized dendriplexes and DPPC:CH-PAMAM lipodendriplexes (liposome to PAMAM dendrimer mass ratio 0.5; N/P ratio 12) without or with IM (75 μ M) treatment. Graphical representation of % positive cells (live, dead, early apoptotic and late apoptotic, respectively). Black bar graph; cells incubated only with si-Control, dendriplexes and lipodendriplexes. Red bar graph; cells incubated with sequential treatment with si-Control, dendriplexes and lipodendriplexes for 48 h and then with IM (75 μ M) for 24 h. Cells treated with lipodendriplexes containing non-specific scrambled siRNA were considered as si-Control. Values are represented as mean \pm S.D (n=3) and statistical significances are indicated as *p < 0.05, ***p < 0.001.

3.9 Apoptosis determination of spheroids by live dead viability assay

In contrast to 2D culture, the live dead viability assay was performed in 3D tumor spheroidal model for apoptosis investigation. The live cells were stained with syto 9 while dead and late apoptotic cells were stained with PI. For the apoptotic determination, the equilibrated spheroids of si-Control, dendriplexes and lipodendriplexes were incubated with IM (75 μ M) or without IM treatment for 24 h. The spheroids only incubated with si-Control, dendriplexes and

Chapter III: Results and Discussion

lipodendriplexes maintain their cellular integrity and showed a dense outer layer of live cells, with a small portion of dead cells while the IM treated spheroids exhibited a change in shape depicted a hollow cellular structure, indicating the loss of cell fragments from spheroids. Results of Fig. 44 showed that after the IM treatment, the lipodendriplexes treated cells exhibited maximum apoptotic effects and showed an enhanced red fluorescence of PI channel in spheroidal structure as compared to dendriplexes and si-Control treated group. These results further confirmed the enhanced intracellular accumulation of IM following the efficient knockdown by lipodendriplexes system. These results were in good correlation with the results obtained from apoptosis assay in 2D culture.

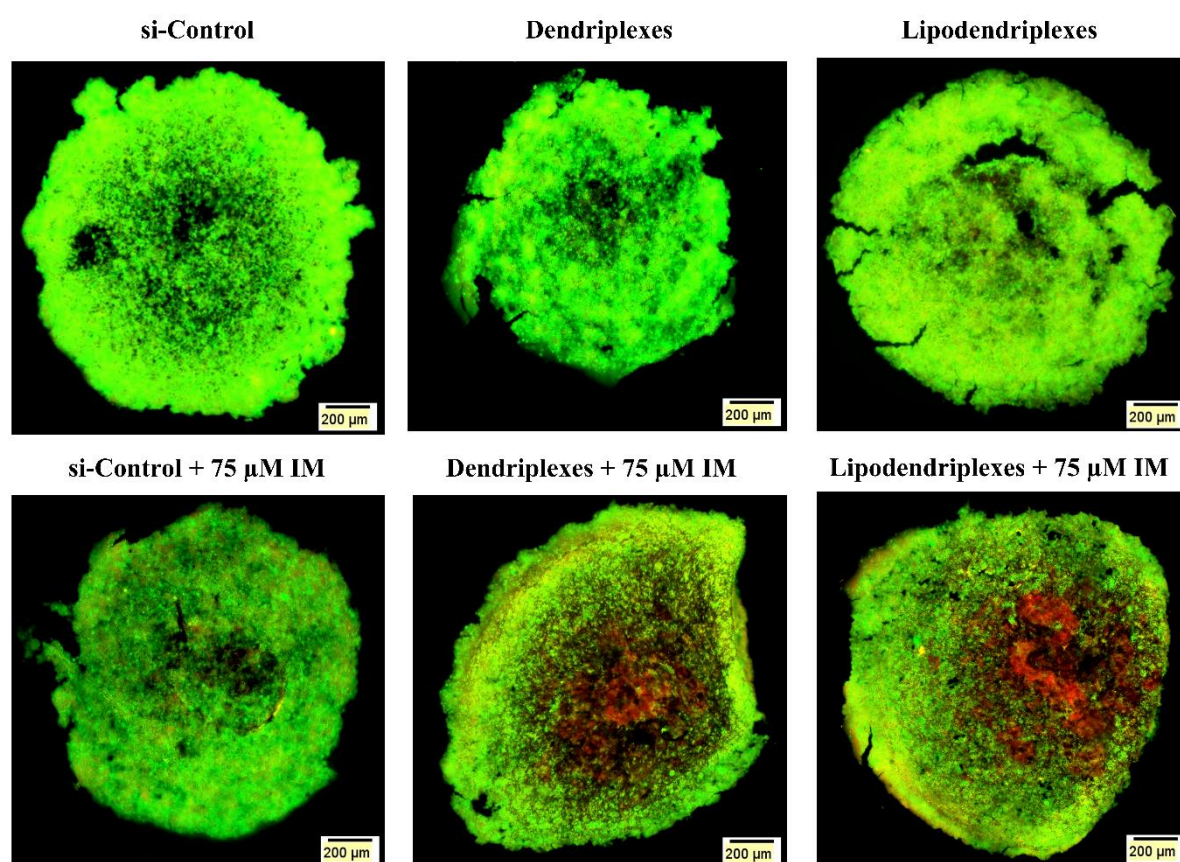


Figure 44. Live dead viability assay of spheroids for apoptosis determination by fluorescence microscopy in Caco-2 cell line of optimized dendriplexes and DPPC:CH-PAMAM lipodendriplexes (liposome to PAMAM dendrimer mass ratio 0.5; N/P ratio 12) without or with IM (75 μ M) treatment. Green fluorescence (syto 9) representing the live cells while red fluorescence (PI) indicating dead and late apoptotic cells. Cells treated with lipodendriplexes containing non-specific scrambled siRNA were considered as si-Control. Scale bar represents 200 μ m.

Chapter III: Results and Discussion

3.10 Cell cycle analysis and accumulation of Sub-G1 phase

The cell cycle analysis was performed to determine the cell phase distribution by flow cytometry analysis. Results of Fig. 45 depicted the effective downregulation of P-gp expression contributes to the apoptosis induced by IM and arrest the cell cycle at Sub-G1 phase [120]. Fig. 46 showed that the cells incubated with si-Control, dendriplexes and lipodendriplexes exhibited $12.0 \pm 5.5\%$, $8.6 \pm 3.5\%$ and $14.2 \pm 7.7\%$ Sub-G1 phase distribution. While an increased percentage in Sub-G1 phase was observed after the sequential treatment, depicting an increased Sub-G1 phase with lipodendriplexes treated group ($34.7 \pm 10.3\%$) in comparison to dendriplexes ($28.2 \pm 4.4\%$) and si-Control groups ($23.4 \pm 3.7\%$). These findings suggest that enhanced intracellular accumulation of IM arrests Caco-2 cells at the Sub-G1 phase and inhibit the cell cycle progression.

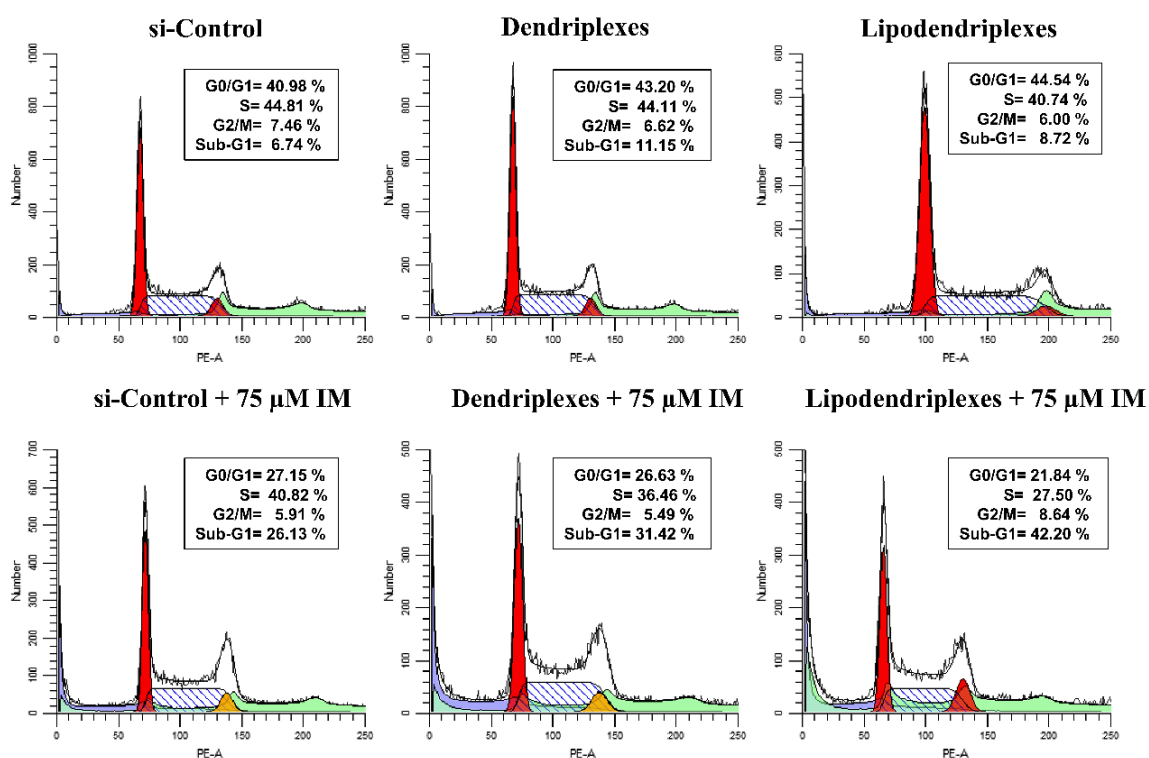


Figure 45. Cell cycle analysis (FACS micrographs) by flow cytometry in Caco-2 cell line by optimized dendriplexes and DPPC:CH-PAMAM lipodendriplexes (liposome to PAMAM dendrimer mass ratio 0.5; N/P ratio 12) without or with IM (75 μ M) treatment. Cells treated with lipodendriplexes containing non-specific scrambled siRNA were considered as si-Control.

Chapter III: Results and Discussion

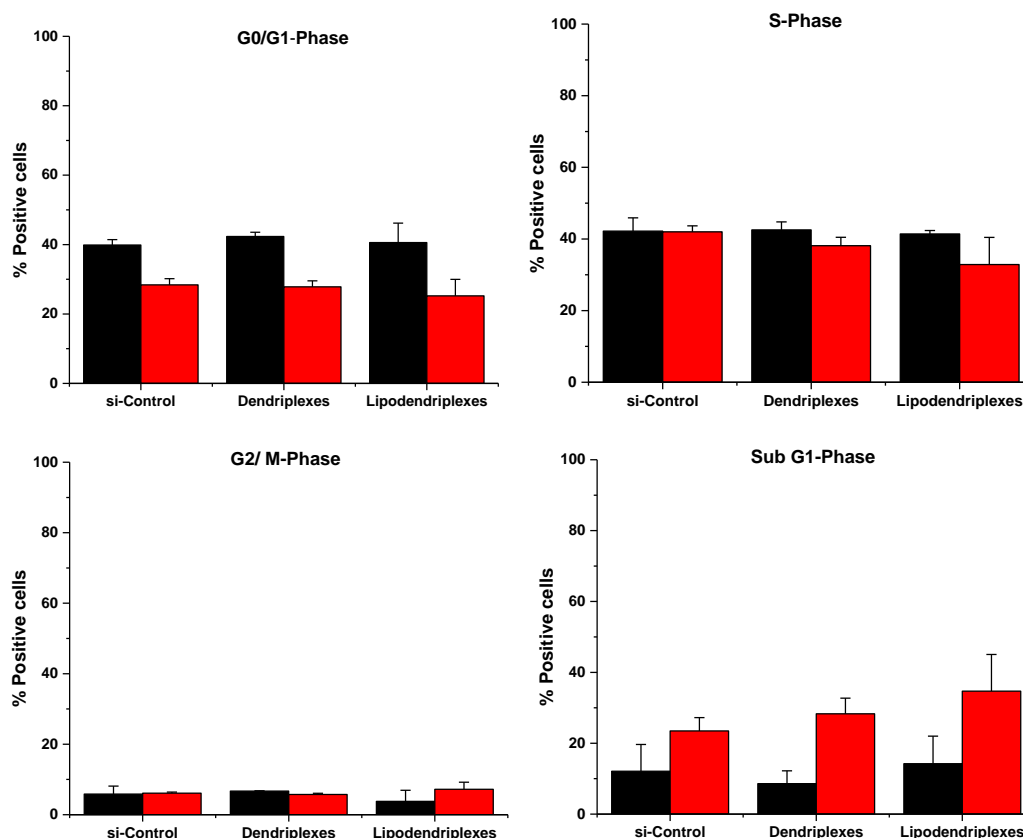


Figure 46. Cell cycle analysis (graphical representation) by flow cytometry in Caco-2 cell line by optimized dendriplexes and of DPPC:CH-PAMAM lipodendriplexes (liposome to PAMAM dendrimer mass ratio 0.5; N/P ratio 12) without or with IM (75 μ M) treatment. Graphical representation of % positive cells (G0/G1, S, G2/ M and Sub-G1 phases, respectively). Black bar graph; cells incubated only with si-Control, dendriplexes and lipodendriplexes. Red bar graph; cells incubated with sequential treatment with si-Control, dendriplexes and lipodendriplexes for 48 h followed by IM (75 μ M) for further 24 h. Cells treated with lipodendriplexes containing non-specific scrambled siRNA were considered as si-Control. Values are represented as mean \pm S.D (n=2).

3.11 *In ovo* chorioallantoic membrane (CAM) analysis

According to the strategy of 3Rs principle (i.e. replacement, refinement, and reduction), different alternative methods should be used to avoid the unethical use of animals. Therefore, at the initial level of research, an alternative method should be first evaluated, which can reduce the exposure of testing drug products on laboratory animal [121]. In the present study, the chorioallantoic membrane (CAM) model was used to evaluate the GFP expression and safety profile of the dendriplexes and lipodendriplexes. The results showed that the lipodendriplexes

Chapter III: Results and Discussion

exhibited an enhanced GFP expression as compared to its parent dendriplexes. The GFP expression was observed in the epithelial cells (Fig. 47). Similar results were obtained by Baghdan et al. [122]. In addition, 48 h post-transfection, the optimized complexes did not produce any toxicity in the developing embryo and showed no injury of the CAM microvasculature. Thereby, the optimized lipodendriplexes exhibited transfection efficiency with a good safety profile *in ovo* environment.

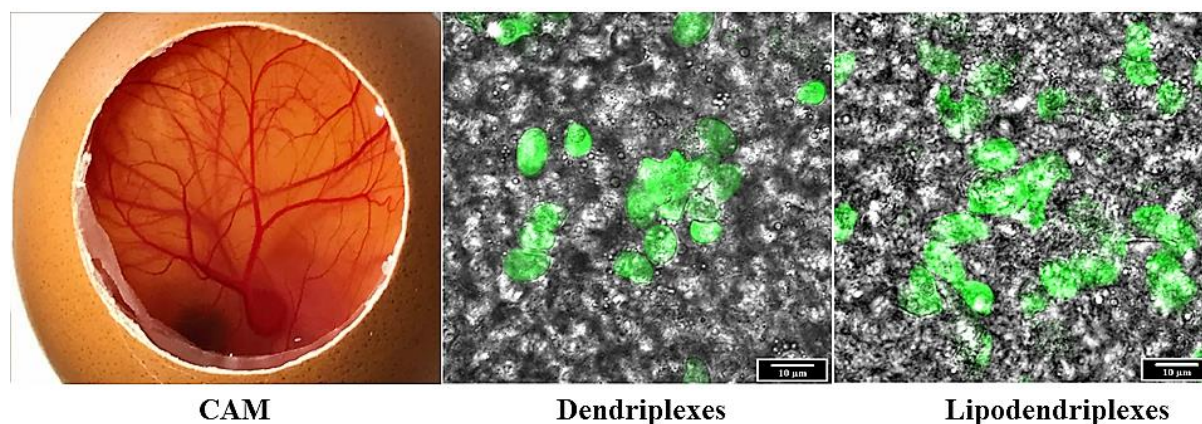


Figure 47. Apical view of CAM on the egg development day 11 and CLSM micrographs of GFP expression in CAM (epithelial cells) with optimized dendriplexes and DPPC:CH-PAMAM lipodendriplexes (liposome to PAMAM dendrimer mass ratio 0.5; N/P ratio 12). Green channel represents GFP expression. Scale bar represents 10 μm.

3.12 *In vivo* experiments

3.12.1 Acute *in vivo* toxicity

3.12.1.1 Body weight and behaviour monitoring

Acute *in vivo* toxicity was investigated in mice following *i.v.* injection of optimized complexes (dendriplexes and lipodendriplexes) containing at 10 μg of pDNA by tail vein route and compared to untreated group. The animal body weight was monitored daily for 7 days. There was no significant difference in the body weight found during the experimental period in both treated and untreated groups as shown in Fig. 48. The survival rate was 100% with no alteration in physical and social behaviours among the animals.

(A)



(B)

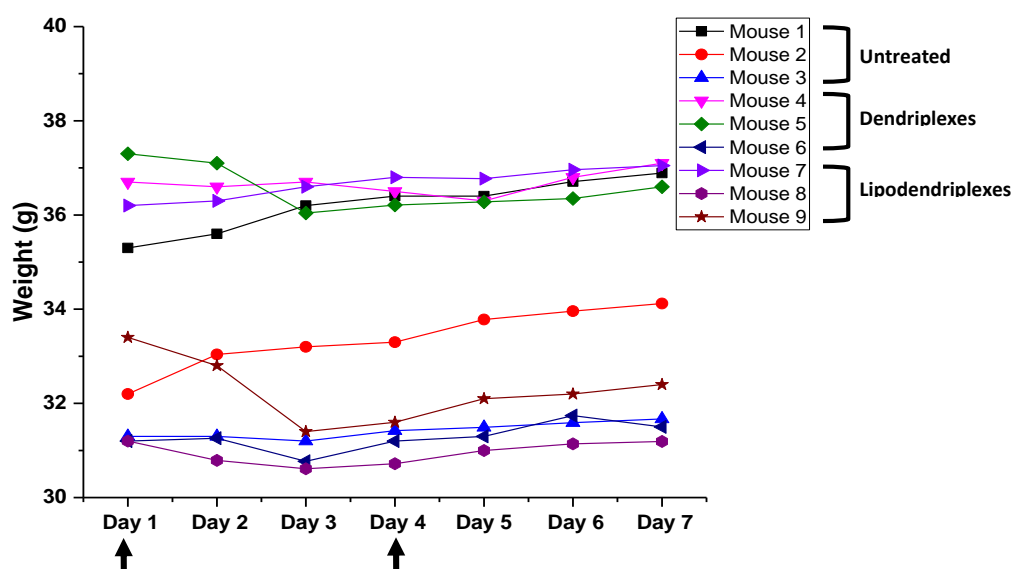


Figure 48. (A) Process of: *i.v.* administration, blood collection by cardiac puncture and sacrifice of mice by cervical dislocation method, respectively (B) Changes in body weight of mice for 7 days in untreated group (mice 1-3) and after the administration of the complexes containing 10 μg of pDNA (mice 4-6 dendriplexes and mice 7-9 lipodendriplexes of DPPC:CH-PAMAM; liposome to PAMAM dendrimer mass ratio 0.5 with N/P ratio 12). No changes in body weight of the mice were observed. (Arrows representing the repeated dose).

3.12.1.2 Organ to body ratio

At the termination of the study, mice were sacrificed by cervical dislocation and the major vital organs were carefully removed to calculate the organ index of heart, lungs, liver, spleen and kidneys. No significant increase in the organs index was found after the treatment with dendriplexes and lipodendriplexes except in the liver index, which was significantly reduced

Chapter III: Results and Discussion

after treatment with dendriplexes as depicted in Fig. 49. The results showed that the liver to body index in dendriplexes treated group was $4.9 \pm 0.6\%$ which was significantly less ($p < 0.05$) than the liver index of untreated group (i.e. $6.2 \pm 0.5\%$). PAMAM dendrimers induced autophagy process could be responsible for a reduced liver weight of the mice [68].

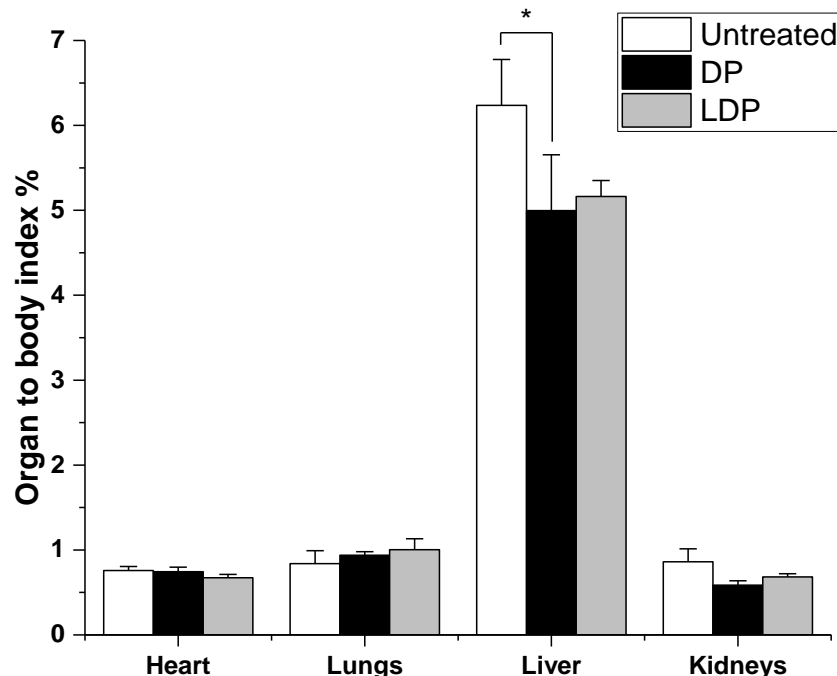


Figure 49. The organ to body index (%) of untreated group (white bar graph) and treated groups (dendriplexes (DP): black graph bar; lipodendriplexes (LDP): grey bar graph) after the sacrifice of animals by cervical dislocation. Values are represented as mean \pm S.D (n=3) and statistical significance is indicated as * $p < 0.05$.

3.12.1.3 Serum biochemistry analysis

Results of serum biochemistry markers showed a significant increase ($p < 0.001$) in the levels of alanine aminotransferase (ALT), aspartate aminotransferase (AST) and alkaline phosphatase (ALP) in dendriplexes treated group, as compared to lipodendriplexes treated and untreated groups as depicted in Fig. 50 A-C. In case of dendriplexes treated group, hepatocellular injury and necrosis may be responsible for an increased leakage of ALT and AST in the bloodstream while an increase in the level of ALP suggested a bile obstruction in the bile duct. Significant elevation in total bilirubin ($p < 0.001$) was also associated with hepatotoxicity induced by dendriplexes in comparison to other groups. Changes in blood glucose and total protein level by dendriplexes group were also indicated some of their interference with the liver functioning

Chapter III: Results and Discussion

and glucose metabolism (Fig. 51 A-C). The level of blood urea nitrogen and creatinine was also higher in dendriplexes treated groups, indicating the decreased efficiency of glomerulus or proximal tubule (Fig. 52 A-B). These findings were in agreement with the studies conducted by Tang et al. and Wang et al. [123, 124].

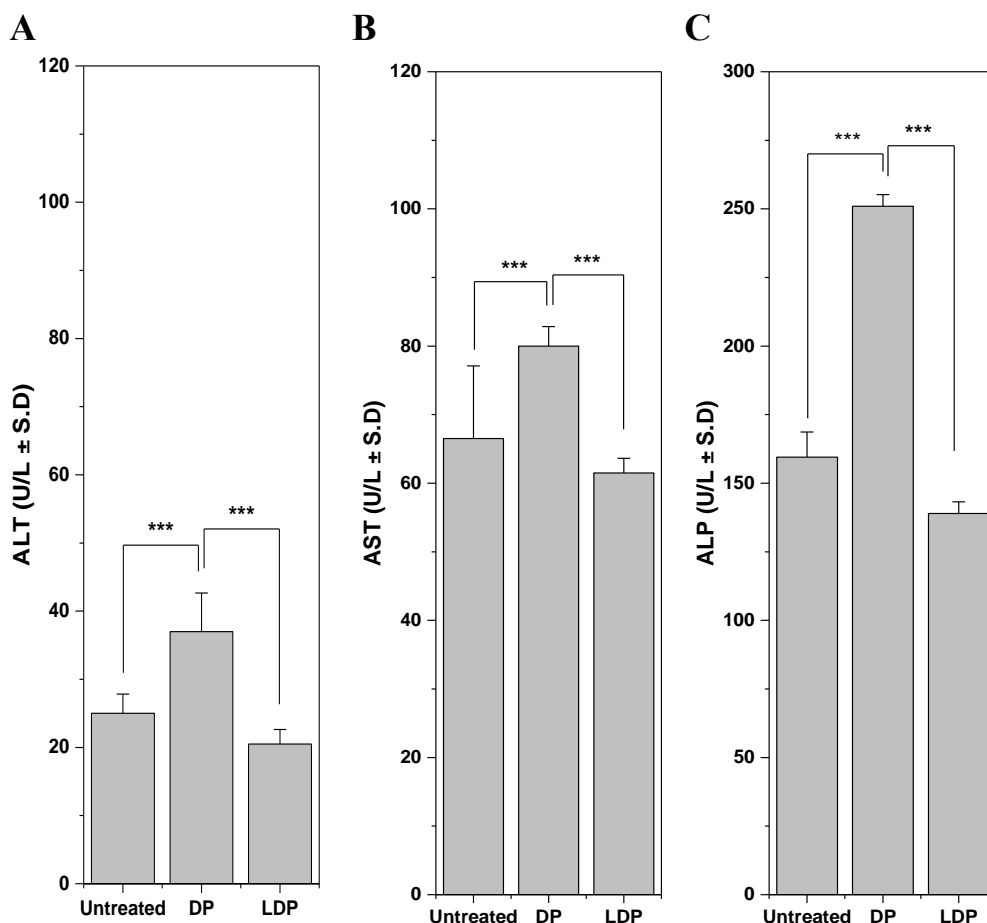


Figure 50. Typical liver function tests (LFTs) parameters including (A) ALT, (B) AST and (C) ALP levels of untreated group and after *i.v.* administration of the complexes containing 10 μg of pDNA (dendriplexes (DP) and lipodendriplexes of DPPC:CH-PAMAM (LDP); liposome to PAMAM dendrimer mass ratio 0.5 with N/P ratio 12). Values are represented as mean \pm S.D (n=3) and statistical significance is indicated as ***p < 0.001.

Chapter III: Results and Discussion

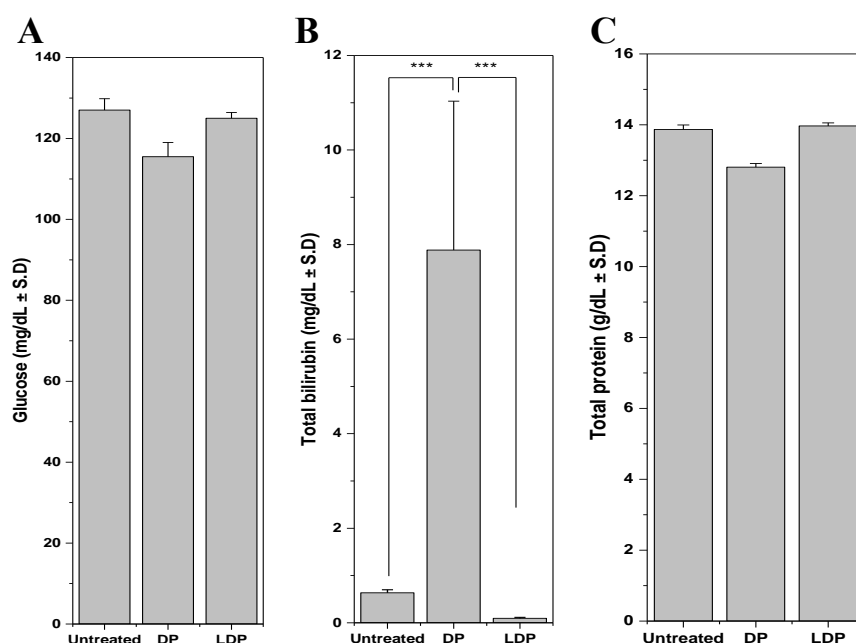


Figure 51. Typical serum biochemical parameters including (A) blood glucose, (B) total bilirubin and (C) total protein parameters of untreated group and after *i.v.* administration of the complexes containing 10 μg of pDNA (dendriplexes (DP) and lipodendriplexes of DPPC:CH-PAMAM (LDP); liposome to PAMAM dendrimer mass ratio 0.5 with N/P ratio 12). Values are represented as mean \pm S.D (n=3) and statistical significance is indicated as *** $p < 0.001$.

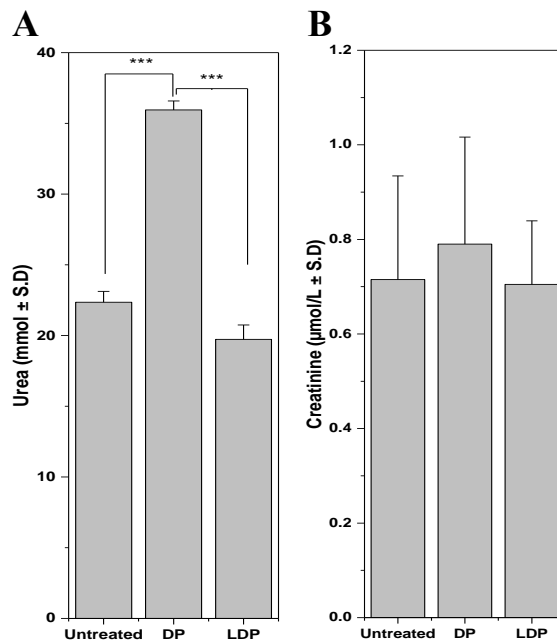


Figure 52. Typical renal function tests (RFTs) parameters including (A) blood urea nitrogen and (B) creatinine levels of untreated group and after *i.v.* administration of the complexes containing 10 μg of pDNA (dendriplexes (DP) and lipodendriplexes of DPPC:CH-PAMAM (LDP); liposome to PAMAM dendrimer mass ratio 0.5 with N/P ratio 12). Values are represented as mean \pm S.D (n=3) and statistical significance is indicated as *** $p < 0.001$.

Chapter III: Results and Discussion

3.12.1.4 Hematological evaluation

In hematological analysis, the major biomarkers including red blood cells count (RBCs), hematocrit (HCT), white blood cells count (WBCs), hemoglobin (Hb), mean corpuscular volume (MCV), neutrophils, eosinophils, lymphocytes, monocytes, platelets count (PLT), mean corpuscular hemoglobin (MCH), mean corpuscular hemoglobin concentration (MCHC), mean platelet volume (MPV) and percentage of neutrophils, monocytes, lymphocytes, eosinophils were monitored (Table 2). The results revealed the cationic dendriplexes triggered hemolysis of RBCs, which was depicted by a lower RBC and hematocrit count with a decreased level of Hb. While lipodendriplexes exhibited a slight decrease in Hb level in comparison to untreated groups. Total leukocytes count was increased in both treated groups in comparison to untreated group, which has suggested the induction of some acute inflammatory response by the immune system. Neutropenia was observed in both treated group while an increase in lymphocytes was monitored in dendriplexes treated group. It was also observed that in the case of dendriplexes treated group the PLT count was high stating the role of cationic PAMAM dendrimers in activation of platelets and in blood clot formation. This finding was in agreement with the results obtained by Jones et al. [125].

Table 2. Hematological parameters of mice in treated (dendriplexes, lipodendriplexes) and untreated group (mean± S.D) (n=3).

Blood parameter	Untreated	Dendriplexes	Lipodendriplexes
Hb (g/dl)	12.9 ± 1.4	12.1 ± 2.0	12.6 ± 1.6
WBCs (10 ⁹ /L)	3.2 ± 1.2	4.4 ± 1.6	6.4 ± 0.8
RBCs (10 ¹² /L)	7.1 ± 1.2	6.6 ± 1.2	7.19 ± 1.9
HCT (PCV) %	35.6 ± 6.8	33.5 ± 6.2	39.2 ± 7.1
MCV (fl)	49.6 ± 5.2	50.0 ± 6.0	54.5 ± 5.6
MCH (pg)	18.0 ± 2.7	18.0 ± 3.1	17.5 ± 1.8
MCHC %	36.3 ± 8.5	36.1 ± 7.4	32.1 ± 8.1
PLT (10 ⁹ /L)	747.0 ± 25.2	794.0 ± 36.4	731.0 ± 19.2
Neutrophils %	10.0 ± 1.3	2.0 ± 1.4	2.0 ± 1.0
Lymphocytes %	80.0 ± 9.4	95.0 ± 10.7	88.0 ± 8.1
Monocytes %	7.0 ± 1.6	2.0 ± 0.5	8.0 ± 1.1
Eosinophils %	3.0 ± 0.8	1.0 ± 0.4	2.0 ± 0.4

Chapter III: Results and Discussion

3.12.1.5 Erythrocytes aggregation assay

An erythrocyte aggregation analysis was performed to check the *ex vivo* behaviour of complexes on the blood cells. The dendriplexes treatment with erythrocytes exhibited a high level of aggregation with some hemolysis of the cells while the lipodendriplexes exhibited very low levels of interaction among the erythrocytes (Fig. 53). Similar work was done by Ewe et al. [126].

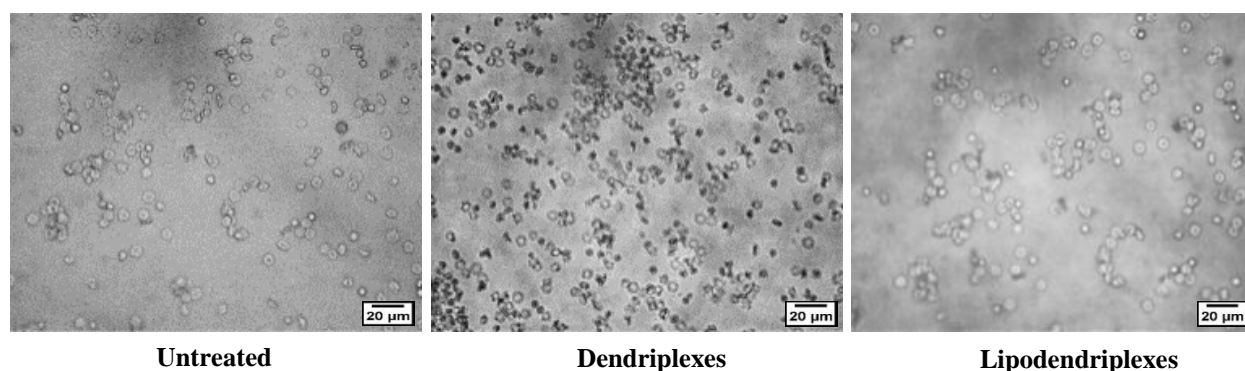


Figure 53. *Ex vivo* erythrocytes aggregation assay after treatment of complexes (dendriplexes and lipodendriplexes of DPPC:CH-PAMAM; liposome to PAMAM dendrimer mass ratio 0.5 with N/P ratio 12) with 100 µl of erythrocytes suspension (2% v/v) compared to untreated cells. Scale bar represents 20 µm.

3.12.1.6 Histopathology of vital organs

Histopathological analysis of major organs was done using H & E stained tissue sections (Fig. 54). No discriminable changes were seen among the vital organs (heart, lung, and kidneys) of all groups. However, some scattered hepatocytic necrosis dots with pronounced vacuolization were observed in the dendriplexes treated group, indicating PAMAM dendrimers induced damages of the liver tissue. In the case of dendriplexes treated group some thickness in the glomerulus was also observed. These hepatic damage and glomerulus thickness by dendriplexes were in compliance with the results, illustrated in Fig. 51 & 52, showed the high bilirubin, blood urea nitrogen and creatinine levels, respectively. There was no renal toxicity observed in the untreated and lipodendriplexes treated groups.

Chapter III: Results and Discussion

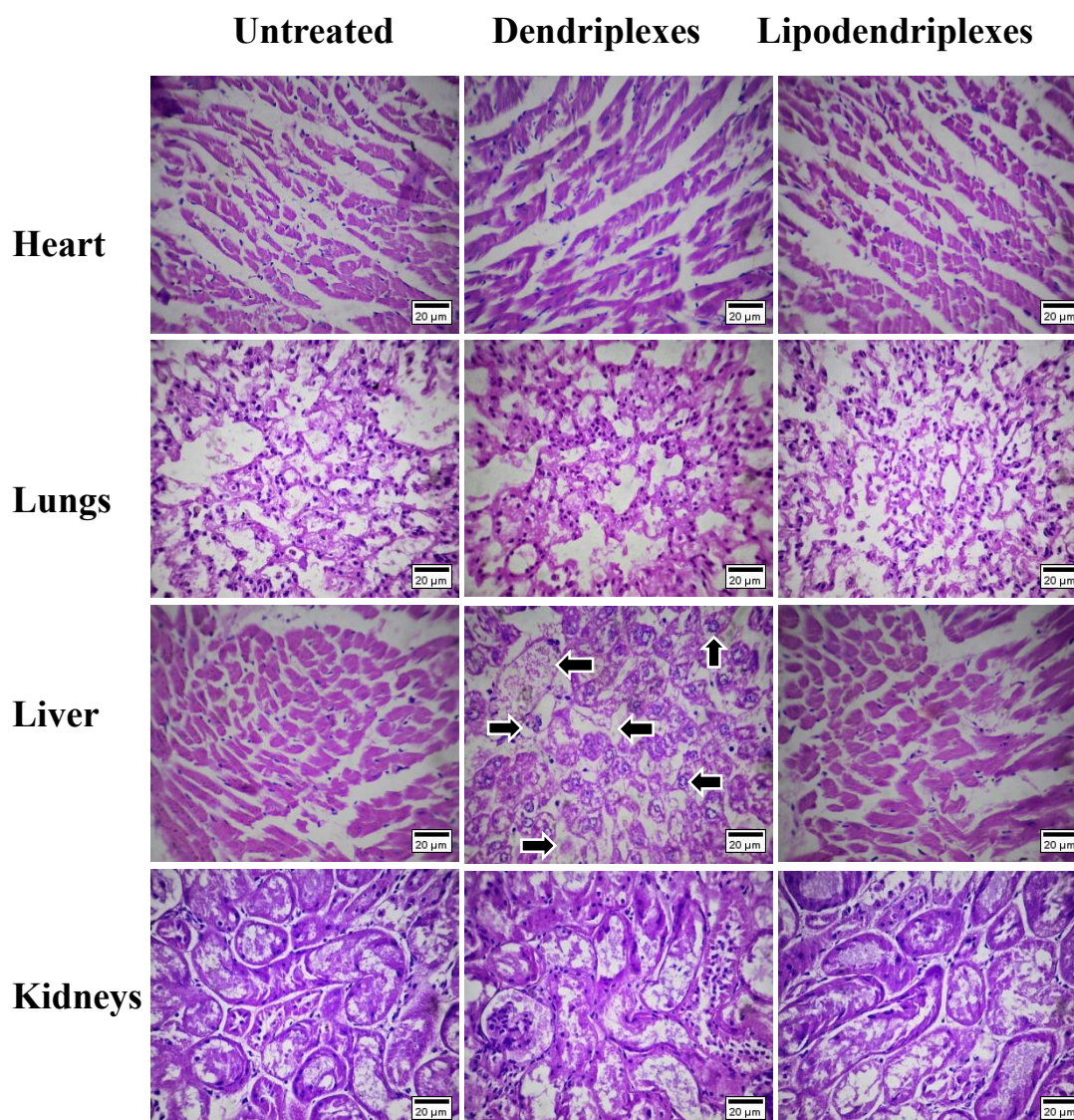


Figure 54. Histopathology studies: H & E stained sections of vital organs from mice (heart, lungs, liver and kidney) of untreated group and after *i.v.* administration of the complexes containing 10 μg of pDNA (dendriplexes and lipodendriplexes of DPPC:CH-PAMAM; liposome to PAMAM dendrimer mass ratio 0.5 with N/P ratio 12). All images were taken at 40 x magnification. Scale bar represents 20 μm .

Results of *in vitro* and acute *in vivo* toxicity showed that the lipid modification of cationic dendriplexes markedly reduces the toxic properties of naked dendriplexes such as their cytotoxicity towards cultured cells, blood cells and in vital organs as well [127].

Chapter III: Results and Discussion

3.12.2 *In vivo* biodistribution and imaging analysis

The precise biodistribution of GFP labeled DNA complexes following *i.v.* administration was assessed in vital organs, using a fluorescence iBox[®] Explorer2[™] imaging system. The images of the dissected organs were taken 24 h after the administration of the complexes to detect the fluorescence signals of GFP expression. The higher fluorescence signals of GFP expression were observed in liver, lungs, kidneys and heart as shown in Fig. 55 A. In case of dendriplexes the highest signals were detected in liver ($24,606 \pm 1,047$ a.u. per organ), followed by the lungs ($19,953 \pm 3,028$ a.u. per organ), kidneys ($7,652 \pm 1,016$ a.u. per organ), heart ($4,923 \pm 287$ a.u. per organ) and then in spleen ($4,421 \pm 932$ a.u. per organ). The liposome modification with dendriplexes significantly increases the fluorescence intensity in all organs, except the spleen, in comparison to naked dendriplexes. The fluorescence signals in the liver appeared to be highest with lipodendriplexes treatment ($1,43,916 \pm 15,876$ a.u. per organ), followed by lungs ($54,517 \pm 4,552$ a.u. per organ), kidneys ($41,582 \pm 3,804$ a.u. per organ), heart ($10,483 \pm 698$ a.u. per organ) and then in spleen ($4,623 \pm 932$ a.u. per organ) (Fig. 55 B).

In vivo biodistribution of dendriplexes exhibited low gene expression, which was due to the rapid plasma clearance by reticuloendothelial system (RES) sites. Less uptake of dendriplexes was also due to possible interaction of some anionic blood and cell membranes components with the terminal amino groups on the complexes, to get clearance from blood circulation. The short blood circulation time limits the possibility of effective delivery of dendriplexes. However, the protective shielding of liposome over the dendriplexes exhibited an increased cellular uptake with prolonged circulation time and decreased clearance. Similar results were described by Ko et al. [128].

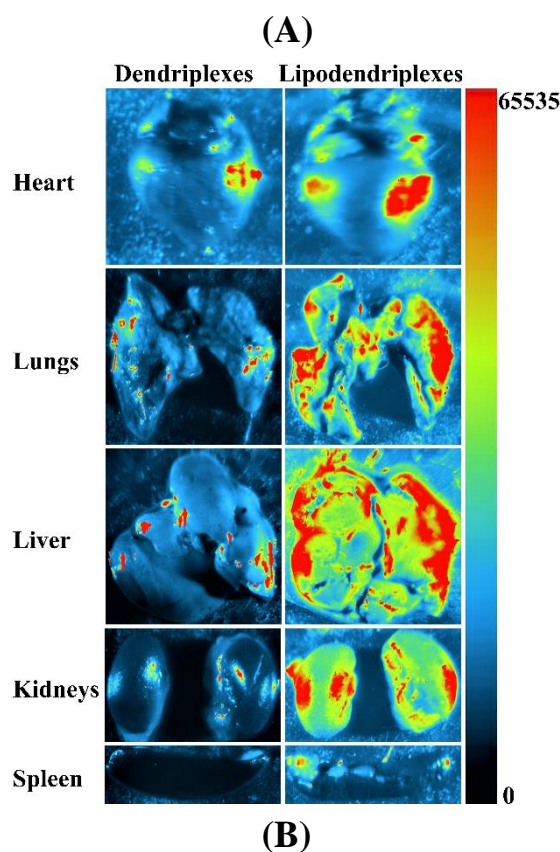


Figure 55. (A) *Ex vivo* fluorescence images of vital organs (heart, lungs, liver, kidneys and spleen) after *i.v.* administration of the complexes containing 10 μg of pCMV-GFP (dendriplexes and lipodendriplexes of DPPC:CH-PAMAM; liposome to PAMAM dendrimer mass ratio 0.5 with N/P ratio 12). The mice were sacrificed 24 h after the administration of the complexes. The organs were collected carefully and washed with normal saline to remove any blood traces. Fluorescence intensity is demonstrated by a color scale bar (red depicting maximum fluorescence intensity; 65535, while dark blue is minimum fluorescence intensity; 0) and (B) quantitative biodistribution (fluorescence intensity a.u.) of pCMV-GFP labeled DNA complexes in vital organs. Values are represented as mean \pm S.D (n=3) and statistical significances are

Chapter III: Results and Discussion

indicated as ** $p < 0.01$, *** $p < 0.001$. (Black graph bar represents dendriplexes (DP) and grey bar graph represents lipodendriplexes (LDP)).

3.12.3 Frozen tissues GFP distribution analysis

To investigate the GFP biodistribution in vital organs, a less expensive *ex vivo* fluorescence imaging technique was employed, using thin frozen sections of the organs. It has been observed that a marked distribution of GFP fluorescence was observed in all organs but with of different intensity. Results of Fig. 56 showed the same pattern of GFP expression, as observed in section 3.12.2. The highest no. of green fluorescent signals was detected in liver followed by the lungs, kidneys, heart and then in spleen, respectively. These results also indicated that lipid modified complexes contributes to the efficient cellular internalization of the cargo as compared to naked dendriplexes system.

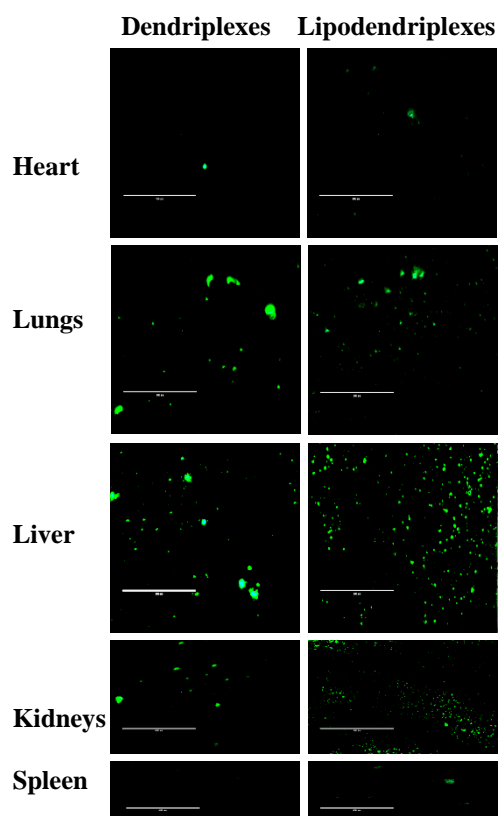


Figure 56. *Ex vivo* fluorescence imaging in the frozen thin section of dissected vital organs (heart, lungs, liver, kidneys and spleen) after *i.v.* administration of the complexes containing 10 μg of pCMV-GFP (dendriplexes and lipodendriplexes of DPPC:CH-PAMAM; liposome to PAMAM dendrimer mass ratio 0.5 with N/P ratio 12). Green spots indicating the GFP expression in the cells. Scale bar represents 100 μm

Chapter IV: Summary and outlook

Chapter IV: Summary and Outlook

4.1 Summary and outlook

The main objective of the current study was to develop an optimized system for enhanced nucleic acid delivery with minimum cytotoxicity. For efficient therapeutic gene delivery, PAMAM dendrimer, with ethylenediamine core was chosen due to its biodegradable and non-immunogenic nature. However, the cytotoxicity and unusual biodistribution by this polycationic polymeric system urged the need of protective shielding. Therefore, a non-covalent interaction of dendriplexes with lipids i.e. liposomal modification was chosen as a technique to overcome the associated drawbacks.

The methodology section of the thesis deals with the preparation of liposomes, dendriplexes, lipodendriplexes, their subsequent physicochemical characterization and *in vitro*, *in ovo* and *in vivo* studies.

In the results section, the characterization of dendriplexes has been discussed, which was the prerequisite of lipodendriplex formation. Dendriplexes formation was confirmed by gel retardation and fluorescence quenching assay. Dynamic light scattering and laser Doppler anemometry also confirmed the stable complex formation, with a desired size range suitable for cellular internalization. Based on highest pDNA transfection efficiency and appropriate cell viability profile, an N/P ratio of 12 has been chosen for complexation with the liposomal formulation.

A broad range of liposomal formulations has been investigated and the influence of liposome to PAMAM ratios on surface charge and size of lipodendriplexes are described in detail. Surface morphology of the liposomes and lipodendriplexes has been analysed using atomic force microscopy and their sizes were compared with the results obtained from dynamic light scattering.

Transfection studies have been discussed for different lipodendriplexes formulations. It has been observed that the DPPC:CH-PAMAM lipodendriplexes showed a significant improvement in pDNA transfection as compared to other lipodendriplexes formulations and their parent dendriplexes. The higher gene expression was also confirmed using fluorescence microscopy by GFP expression analysis.

Cytotoxicity studies including MTT, ROS, lysosomal disruption and DNA damage assays has been discussed in detail. From the results, it has been depicted that the lipid modification of dendriplexes shields the terminal amino group induced toxicity and consequently improves the cell viability.

Chapter IV: Summary and Outlook

Biocompatibility studies has been performed to check to the compatibility of the complexes in the presence of blood components. Heparin competition and erythrocyte hemolysis assay revealed the biocompatible nature of the lipodendriplexes.

Another objective of the study was to deliver the siRNA to investigate the gene silencing effect. Knockdown experiments showed a pronounced downregulation of luciferase, GFP and MDR1 genes by lipodendriplexes compared to dendriplexes or the control siRNA groups.

The role of MDR1 in cell migration and colonization of cancer cells has also been described in detail. Downregulation of MDR1 gene by lipodendriplexes exhibited significant inhibition of tumor metastasis and colonization.

The knockdown effect of MDR1 gene was also investigated in 3D cell culture environment. Cell migration and ring closure assays were performed using 3D tumor spheroid and ring bioprinting model. A significant reduction in the cell migration was observed in the case of lipodendriplexes treated group.

Next step was to investigate the enhanced intracellular accumulation of tyrosine kinase inhibitor (imatinib mesylate) after the downregulation of P-gp (responsible for drug efflux) and subsequent apoptosis in colon carcinoma. Apoptosis assay was done in 2D and 3D cultures using flow cytometry and live dead staining, respectively. The results of 2D culture were in agreement with the data from 3D cell cultures.

Cell cycle analysis also confirmed the imatinib mesylate induced apoptosis, indicated by an arrest of Sub-G1 phase depicting an effective downregulation of P-glycoprotein by lipodendriplexes.

In order to minimise the unethical use of animals, an alternative *in ovo* chorioallantoic membrane model (an *in vivo* like environment) has been used to determine the efficacy and biocompatibility of the complexes. Lipodendriplexes exhibited successful reporter gene (GFP) expression in the CAM with no toxicity observed within the CAM vasculature.

After establishing the improved gene transfection and toxicity profile in *in vitro* conditions, *in vivo* biodistribution and toxicity assessment of the complexes has performed in female BALB/c mice and discussed in detail. *In vivo* biodistribution has revealed that encapsulation of dendriplexes with liposomes has essentially increased the cellular uptake of the complexes, which was confirmed by *ex vivo* imaging of the dissected organs. Acute toxicity studies showed that the lipodendriplexes treated group did not produce any change in body weight, organ to body ratio and in organ tissue histopathology. Serum biomarkers and hematological studies also revealed the biocompatibility in an *in vivo* environment.

Chapter IV: Summary and Outlook

From the findings in this thesis, it can be concluded that development of such non-viral nano carrier system could serve for an efficient gene transfection with better safety profile, both for *in vitro* and *in vivo* therapeutics. Further *in vivo* studies using different pre-clinical models for specific targeted delivery against different types of cancer and genetic disorders will help to realise the therapeutic potential of this system.

Chapter IV: Summary and outlook

4.2 Zusammenfassung und Ausblick

Das Hauptziel der aktuellen Studie war die Entwicklung eines optimierten Gentransfersystems mit minimaler Zytotoxizität und maximaler Effizienz. Für einen effizienten Gentransfer dienten PAMAM-Dendrimere, die aus einem Ethylendiamin-Kern bestehen und biologisch abbaubar und wenig immunogen sind.

Die Zytotoxizität und die ungewöhnliche Verteilung in biologischen Systemen erforderten jedoch eine Schutzabschirmung dieser polykationischen Polymersysteme. Die Ausnutzung von nichtkovalenten Wechselwirkungen von Dendriplexen mit Lipiden wurde als ein nützliches technologisches Instrument genutzt, um diese Nachteile zu überwinden. Der methodische Teil der Arbeit beschreibt die Herstellung von Liposomen, Dendriplexen, Lipodendriplexen und deren anschließende physikalisch-chemische Charakterisierung bis hin zu *in-vitro*-, *in-ovo*- bzw. *in-vivo*-Studien.

Der Ergebnisabschnitt der Arbeit umfasst die Charakterisierung von Dendriplexen, welche die Voraussetzung für die Bildung von Lipodendriplexen darstellen. Die Überprüfung der Integrität der Bildung stabiler Dendriplexen wurde mit Hilfe der Gel-Retardations Chromatographie und des Fluoreszenzlöschungassays durchgeführt. Dynamische Lichtstreuung und Laser-Doppler-Anemometrie bestätigten ebenfalls die stabile Komplexbildung in einem gewünschten Größenbereich (von unter 200 nm), der für eine optimale zelluläre Aufnahme geeignet ist. Auf Grund der höchsten pDNA-Transfektionseffizienz und einer geringen Zelltoxizität wurde ein N/P-Verhältnis von 12 für die Liposomenkomplexierung verwendet. Ein breites Spektrum liposomaler Formulierungen wurde zur Komplexierung mit Dendriplexen untersucht und der Einfluss des Liposom-PAMAM-Verhältnisses auf die Oberflächenladung und die Größe von Lipodendriplexen wurde detailliert beschrieben.

Die Untersuchung der Oberflächenmorphologie der Liposomen und Lipodendriplexe fand mit Hilfe der Rasterkraftmikroskopie statt. Die gemessenen Durchmesser wurden mit den Ergebnissen der dynamischen Lichtstreuung verglichen.

Eine breite Vielfalt an verschiedenen Lipodendriplex-Formulierungen sind hergestellt, charakterisiert und deren Transfektionsstudien diskutiert worden. Die DPPC:CH-PAMAM-Lipodendriplexe zeigten eine signifikante Verbesserung der pDNA-Transfektion im Vergleich zu anderen Lipodendriplex Formulierungen und Dendriplexen. Eine GFP-Expressionsanalyse bestätigte die erhöhte Genexpression.

Untersuchungen zur Zytotoxizität, einschließlich MTT-, ROS-, Lysosomal-Disruptions und DNA-Schädigungs Assays, wurden ausführlich diskutiert. Aus den Ergebnissen ist ersichtlich,

Chapter IV: Summary and outlook

dass die Lipidmodifikation, die für Zelltoxizität verantwortlichen terminalen Aminogruppen von Dendriplexen abschirmen und letztendlich zu einer erhöhten Zellüberlebensrate führen.

Das Biokompatibilitätsprofil wurde untersucht, um die Verträglichkeit der Komplexe in Blutbestandteilen zu überprüfen. Der Heparin-Kompetitions- und Hämolysetest bestätigte die deutlich verbesserte Biokompatibilität von Lipodendriplexen im Vergleich zu den Dendriplexen.

Ein weiteres Ziel der Arbeit bestand darin, den siRNA Gen-Silencing-Effekt zu untersuchen. Im Vergleich zu Dendriplexen und zu der siRNA-Kontrollgruppe zeigten Lipodendriplexe eine ausgeprägte Herunterregulierung des Luciferase-, GFP- und des therapeutisch relevanten MDR1-Gens.

Die Rolle von MDR1 bei der Zellmigration und Kolonisierung von Krebszellen wurde ebenfalls ausführlich beschrieben. Die Herunterregulierung des MDR1 Gens durch Lipodendriplexe zeigte eine signifikante Hemmung des Tumormetastasenwachstums und deren Abwanderung/Weiterverbreitung. Die Untersuchung des Knockdown-Effekts des MDR1-Gens erfolgte in einer 3D-Zellkulturumgebung, die eine ähnliche Situation wie *in-vivo* simuliert. Die Zellmigrations- und Ringschluss-Assays wurden unter Verwendung eines 3D-Tumor-Sphäroid- und Ring-Bioprinting-Modells durchgeführt. Eine deutliche Hemmung der Zellmigration wurde dabei festgestellt.

Der nächste Schritt bestand in der Untersuchung der verstärkten intrazellulären Akkumulation des Tyrosinkinaseinhibitors (Imatinib-Mesylat) nach der Herunterregulierung von P-gp, das vornehmlich für die zelluläre Arzneimittelausschleusung verantwortlich ist, und der anschließenden Apoptose beim Kolonkarzinom. Der Apoptosetest wurde in 2D- und 3D-Kulturen unter Verwendung von Durchflusszytometrie bzw. Lebendtotfärbung durchgeführt. Die Ergebnisse der 2D-Kultur haben eine Bestätigung der in 3D-Zellkulturen erhaltenen Daten erbracht.

Aus den Befunden konnte geschlossen werden, dass nach der wirksamen Herunterregulierung von P-gp durch Lipodendriplexe die intrazelluläre Akkumulation des Wirkstoffs und anschließend die zelluläre Apoptose erhöht wurde.

Die Zellzyklusanalyse bestätigte auch die durch Imatinib-Mesylat induzierte Apoptose, die durch einen Stillstand der Sub-G1-Phase angezeigt wird und eine wirksame Herunterregulierung von P-gp durch Lipodendriplexe darstellt.

Chapter IV: Summary and outlook

Um die Verwendung von Tieren in vorklinischen Experimenten zu verringern, ist eine Alternative, das sogenannte *in-ovo chorio allantois* Membranmodell verwendet worden, um die Exposition von Komplexen *in-vivo*-ähnlicher Umgebung zu untersuchen. Es wurde beobachtet, dass die Lipodendriplexe eine erfolgreiche GFP-Expression auf der CAM-Oberfläche und kein toxisches Verhalten in den CAM-Gefäßen aufwiesen.

Danach konnten die Komplexe nach Festlegung des verbesserten Gentransfektions- und Toxizitätsprofils unter *in-vitro*-Bedingungen, *in-vivo*-Bioverteilung und Toxizitätsbewertung geplant und ausführlich erörtert werden.

Die *in-vivo*-Bioverteilung zeigte, dass die Verkapselung von Dendriplexen in Liposomen die zelluläre Aufnahme der Komplexe wesentlich erhöht hat, was durch *ex-vivo*-Bildgebung der präparierten Organe bestätigt wurde. Studien zur akuten Toxizität wurden ebenfalls eingehend untersucht. Es konnte beobachtet werden, dass die mit Lipodendriplexen behandelte Gruppe keine Änderung des Körpergewichts, des Verhältnisses von Organ zu Körper und der Histopathologie des Organgewebes hervorrief. Serumbiomarker und hämatologische Studien zeigten auch die Biokompatibilität in einer *in-vivo*-Umgebung.

Die Ergebnisse zeigen, dass die Entwicklung eines solchen nicht-viralen Genvehikels für eine effiziente Gentransfektion mit einem besseren Sicherheitsprofil sowohl *in-vitro* als auch *in-vivo* verwendbar wird. Weitere *in-vivo*-Studien mit verschiedenen präklinischen Modellen zur gezielten Therapie von verschiedenen Arten von Tumoren und genetischen Störungen könnte das therapeutische Potential diesen neuartigen Lipodendriplexen bestätigen.

Chapter V: Appendix

5.1 References:

- [1] T. Wirth, N. Parker, S. Ylä-Herttuala, History of gene therapy, *Gene*, 525 (2013) 162-169.
- [2] C. Dufes, I.F. Uchegbu, A.G. Schätzlein, Dendrimers in gene delivery, *Advanced drug delivery reviews*, 57 (2005) 2177-2202.
- [3] L. García, M. Bunuales, N. Düzgüneş, C.T. de Ilarduya, Serum-resistant lipopolyplexes for gene delivery to liver tumor cells, *European journal of pharmaceutics and biopharmaceutics*, 67 (2007) 58-66.
- [4] J. Li, L. Chen, N. Liu, S. Li, Y. Hao, X. Zhang, EGF-coated nano-dendriplexes for tumor-targeted nucleic acid delivery in vivo, *Drug delivery*, 23 (2016) 1718-1725.
- [5] D. Ibraheem, A. Elaissari, H. Fessi, Gene therapy and DNA delivery systems, *International journal of pharmaceutics*, 459 (2014) 70-83.
- [6] M.A. Kay, J.C. Glorioso, L. Naldini, Viral vectors for gene therapy: The art of turning infectious agents into vehicles of therapeutics, *Nature medicine*, 7 (2001) 33-40.
- [7] H. Lv, S. Zhang, B. Wang, S. Cui, J. Yan, Toxicity of cationic lipids and cationic polymers in gene delivery, *Journal of controlled release*, 114 (2006) 100-109.
- [8] O.M. Merkel, M.A. Mintzer, J. Sitterberg, U. Bakowsky, E.E. Simanek, T. Kissel, Triazine dendrimers as nonviral gene delivery systems: Effects of molecular structure on biological activity, *Bioconjugate chemistry*, 20 (2009) 1799-1806.
- [9] Z. Zhou, X. Liu, D. Zhu, Y. Wang, Z. Zhang, X. Zhou, N. Qiu, X. Chen, Y. Shen, Nonviral cancer gene therapy: Delivery cascade and vector nanoproperty integration, *Advanced drug delivery reviews*, 115 (2017) 115-154.
- [10] T. Niidome, L. Huang, Gene therapy progress and prospects: Nonviral vectors, *Gene therapy*, 9 (2002) 1647-1652.
- [11] D.V. Morrissey, J.A. Lockridge, L. Shaw, K. Blanchard, K. Jensen, W. Breen, K. Hartsough, L. Machemer, S. Radka, V. Jadhav, Potent and persistent in vivo anti-HBV activity of chemically modified siRNAs, *Nature biotechnology*, 23 (2005) 1002-1006.
- [12] K.A. Whitehead, R. Langer, D.G. Anderson, Knocking down barriers: Advances in siRNA delivery, *Nature reviews drug discovery*, 8 (2009) 129-138.
- [13] J.P. Dassie, X. Liu, G.S. Thomas, R.M. Whitaker, K.W. Thiel, K.R. Stockdale, D.K. Meyerholz, A.P. McCaffrey, J.O. McNamara II, P.H. Giangrande, Systemic administration of optimized aptamer-siRNA chimeras promotes regression of PSMA-expressing tumors, *Nature biotechnology*, 27 (2009) 839-846.

Chapter V: Appendix

- [14] Y. Sato, K. Murase, J. Kato, M. Kobune, T. Sato, Y. Kawano, R. Takimoto, K. Takada, K. Miyanishi, T. Matsunaga, T. Takayama, Y. Niitsu, Resolution of liver cirrhosis using vitamin A-coupled liposomes to deliver siRNA against a collagen-specific chaperone, *Nature biotechnology*, 26 (2008) 431-442.
- [15] M.E. Davis, J.E. Zuckerman, C.H.J. Choi, D. Seligson, A. Tolcher, C.A. Alabi, Y. Yen, J.D. Heidel, A. Ribas, Evidence of RNAi in humans from systemically administered siRNA via targeted nanoparticles, *Nature*, 464 (2010) 1067-1070.
- [16] E.P. Thi, C.E. Mire, A.C. Lee, J.B. Geisbert, J.Z. Zhou, K.N. Agans, N.M. Snead, D.J. Deer, T.R. Barnard, K.A. Fenton, Lipid nanoparticle siRNA treatment of Ebola-virus-Makona-infected nonhuman primates, *Nature*, 521 (2015) 362-365.
- [17] M. Foldvari, D.W. Chen, N. Nafissi, D. Calderon, L. Narsineni, A. Rafiee, Non-viral gene therapy: Gains and challenges of non-invasive administration methods, *Journal of controlled release*, 240 (2016) 165-190.
- [18] G.D. Schmidt-Wolf, I.G. Schmidt-Wolf, Non-viral and hybrid vectors in human gene therapy: An update, *Trends in molecular medicine*, 9 (2003) 67-72.
- [19] M.N. Sarbolouki, M. Sadeghizadeh, M.M. Yaghoobi, A. Karami, T. Lohrasbi, Dendrosomes: A novel family of vehicles for transfection and therapy, *Journal of chemical technology and biotechnology*, 75 (2000) 919-922.
- [20] M.X. Tang, C.T. Redemann, F.C. Szoka, In vitro gene delivery by degraded polyamidoamine dendrimers, *Bioconjugate chemistry*, 7 (1996) 703-714.
- [21] S.C. De Smedt, J. Demeester, W.E. Hennink, Cationic polymer based gene delivery systems, *Pharmaceutical research*, 17 (2000) 113-126.
- [22] D.W. Pack, A.S. Hoffman, S. Pun, P.S. Stayton, Design and development of polymers for gene delivery, *Nature reviews drug discovery*, 4 (2005) 581-593.
- [23] E. Wagner, K. Zatloukal, M. Cotten, H. Kirlappos, K. Mechtler, D.T. Curiel, M.L. Birnstiel, Coupling of adenovirus to transferrin-polylysine/DNA complexes greatly enhances receptor-mediated gene delivery and expression of transfected genes, *Proceedings of the national academy of sciences*, 89 (1992) 6099-6103.
- [24] D. Goula, J. Remy, P. Erbacher, M. Wasowicz, G. Levi, B. Abdallah, B. Demeneix, Size, diffusibility and transfection performance of linear PEI/DNA complexes in the mouse central nervous system, *Gene therapy*, 5 (1998) 712-717.
- [25] M. Hanzlíková, P. Soininen, P. Lampela, P.T. Männistö, A. Raasmaja, The role of PEI structure and size in the PEI/liposome-mediated synergism of gene transfection, *Plasmid*, 61 (2009) 15-21.

Chapter V: Appendix

- [26] A.U. Bielinska, A. Yen, H.L. Wu, K.M. Zahos, R. Sun, N.D. Weiner, J.R. Baker Jr, B.J. Roessler, Application of membrane-based dendrimer/DNA complexes for solid phase transfection in vitro and in vivo, *Biomaterials*, 21 (2000) 877-887.
- [27] P. Lampela, P. Soininen, A. Urtti, P.T. Männistö, A. Raasmaja, Synergism in gene delivery by small PEIs and three different nonviral vectors, *International journal of pharmaceutics*, 270 (2004) 175-184.
- [28] B.J. Roessler, A.U. Bielinska, K. Janczak, I. Lee, J.R. Baker, Substituted β -cyclodextrins interact with PAMAM dendrimer–DNA complexes and modify transfection efficiency, *Biochemical and biophysical research communications*, 283 (2001) 124-129.
- [29] S. Biswas, P.P. Deshpande, G. Navarro, N.S. Dodwadkar, V.P. Torchilin, Lipid modified triblock PAMAM-based nanocarriers for siRNA drug co-delivery, *Biomaterials*, 34 (2013) 1289-1301.
- [30] H.Y. Nam, H.J. Hahn, K. Nam, W. Choi, Y. Jeong, D. Kim, J. Park, Evaluation of generations 2, 3 and 4 arginine modified PAMAM dendrimers for gene delivery, *International journal of pharmaceutics*, 363 (2008) 199-205.
- [31] M. Labieniec-Watala, K. Karolczak, K. Siewiera, C. Watala, The Janus face of PAMAM dendrimers used to potentially cure nonenzymatic modifications of biomacromolecules in metabolic disorders—A critical review of the pros and cons, *Molecules*, 18 (2013) 13769-13811.
- [32] N. Silva, F. Menacho, M. Chorilli, Dendrimers as potential platform in nanotechnology-based drug delivery systems, *IOSR journal of pharmacy*, 2 (2012) 23-30.
- [33] T. Kim, H.J. Seo, J.S. Choi, H. Jang, J. Baek, K. Kim, J. Park, PAMAM-PEG-PAMAM: Novel triblock copolymer as a biocompatible and efficient gene delivery carrier, *Biomacromolecules*, 5 (2004) 2487-2492.
- [34] Y.J. Choi, S.J. Kang, Y.J. Kim, Y. Lim, H.W. Chung, Comparative studies on the genotoxicity and cytotoxicity of polymeric gene carriers polyethylenimine (PEI) and polyamidoamine (PAMAM) dendrimer in Jurkat T-cells, *Drug and chemical toxicology*, 33 (2010) 357-366.
- [35] D.W. Pack, A.S. Hoffman, S. Pun, P.S. Stayton, Design and development of polymers for gene delivery, *Nature reviews drug discovery*, 4 (2005) 581-593.
- [36] C.M. Paleos, D. Tsiourvas, Z. Sideratou, A. Pantos, Formation of artificial multicompartement vesosome and dendrosome as prospected drug and gene delivery carriers, *Journal of controlled release*, 170 (2013) 141-152.

- [37] L. Wu, M. Ficker, J.B. Christensen, P.N. Trohopoulos, S.M. Moghimi, Dendrimers in medicine: Therapeutic concepts and pharmaceutical challenges, *Bioconjugate chemistry*, 26 (2015) 1198-1211.
- [38] T. Dutta, H.B. Aghase, P. Vijayarajkumar, M. Joshi, N. Jain, Dendrosome-based gene delivery, *Journal of experimental nanoscience*, 1 (2006) 235-248.
- [39] T. Dutta, M. Burgess, N.A. McMillan, H.S. Parekh, Dendrosome-based delivery of siRNA against E6 and E7 oncogenes in cervical cancer, *Nanomedicine: Nanotechnology, biology and medicine*, 6 (2010) 463-470.
- [40] H.K. Alajangi, P. Natarajan, M. Vij, M. Ganguli, D. Santhiya, Role of unmodified low generation–PAMAM dendrimers in efficient non-toxic gene transfection, *Chemistry select*, 1 (2016) 5206-5217.
- [41] M.K. Khan, S.S. Nigavekar, L.D. Minc, M.S. Kariapper, B.M. Nair, W.G. Lesniak, L.P. Balogh, In vivo biodistribution of dendrimers and dendrimer nanocomposites—implications for cancer imaging and therapy, *Technology in cancer research and treatment*, 4 (2005) 603-613.
- [42] Y. Li, X. Zeng, S. Wang, Y. Sun, Z. Wang, J. Fan, P. Song, D. Ju, Inhibition of autophagy protects against PAMAM dendrimers-induced hepatotoxicity, *Nanotoxicology*, 9 (2015) 344-355.
- [43] L. Albertazzi, L. Gherardini, M. Brondi, S. Sulis Sato, A. Bifone, T. Pizzorusso, G.M. Ratto, G. Bardi, In vivo distribution and toxicity of PAMAM dendrimers in the central nervous system depend on their surface chemistry, *Molecular pharmaceutics*, 10 (2012) 249-260.
- [44] D. Shcharbin, A. Janaszewska, B. Klajnert-Maculewicz, B. Ziemia, V. Dzmitruk, I. Halets, S. Loznikova, N. Shcharbina, K. Milowska, M. Ionov, How to study dendrimers and dendriplexes III. Biodistribution, pharmacokinetics and toxicity in vivo, *Journal of controlled release*, 181 (2014) 40-52.
- [45] T. Dutta, M. Garg, V. Dubey, D. Mishra, K. Singh, D. Pandita, A.K. Singh, A.K. Ravi, T. Velpandian, N.K. Jain, Toxicological investigation of surface engineered fifth generation poly (propyleneimine) dendrimers in vivo, *Nanotoxicology*, 2 (2008) 62-70.
- [46] S. Akhtar, B. Al-Zaid, A.Z. El-Hashim, B. Chandrasekhar, S. Attur, M.H. Yousif, I.F. Benter, Cationic polyamidoamine dendrimers as modulators of EGFR signaling in vitro and in vivo, *Public library of science one*, 10 (2015) 1-22.
- [47] S. Kulkarni, G. Betageri, M. Singh, Factors affecting microencapsulation of drugs in liposomes, *Journal of microencapsulation*, 12 (1995) 229-246.

- [48] M. Gulati, M. Grover, S. Singh, M. Singh, Lipophilic drug derivatives in liposomes, *International journal of pharmaceutics*, 165 (1998) 129-168.
- [49] T. Nii, F. Ishii, Encapsulation efficiency of water-soluble and insoluble drugs in liposomes prepared by the microencapsulation vesicle method, *International journal of pharmaceutics*, 298 (2005) 198-205.
- [50] A. Ewe, A. Aigner, Nebulization of liposome–polyethylenimine complexes (lipopolyplexes) for DNA or siRNA delivery: Physicochemical properties and biological activity, *European journal of lipid science and technology*, 116 (2014) 1195-1204.
- [51] S. Movassaghian, H.R. Moghimi, F.H. Shirazi, A. Koshkaryev, M.S. Trivedi, V.P. Torchilin, Efficient down-regulation of PKC- α gene expression in A549 lung cancer cells mediated by antisense oligodeoxynucleotides in dendrosomes, *International journal of pharmaceutics*, 441 (2013) 82-91.
- [52] T. Date, V. Nimbalkar, J. Kamat, A. Mittal, R.I. Mahato, D. Chitkara, Lipid-polymer hybrid nanocarriers for delivering cancer therapeutics, *Journal of controlled release*, 271 (2018) 60-73.
- [53] S. Movassaghian, H.R. Moghimi, F.H. Shirazi, V.P. Torchilin, Dendrosome-dendriplex inside liposomes: As a gene delivery system, *Journal of drug targeting*, 19 (2011) 925-932.
- [54] Y. Liu, Y. Ng, M.R. Toh, G.N. Chiu, Lipid-dendrimer hybrid nanosystem as a novel delivery system for paclitaxel to treat ovarian cancer, *Journal of controlled release*, 220 (2015) 438-446.
- [55] K. Hadinoto, A. Sundaresan, W.S. Cheow, Lipid–polymer hybrid nanoparticles as a new generation therapeutic delivery platform: A review, *European journal of pharmaceutics and biopharmaceutics*, 85 (2013) 427-443.
- [56] A. Kwok, G.A. Eggimann, J.L. Reymond, T. Darbre, F. Hollfelder, Peptide dendrimer/lipid hybrid systems are efficient DNA transfection reagents: Structure–activity relationships highlight the role of charge distribution across dendrimer generations, *ACS nano*, 7 (2013) 4668-4682.
- [57] F. Pourasgari, S. Ahmadian, A.H. Salmanian, M.N. Sarbolouki, M. Massumi, Low cytotoxicity effect of dendrosome as an efficient carrier for rotavirus VP2 gene transferring into a human lung cell line, *Molecular biology reports*, 36 (2009) 105-109.
- [58] T. Tsuruo, M. Naito, A. Tomida, N. Fujita, T. Mashima, H. Sakamoto, N. Haga, Molecular targeting therapy of cancer: Drug resistance, apoptosis and survival signal, *Cancer science*, 94 (2003) 15-21.

- [59] C. Risnayanti, Y. Jang, J. Lee, H.J. Ahn, PLGA nanoparticles co-delivering MDR1 and BCL2 siRNA for overcoming resistance of paclitaxel and cisplatin in recurrent or advanced ovarian cancer, *Scientific reports*, 8 (2018) 1-12.
- [60] F. Mahon, F. Belloc, V. Lagarde, C. Chollet, F. Moreau-Gaudry, J. Reiffers, J.M. Goldman, J.V. Melo, MDR1 gene overexpression confers resistance to imatinib mesylate in leukemia cell line models, *Blood*, 101 (2003) 2368-2373.
- [61] A.H. Dantzig, D.P. de Alwis, M. Burgess, Considerations in the design and development of transport inhibitors as adjuncts to drug therapy, *Advanced drug delivery reviews*, 55 (2003) 133-150.
- [62] L. Ni, J. Li, K. Miao, C. Qiao, S.-J. Zhang, H. Qiu, S. Qian, Multidrug resistance gene (MDR1) polymorphisms correlate with imatinib response in chronic myeloid leukemia, *Medical oncology*, 28 (2011) 265-269.
- [63] S. Essex, G. Navarro, P. Sabhachandani, A. Chordia, M. Trivedi, S. Movassaghian, V.P. Torchilin, Phospholipid-modified PEI-based nanocarriers for in vivo siRNA therapeutics against multidrug-resistant tumors, *Gene therapy*, 22 (2014) 257-266.
- [64] J.A. MacDiarmid, N.B. Amaro-Mugridge, J. Madrid-Weiss, I. Sedliarou, S. Wetzel, K. Kochar, V.N. Brahmabhatt, L. Phillips, S.T. Pattison, C. Petti, Sequential treatment of drug-resistant tumors with targeted minicells containing siRNA or a cytotoxic drug, *Nature biotechnology*, 27 (2009) 643-651.
- [65] J. Jiang, S. Yang, J. Wang, L. Yang, Z. Xu, T. Yang, X. Liu, Q. Zhang, Sequential treatment of drug-resistant tumors with RGD-modified liposomes containing siRNA or doxorubicin, *European journal of pharmaceuticals and biopharmaceutics*, 76 (2010) 170-178.
- [66] B.J. Druker, C.L. Sawyers, H. Kantarjian, D.J. Resta, S.F. Reese, J.M. Ford, R. Capdeville, M. Talpaz, Activity of a specific inhibitor of the BCR-ABL tyrosine kinase in the blast crisis of chronic myeloid leukemia and acute lymphoblastic leukemia with the Philadelphia chromosome, *New england journal of medicine*, 344 (2001) 1038-1042.
- [67] N. Iqbal, N. Iqbal, Imatinib: A breakthrough of targeted therapy in cancer, *Chemotherapy research and practice*, 2014 (2014) 1-9.
- [68] V.P. Balachandran, M.J. Cavnar, S. Zeng, Z.M. Bamboat, L.M. Ocuin, H. Obaid, E.C. Sorenson, R. Popow, C. Ariyan, F. Rossi, Imatinib potentiates antitumor T cell responses in gastrointestinal stromal tumor through the inhibition of Ido, *Nature medicine*, 17 (2011) 1094-1100.

- [69] A. Graber-Maier, H. Gutmann, J. Drewe, A new intestinal cell culture model to discriminate the relative contribution of P-gp and BCRP on transport of substrates such as imatinib, *Molecular pharmaceutics*, 7 (2010) 1618-1628.
- [70] S. Galimberti, G. Cervetti, F. Guerrini, R. Testi, S. Pacini, R. Fazzi, P. Simi, M. Petrini, Quantitative molecular monitoring of BCR-ABL and MDR1 transcripts in patients with chronic myeloid leukemia during Imatinib treatment, *Cancer genetics and cytogenetics*, 162 (2005) 57-62.
- [71] P.E. Saw, J. Park, S. Jon, O.C. Farokhzad, A drug-delivery strategy for overcoming drug resistance in breast cancer through targeting of oncofetal fibronectin, *Nanomedicine: Nanotechnology, biology and medicine*, 13 (2017) 713-722.
- [72] C. Sarisozen, J. Pan, I. Dutta, V.P. Torchilin, Polymers in the co-delivery of siRNA and anticancer drugs to treat multidrug-resistant tumors, *Journal of pharmaceutical investigation*, 47 (2017) 37-49.
- [73] L.M. Negi, M. Jaggi, V. Joshi, K. Ronodip, S. Talegaonkar, Hyaluronan coated liposomes as the intravenous platform for delivery of imatinib mesylate in MDR colon cancer, *International journal of biological macromolecules*, 73 (2015) 222-235.
- [74] T. Stromskaya, E.Y. Rybalkina, S. Kruglov, T. Zabolina, E. Mechetner, A. Turkina, A. Stavrovskaya, Role of P-glycoprotein in evolution of populations of chronic myeloid leukemia cells treated with imatinib, *Biochemistry*, 73 (2008) 29-37.
- [75] J. Gilleron, W. Querbes, A. Zeigerer, A. Borodovsky, G. Marsico, U. Schubert, K. Manygoats, S. Seifert, C. Andree, M. Stöter, Image-based analysis of lipid nanoparticle-mediated siRNA delivery, intracellular trafficking and endosomal escape, *Nature biotechnology*, 31 (2013) 1-12.
- [76] P.K. Maiti, T. Çağın, G. Wang, W.A. Goddard, Structure of PAMAM dendrimers: Generations 1 through 11, *Macromolecules*, 37 (2004) 6236-6254.
- [77] R. Esfand, D.A. Tomalia, Poly(amidoamine) (PAMAM) dendrimers: From biomimicry to drug delivery and biomedical applications, *Drug discovery today*, 6 (2001) 427-436.
- [78] O.M. Milhem, C. Myles, N.B. McKeown, D. Attwood, A. D'Emanuele, Polyamidoamine Starburst® dendrimers as solubility enhancers, *International journal of pharmaceutics*, 197 (2000) 239-241.
- [79] M. Wang, T. Zander, X. Liu, C. Liu, A. Raj, D.C. Florian Wieland, V.M. Garamus, R. Willumeit-Römer, P.M. Claesson, A. Dédinaite, The effect of temperature on supported dipalmitoylphosphatidylcholine (DPPC) bilayers: Structure and lubrication performance, *Journal of colloid and interface science*, 445 (2015) 84-92.

Chapter V: Appendix

- [80] B. Kim, G. Hwang, Y. Seu, J. Choi, K.S. Jin, K. Doh, DOTAP/DOPE ratio and cell type determine transfection efficiency with DOTAP-liposomes, *Biochimica et biophysica acta-Biomembranes*, 1848 (2015) 1996-2001.
- [81] S. Mochizuki, N. Kanegae, K. Nishina, Y. Kamikawa, K. Koiwai, H. Masunaga, K. Sakurai, The role of the helper lipid dioleoylphosphatidylethanolamine (DOPE) for DNA transfection cooperating with a cationic lipid bearing ethylenediamine, *Biochimica et biophysica acta-Biomembranes*, 1828 (2013) 412-418.
- [82] D.A. Balazs, W. Godbey, Liposomes for use in gene delivery, *Journal of drug delivery*, 2011 (2011) 1-12.
- [83] E. Nogueira, A.C. Gomes, A. Preto, A. Cavaco-Paulo, Design of liposomal formulations for cell targeting, *Colloids and surfaces B: Biointerfaces*, 136 (2015) 514-526.
- [84] K.H. Engelhardt, S.R. Pinnapireddy, E. Baghdan, J. Jedelská, U. Bakowsky, Transfection studies with colloidal systems containing highly purified bipolar tetraether lipids from *Sulfolobus acidocaldarius*, *Archaea*, 2017 (2017) 1-12.
- [85] I. Tariq, S.R. Pinnapireddy, L. Duse, M.Y. Ali, S. Ali, M.U. Amin, N. Goergen, J. Jedelská, J. Schäfer, U. Bakowsky, Lipodendriplexes: A promising nanocarrier for enhanced gene delivery with minimal cytotoxicity, *European journal of pharmaceuticals and biopharmaceutics*, 135 (2019) 72-82.
- [86] M. Tang, F. Szoka, The influence of polymer structure on the interactions of cationic polymers with DNA and morphology of the resulting complexes, *Gene therapy*, 4 (1997) 823.
- [87] S.R. Pinnapireddy, L. Duse, B. Strehlow, J. Schäfer, U. Bakowsky, Composite liposome-PEI/nucleic acid lipopolyplexes for safe and efficient gene delivery and gene knockdown, *Colloids and surfaces B: Biointerfaces*, 158 (2017) 93-101.
- [88] F. Lemarié, D.R. Croft, R.J. Tate, K.M. Ryan, C. Dufès, Tumor regression following intravenous administration of a tumor-targeted p73 gene delivery system, *Biomaterials*, 33 (2012) 2701-2709.
- [89] L. Duse, S.R. Pinnapireddy, B. Strehlow, J. Jedelská, U. Bakowsky, Low level LED photodynamic therapy using curcumin loaded tetraether liposomes, *European journal of pharmaceuticals and biopharmaceutics*, 126 (2018) 233-241.
- [90] G. Mahmoud, J. Jedelská, S.M. Omar, B. Strehlow, M. Schneider, U. Bakowsky, Stabilized tetraether lipids based particles guided porphyrins photodynamic therapy, *Drug delivery*, 25 (2018) 1526-1536.

- [91] N. Guo, C. Gao, J. Liu, J. Li, N. Liu, Y. Hao, L. Chen, X. Zhang, Reversal of ovarian cancer multidrug resistance by a combination of LAH4-L1-siMDR1 nanocomplexes with chemotherapeutics, *Molecular pharmaceutics*, 15 (2018) 1853-1861.
- [92] B.C. Evans, C.E. Nelson, S.Y. Shann, K.R. Beavers, A.J. Kim, H. Li, H.M. Nelson, T.D. Giorgio, C.L. Duvall, Ex vivo red blood cell hemolysis assay for the evaluation of pH-responsive endosomolytic agents for cytosolic delivery of biomacromolecular drugs, *Journal of visualized experiments*, 73 (2013) 1-5.
- [93] S. Pinnapireddy, L. Duse, D. Akbari, U. Bakowsky, Photo-Enhanced delivery of genetic material using curcumin loaded composite nanocarriers, *Clinical oncology*, 2 (2017) 1-5.
- [94] J. Nguyen, X. Xie, M. Neu, R. Dumitrascu, R. Reul, J. Sitterberg, U. Bakowsky, R. Schermuly, L. Fink, T. Schmehl, Effects of cell-penetrating peptides and pegylation on transfection efficiency of polyethylenimine in mouse lungs, *The journal of gene medicine*, 10 (2008) 1236-1246.
- [95] H. Tseng, J.A. Gage, W.L. Haisler, S.K. Neeley, T. Shen, C. Hebel, H.G. Barthlow, M. Wagoner, G.R. Souza, A high-throughput in vitro ring assay for vasoactivity using magnetic 3D bioprinting, *Scientific reports*, 6 (2016) 1-8.
- [96] D.M. Timm, J. Chen, D. Sing, J.A. Gage, W.L. Haisler, S.K. Neeley, R.M. Raphael, M. Dehghani, K.P. Rosenblatt, T. Killian, A high-throughput three-dimensional cell migration assay for toxicity screening with mobile device-based macroscopic image analysis, *Scientific reports*, 3 (2013) 1-8.
- [97] P.K. Maiti, T. Çağın, S. Lin, W.A. Goddard, Effect of solvent and pH on the structure of PAMAM dendrimers, *Macromolecules*, 38 (2005) 979-991.
- [98] A. Kumar, V.K. Yellepeddi, G.E. Davies, K.B. Strychar, S. Palakurthi, Enhanced gene transfection efficiency by polyamidoamine (PAMAM) dendrimers modified with ornithine residues, *International journal of pharmaceutics*, 392 (2010) 294-303.
- [99] Y. Zhang, H. Li, J. Sun, J. Gao, W. Liu, B. Li, Y. Guo, J. Chen, DC-Chol/DOPE cationic liposomes: A comparative study of the influence factors on plasmid pDNA and siRNA gene delivery, *International journal of pharmaceutics*, 390 (2010) 198-207.
- [100] P. Laskar, S. Somani, N. Altwaijry, M. Mullin, D. Bowering, M. Warzecha, P. Keating, R.J. Tate, H.Y. Leung, C. Dufès, Redox-sensitive, cholesterol-bearing PEGylated poly(propylene imine)-based dendrimersomes for drug and gene delivery to cancer cells, *Nanoscale*, 10 (2018) 22830-22847.
- [101] J. Schäfer, S. Höbel, U. Bakowsky, A. Aigner, Liposome–polyethylenimine complexes for enhanced DNA and siRNA delivery, *Biomaterials*, 31 (2010) 6892-6900.

Chapter V: Appendix

- [102] P.C. Naha, M. Davoren, F.M. Lyng, H.J. Byrne, Reactive oxygen species (ROS) induced cytokine production and cytotoxicity of PAMAM dendrimers in J774A. 1 cells, *Toxicology and applied pharmacology*, 246 (2010) 91-99.
- [103] J. Nguyen, T.W. Steele, O. Merkel, R. Reul, T. Kissel, Fast degrading polyesters as siRNA nano-carriers for pulmonary gene therapy, *Journal of controlled release*, 132 (2008) 243-251.
- [104] T.P. Thomas, I. Majoros, A. Kotlyar, D. Mullen, M.M. Banaszak Holl, J.R. Baker, Cationic Poly(amidoamine) dendrimer induces lysosomal apoptotic pathway at therapeutically relevant concentrations, *Biomacromolecules*, 10 (2009) 3207-3214.
- [105] K.M. Kitchens, A.B. Foraker, R.B. Kolhatkar, P.W. Swaan, H. Ghandehari, Endocytosis and interaction of poly (amidoamine) dendrimers with Caco-2 cells, *Pharmaceutical research*, 24 (2007) 2138-2145.
- [106] S.T. Stern, P.P. Adisheshaiah, R.M. Crist, Autophagy and lysosomal dysfunction as emerging mechanisms of nanomaterial toxicity, *Particle and fibre toxicology*, 9 (2012) 1-15.
- [107] P. Ruenraroengsak, A.T. Florence, Biphasic interactions between a cationic dendrimer and actin, *Journal of drug targeting*, 18 (2010) 803-811.
- [108] Z. Shen, W. Tian, K. Chen, Y. Ma, Molecular dynamics simulation of G-actin interacting with PAMAM dendrimers, *Journal of molecular graphics and modelling*, 84 (2018) 145-151.
- [109] P.C. Naha, H.J. Byrne, Generation of intracellular reactive oxygen species and genotoxicity effect to exposure of nanosized polyamidoamine (PAMAM) dendrimers in PLHC-1 cells in vitro, *Aquatic toxicology*, 132 (2013) 61-72.
- [110] B. Birdhariya, P. Kesharwani, N.K. Jain, Effect of surface capping on targeting potential of folate decorated poly (propylene imine) dendrimers, *Drug development and industrial pharmacy*, 41 (2015) 1393-1399.
- [111] H. Engelberg, A. Dudley, Plasma heparin levels in normal man, *Circulation*, 23 (1961) 578-581.
- [112] X. Guan, Cancer metastases: Challenges and opportunities, *Acta pharmaceutica sinica B*, 5 (2015) 402-418.
- [113] P.C. Hermann, S.L. Huber, T. Herrler, A. Aicher, J.W. Ellwart, M. Guba, C.J. Bruns, C. Heeschen, Distinct populations of cancer stem cells determine tumor growth and metastatic activity in human pancreatic cancer, *Cell stem cell*, 1 (2007) 313-323.
- [114] H. Yamaguchi, J. Wyckoff, J. Condeelis, Cell migration in tumors, *Current opinion in cell biology*, 17 (2005) 559-564.

- [115] F. Zhang, H. Zhang, Z. Wang, M. Yu, R. Tian, W. Ji, Y. Yang, R. Niu, P-glycoprotein associates with Anxa2 and promotes invasion in multidrug resistant breast cancer cells, *Biochemical pharmacology*, 87 (2014) 292-302.
- [116] S. Katoh, M. Ueno, N. Takakura, Involvement of MDR1 function in proliferation of tumor cells, *Journal of biochemistry*, 143 (2008) 517-524.
- [117] E. Wiercinska, H.P. Naber, E. Pardali, G. van der Pluijm, H. van Dam, P. Ten Dijke, The TGF- β /Smad pathway induces breast cancer cell invasion through the up-regulation of matrix metalloproteinase 2 and 9 in a spheroid invasion model system, *Breast cancer research and treatment*, 128 (2011) 657-666.
- [118] H. Tseng, J.A. Gage, T. Shen, W.L. Haisler, S.K. Neeley, S. Shiao, J. Chen, P.K. Desai, A. Liao, C. Hebel, A spheroid toxicity assay using magnetic 3D bioprinting and real-time mobile device-based imaging, *Scientific reports*, 5 (2015) 1-11.
- [119] J. Liu, J. Li, N. Liu, N. Guo, C. Gao, Y. Hao, L. Chen, X. Zhang, In vitro studies of phospholipid-modified PAMAM-siMDR1 complexes for the reversal of multidrug resistance in human breast cancer cells, *International journal of pharmaceutics*, 530 (2017) 291-299.
- [120] J.L. Kim, D.H. Lee, S. Jeong, B.R. Kim, Y.J. Na, S.H. Park, M.J. Jo, Y.A. Jeong, S.C. Oh, Imatinib-induced apoptosis of gastric cancer cells is mediated by endoplasmic reticulum stress, *Oncology reports*, 41 (2019) 1616-1626.
- [121] S.K. Doke, S.C. Dhawale, Alternatives to animal testing: A review, *Saudi pharmaceutical journal*, 23 (2015) 223-229.
- [122] E. Baghdan, S.R. Pinnapireddy, B. Strehlow, K.H. Engelhardt, J. Schäfer, U. Bakowsky, Lipid coated chitosan-DNA nanoparticles for enhanced gene delivery, *International journal of pharmaceutics*, 535 (2018) 473-479.
- [123] Y. Tang, S. Han, H. Liu, X. Chen, L. Huang, X. Li, J. Zhang, The role of surface chemistry in determining in vivo biodistribution and toxicity of CdSe/ZnS core-shell quantum dots, *Biomaterials*, 34 (2013) 8741-8755.
- [124] J. Wang, G. Zhou, C. Chen, H. Yu, T. Wang, Y. Ma, G. Jia, Y. Gao, B. Li, J. Sun, Acute toxicity and biodistribution of different sized titanium dioxide particles in mice after oral administration, *Toxicology letters*, 168 (2007) 176-185.
- [125] C.F. Jones, R.A. Campbell, A.E. Brooks, S. Assemi, S. Tadjiki, G. Thiagarajan, C. Mulcock, A.S. Weyrich, B.D. Brooks, H. Ghandehari, Cationic PAMAM dendrimers aggressively initiate blood clot formation, *ACS nano*, 6 (2012) 9900-9910.
- [126] A. Ewe, O. Panchal, S.R. Pinnapireddy, U. Bakowsky, S. Przybylski, A. Temme, A. Aigner, Liposome-polyethylenimine complexes (DPPC-PEI lipopolyplexes) for therapeutic

Chapter V: Appendix

siRNA delivery in vivo, *Nanomedicine: Nanotechnology, biology and medicine*, 13 (2017) 209-218.

[127] T. Kurosaki, S. Kawakami, Y. Higuchi, R. Suzuki, K. Maruyama, H. Sasaki, F. Yamashita, M. Hashida, Development of anionic bubble lipopolyplexes for efficient and safe gene transfection with ultrasound exposure in mice, *Journal of controlled release*, 176 (2014) 24-34.

[128] Y.T. Ko, R. Bhattacharya, U. Bickel, Liposome encapsulated polyethylenimine/ODN polyplexes for brain targeting, *Journal of controlled release*, 133 (2009) 230-237.

5.2 Research output

Imran Tariq, Shashank Reddy Pinnapireddy, Lili Duse, Muhammad Yasir Ali, Sajid Ali, Muhammad Umair Amin, Nathalie Goergen, Jarmila Jedelská, Jens Schäfer and Udo Bakowsky; Lipodendriplexes: A promising nanocarrier for enhanced gene delivery with minimal cytotoxicity, *European journal of pharmaceutics and biopharmaceutics*, 135 (2019) 72-82.

Imran Tariq, Muhammad Yasir Ali, Muhammad Farhan Sohail, Muhammad Umair Amin, Sajid Ali, Nadeem Irfan Bukhari, Abida Raza, Shashank Reddy Pinnapireddy, Jens Schäfer and Udo Bakowsky; Lipodendriplexes mediated enhanced systemic delivery and gene expression. *Manuscript in preparation.*

Imran Tariq, Muhammad Yasir Ali, Harshavardhan Janga, Sajid Ali, Muhammad Umair Amin, Ghazala Ambreen, Uzma Ali, Shashank Reddy Pinnapireddy, Jens Schäfer and Udo Bakowsky; Downregulation of MDR 1 gene contributes to tyrosine kinase inhibitor induced apoptosis and inhibition in tumor metastasis: A gravity to space investigation. *Manuscript in preparation.*

Muhammad Yasir Ali, **Imran Tariq**, Sajid Ali, Muhammad Umair Amin, Shashank Reddy Pinnapireddy, Lili Duse, Konrad Engelhardt, Jens Schäfer and Udo Bakowsky; Targeted ErbB3 cancer therapy: A synergistic approach to effectively combat cancer. *Submitted Manuscript.*

Muhammad Yasir Ali, **Imran Tariq**, Muhammad Farhan Sohail, Asad Ali, Muhammad Umair Amin, Sajid Ali, Shashank Reddy Pinnapireddy, Jens Schäfer and Udo Bakowsky; Anti-ErbB3 aptamer modified sorafenib microparticles: *In vitro* and *in vivo* toxicity assessment. *Submitted Manuscript.*

Sajid Ali, Muhammad Umair Amin, Muhammad Yasir Ali, **Imran Tariq**, Nathalie Goergen, Lili Duse, Christian Wölk, Gerd Hause, Jarmila Jedelská, Shashank Reddy Pinnapireddy, Jens Schäfer, and Udo Bakowsky; Wavelength-dependent Photocytotoxicity to ovarian carcinoma using temoporfin loaded liposomes as efficient drug delivery system. *Manuscript in preparation.*

5.3 Presentations

In vivo biodistribution imaging and acute toxicity profile of lipid modified polymeric nanoparticles- *Oral Presentation*: **Imran Tariq**; Global Experts Meeting on Frontiers in Nanomedicine and Drug Delivery (Nano Delivery 2019) 18-20 March, 2019, London, UK.

In vivo biodistribution and toxicity profile of liposome conjugated polyamidoamine dendrimeric system- *Poster Presentation*: **Imran Tariq**, Muhammad Yasir Ali, Muhammad Farhan Sohail, Sajid Ali, Muhammad Umair Amin, Nadeem Irfan Bukhari, Abida Raza, Jens Schäfer and Udo Bakowsky; 23rd Annual Meeting of Controlled Release Society, German Local Chapter (Functional Biomaterials and Release of Nucleic Acid Drugs) 7-8 March, 2019, Leipzig, Germany.

Enhanced gene delivery by lipid triblock nanocarrier- *Oral Presentation*: **Imran Tariq**; International Conference and Exhibition on Pharmaceutical Nanotechnology and Nanomedicine (Conference series LLC Ltd) 18-19 April, 2018, Las Vegas, USA.

Enhanced gene delivery by lipid triblock nanocarrier- *Moderator speaker*: **Imran Tariq**; International Conference and Exhibition on Pharmaceutical Nanotechnology and Nanomedicine (Conference series LLC Ltd) 18-19 April, 2018, Las Vegas, USA.

Enhanced gene transfection by lipid triblock nano carrier system- *Poster Presentation*: **Imran Tariq**, Jens Schäfer and Udo Bakowsky; 21st Annual Meeting of Controlled Release Society, German Local Chapter (Future Trends in Nanomedicine) 2-3 March, 2017, Marburg, Germany.

5.4 Curriculum Vitae



PERSONAL INFORMATION

Name	IMRAN TARIQ
Adress	SUDETEN STR.7, 35039,MARBURG, GERMANY
Telephone	+4917621422897
E-mail	tariqim@staff.uni-marburg.de / imran.pharmacy@pu.edu.pk
Nationality	Pakistani
Aufenthaltstitel	Y0FZ0H1LJ
Date of Birth	08-09-1982

WORKING EXPERIENCE

Assistant Professor	06 years till to date
University College of Pharmacy, University of the Punjab, Lahore- Pakistan	

Lecturer	03 Months
University College of Pharmacy, University of the Punjab, Lahore- Pakistan	

Research Officer	09 Months
University College of Pharmacy, University of the Punjab, Lahore- Pakistan	

Assistant Professor	01 year and 03 Months
The University of Lahore, Pakistan	

EDUCATION AND CERTIFICATES

Matriculation (BISE, Lahore)	1998	75%
F.Sc. (BISE, Lahore)	2000	63%
B. Pharmacy (University College of Pharmacy, University of the Punjab, Lahore Pakistan)	2000-2004	66%

M. Phil (Pharmaceutics)

University College of Pharmacy,
University of the Punjab, Lahore Pakistan

2006-2008

**3.323
CGPA**

PhD Student

Department of Pharmaceutics and
Biopharmaceutics, Phillips University
Marburg

2016 to present

Two month internship

Mass Pharma (Pvt)Ltd.
Children Hospital, Lahore

**ORGANIZATION
GOALS**

Zur Erzielung einer verantwortlich, herausfordernd und Karriere Wachstum ausgerichteten Position in der Organisation und wollen, effizienter zu arbeiten, indem sie die Potenziale der Ehrlichkeit, harte Arbeit, Hingabe und beruflichen Fähigkeiten nutzen.

OTHER RESPONSIBILITIES

- COORDINATOR OF UNIVERSITY COLLEGE OF PHARMACY, UNIVERSITY OF THE PUNJAB, LAHORE
- MANAGEMENT REPRESENTATIVE ISO 9001:2008

CONFERENCES

- 21st Annual Meeting CRS- German Local chapter "Future trends in Nanomedicines" 2nd-3rd March, Marburg, Germany (Poster Presentation)
- International Conference and Exhibition of Pharmaceutical Nanotechnology and Nanomedicine, 18th-19th April, 2018, Las Vegas, USA (Oral Presentation)
- International Conference and Exhibition of Pharmaceutical Nanotechnology and Nanomedicine, 18th-19th April, 2018, Las Vegas, USA (Moderator of the Conference)

**INTRUMENTATION
HANDLING**

- Fluorescence microscope, Olympus USA.
- Atomic Force Microscope, JPK, Germany
- Fluostar optima micro plate Reader, Germany
- Zeta Sizer, Malvern, Germany
- DSC Apparatus, Q 2000, TA Instruments, USA
- FTIR Apparatus thermo scientific 6700, USA
- Double beam Spectrophotometer Shimadzu UV-2550, Japan
- Zoom stereo microscope with digital camera DF PLAPO 1X-4 Japan
- HPLC Agilent 1200 series, Germany
- Atomic absorption spectrophotometer A Analyst 800 Perkin Elmer, USA

- Dissolution Apparatus Erweka DT- 700, Germany.
- Rheometer AR 1500, TA instruments, USA.
- Freeze Dryer, Christ
- Rotary Evaporator, Hiedolph, Japan.
- pH meter Ino Lab 740, wtw series, Germany
- Refractometer DR-1, Atago, Japan
- Polarimeter Polax- 2L, Atago. Japan

CURRENT PROJECT

- Downregulation of *MDR 1* gene encoded P-glycoprotein contributes to caspase dependant apoptosis induced by tyrosine kinase inhibitors in colon carcinoma
- A comprehensive biodistribution and toxicity profile of PAMAM based lipid triblock nano carriers after system delivery

PUBLICATIONS

- **Imran Tariq ***, Ahmad M. Mumtaz, Tariq Saeed, Pervaiz A. Shah, Syed A. Raza, Najam ul Hassan Jawa, Muhammad Yasir Ali & Ghulam Abbas. In vitro release studies of Diclofenac Potassium tablets from pure and blended mixture of hydrophilic and hydrophobic polymers. Latin American Journal of Pharmacy. 31 (3):380-7 (2012).
- Misbah Sultana, Syed Saeed-ul-Hasan, Tariq Saeed, Rizwan Mahmood, **Imran Tariq ***, Pervaiz A. Shah & Syed A. Raza. The Effect of Silicon Dioxide Concentrations on Drug Release from Poloxamer/Silicon Dioxide Gel Formulations and their Rheological Characterization. Latin American Journal of Pharmacy. 32 (6): 911-6 (2013).
- Syed Saeed ul Hassan , Syeda Fadia Zaidi , **Imran Tariq*** & Muhammad Tayyab Ansari. Development and Validation of Analytical Method for Losartan-Copper Complex Using UV-Vis Spectrophotometry. Tropical Journal of Pharmaceutical Research. 12 (3): 407-411(2013).
- Syed Saeed-ul-Hassan, Ahsan-ul-Haq Ather, Muhammad Tayyab Ansari, **Imran Tariq*** & Sabiha Karim. Determination of Montelukast Sodium in Raw Material and Solid Dosage Form Using Reverse Phase HPLC. Asian Journal of Chemistry. 25 (13): 7481-7484 (2013).
- Syed Saeed-ul-Hassan, **Imran Tariq***, Sabiha Karim, Muhammad Khalil- ur- Rehman, Sajid Bashir & Ghulam Murtaza. Novel Approach for the Determination of Alfalcidol in Bulk and Tablet Dosage Form using Spectrophotometric

Chapter V: Appendix

Method. Latin American Journal of Pharmacy. 32 (5): 784-8 (2013)

- Syed Saeed-ul-Hassan, Muhammad Tayyab Ansari, Shumaila Sadaf, **Imran Tariq*** & Zahid Mahmood. Development of Spectrophotometric Methods for the Determination of Cefixime in Capsule and Suspension by Making Complex with Cobalt Chloride and Cobalt Nitrate. Journal of Chemical Society of Pakistan. 35 (3): 641-646 (2013).
- Muhammad T. Ansari, Muhammad Imran, Syed S.ul. Hassan, **Imran Tariq*** & Ghulam Murtaza. Solubility Enhancement of Dihydroartemisinin using Mixture of Hydroxypropyl- β -cyclodextrin and PEG-6000. Latin American Journal of Pharmacy. 33: 483-491(2014)
- Pervaiz A. Shah, Sajid Bashir, **Imran Tariq*** & Muhammad A. Hafiz. Fabrication of Lornoxicam Loaded Eudragit L-100 Microcapsules by Spray Drying. Latin American Journal of Pharmacy. 33:828-834 (2014).
- Muhammad Farhan Sohail, Pervaiz Akhtar Shah, **Imran Tariq***, Syed Saeed-ul-Hassan, Umair Amin, Syed Atif Raza, Tariq Saeed, Misbah Sultana & Najam ul Hassan Jawa. Development and *In vitro* Evaluation of Flurbiprofen Microcapsules Prepared by Modified Solvent Evaporation Technique. Tropical Journal of Pharmaceutical Research. 13:1031-1038 (2014).
- Syed Saeed Ul Hassan, Uzma Hayat, **Imran Tariq***, Irshad Ahmad, Muhammad Munawar Hayat, Muhammad Uzair & Muhammad Tayyab Ansari. Spectrophotometric method for the determination of *Gemifloxacin mesylate* in pure and tablet dosage form. Pakistan Journal of Pharmaceutical Sciences. 27: 1171-1174 (2014).
- Muhammad A. Hafiz, Sajid Bashir, **Imran Tariq***, Pervaiz A. Shah, Hafiz M.I. Nazar, Sohail Amjad, Abida Latif & Ghulam Murtaza. Development and *In vitro* Evaluation of Swellable Floating Formulation of Captopril. Latin American Journal of Pharmacy. 33: 1001-1008 (2014).
- Pervaiz A. Shah, Sajid Bashir, **Imran Tariq***, Muhammad A. Hafiz, Hafiz I. Nazar, & Muhammad Akhtar. A Simple RP-HPLC Method for Determination of Lornoxicam in Human Plasma. Latin American Journal of Pharmacy. 33:1034-1037 (2014).

- M. Ahsan hafiz, Muhammad idrees, **Imran Tariq***, Sohail Amjad & Arshad Ali Shah. Stress Degradation Studies and HPLC Method Development for Simultaneous Estimation of Prednisolone Acetate and Chloramphenicol in Topical Eye Drops. Asian Journal of Chemistry. 22: 7817-7822 (2014).
- Muhammad Tayyab Ansari, Altaf Hussain, Sumaira Nadeem, HumairaMajeed, Syed Saeed-UI-Hassan, **Imran Tariq***, Qaisar Mahmood, Abida Kalsoom Khan, & Ghulam Murtaza. Preparation and Characterization of Solid Dispersions of Artemether by Freeze-Dried Method. Biomed Research International. 2015:1-11 (2015).
- Muhammad Tayyab Ansari, Sumaira Nadeem, Altaf Hussain, Humaira Majeed, Syed Saeed-UI-Hassan, **Imran Tariq*** & Ghulam Murtaza. Preparation and Characterization of Binary and Ternary Complexes of Dihydroartemisinin with Hydroxypropyl-cyclodextrin, Palmitic acid and Polyvinylpyrrolidone K30. Current Pharmaceutical Analysis. 11: 216-223 (2015).
- Manzoor Ahmad, Mukhtiar Hassan, Anwar Khalid, **Imran Tariq***, Muhammad Hassham Hassan Bin Asad, Abdul Samad, Qaisar Mahmood & Ghulam Murtaza. Prevalence of Extended Spectrum β -Lactamase and Antimicrobial Susceptibility Pattern of Clinical Isolates of *Pseudomonas* from Patients of Khyber Pakhtunkhwa, Pakistan. Biomed Research International. 1-10 (2016).
- **Imran Tariq ***, Shashank Reddy Pinnapireddy, Lili Duse, Muhammad Yasir Ali, Sajid Ali, Muhammad Umair Amin, Nathalie Goergen, Jarmila Jedelská, Jens Schäfer, and Udo Bakowsky. Lipodendriplexes: A promising nanocarrier for enhanced gene delivery with minimal cytotoxicity. European Journal of Pharmaceutics and Biopharmaceutics 135 :72-82. (2019).

REFERENCES

- **Prof. Dr. Udo Bakowsky**
ubakowsky@aol.com
0049 (6421) 2825881
- **Prof. Dr. Nadeem Irfan Bukhari**
nadeem_irfan@hotmail.com
00923004259738
- **Prof. Dr. Syed Nawazish- i- Husain**
nawazish.pharmacy@pu.edu.pk
00923321413544